UNIVERSITY OF BRASILIA
FACULTY OF TECHNOLOGY
DEPARMENT OF CIVILL AND ENVIRONMENTAL ENGINEERING

EVALUATION OF ARTIFICIAL NEURAL NETWORK TO PREDICT SAND-GEOMEMBRANE INTERFACE SHEAR STRENGTH

ANDERSON GUSTAVO VILLAMIL GONZÁLEZ

SUPERVISOR: GREGÓRIO LUIS SILVA ARAÚJO, D.Sc.

CO-SUPERVISOR: FRANCISCO EVANGELISTA JUNIOT, Ph.D.

DISSERTATION OF MASTER IN GEOTECHNICS

PUBLICATION G.DM – 396/2023

BRASILIA/D.F.
2023

UNIVERSITY OF BRASÍLIA
FACULTY OF TECHNOLOGY
DEPARTMENT OF CIVIL AND ENVIRONMENTAL ENGINEERING

EVALUATION OF ARTIFICIAL NEURAL NETWORK TO PREDICT SAND-GEOMEMBRANE INTERFACE SHEAR STRENGTH

ANDERSON GUSTAVO VILLAMIL GONZÁLEZ

Dissertation of MSc. Submitted to the Department of Civil Engineering of the University of Brasília as part of the necessary requirements to obtain the degree of Master of Science in Geotechnics

APPROVED BY:

_____
GREGÓRIO LUIS SILVA ARAÚJO, D.Sc. (ENC/UnB).
(Supervisor)

_____
FRANCISCO EVANGELISTA JUNIOR, Ph.D. (ENC/UnB).
(Co-Supervisor)

_____
PAULO CÉSAR LODI, D.Sc. (EESC/USP)
(External Examiner)

_____
ENNIO MARQUES PALMEIRA, Ph.D. (ENC/UnB)
(Internal Examiner)

Brasília/DF
Agosto/2023

CATALOGUING DATA

VILLAMIL GONZÁLEZ, ANDERSON GUSTAVO

Evaluation of artificial neural network to predict sand-geomembrane interface shear strength, 2023, xix, 96p, 210x297 mm (ENC/FT/UnB, Masters of Science, Geotecnichs, 2023).

Master's dissertation – Graduate Program in Geotechnics – University of Brasilia.
Faculty of Technology, Department of Civil and Environmental Engineering.

1. Artificial Intelligence
2. Artificial Neural Network
3. Geomembrane
4. Interface shear strength

I. ENC/FT/UNB
II. MASTER

BIBLIOGRAPHIC REFERENCE

VILLAMIL, A. (2023). Evaluation of artificial neural network to predict sand-geomembrane interface shear strength. Master's thesis. Publication PPG G.DM – 396/2023, Department of Civil and Environmental Engineering, University of Brasilia, Brasilia, DF, 97 p.

ASSIGNMENT OF RIGHTS

Author: Anderson Gustavo Villamil González

Title: Evaluation of artificial neural network to predict sand-geomembrane interface shear strength.

Degree: Master of Science - Year: 2023

Anderson Gustavo Villamil González
University of Brasilia – UnB
Campus Darcy Ribeiro
Graduate Program in Geotechnics
70910-900, Asa Norte, Brasília/DF - Brasil.

DEDICATION

A mi amada madre, y querido hermano (q.e.p.d.)

ACKNOWLEDEGMENTS

I am grateful to God for continuously blessing me, leading me through each stage of my life, and providing me with the necessary resources to accomplish my goals. To every family member for believing in my decisions and capabilities, and motivating me to strive for personal growth.

To the University of Brasilia and the Graduate Program in Geotechnics for allowing me to enhance my knowledge and skills. Also, I want to thank CNPq and FAPDF for providing financial assistance to carry out this research.

To my Supervisor, Professor Gregório Luis Silva Araújo, for guiding and supporting me in this new stage of my professional career and for his dedication, friendship, and constant motivation. Also, to my Co-Supervisor, Professor Francisco Evangelista Junior, for sharing his knowledge and helping me achieve the objectives of this work.

To María Camila and Mayara for always being present throughout this time, supporting me, offering their care, friendship, and trust, and sharing day by day with me, making every moment joyful.

To all my colleagues in SG-12 and the people I met throughout this journey, thank you for your sincere friendship and kindness. To the professors of the PPG for their commitment to improving students' knowledge.

To my friends Julieth and Zorany, for always being aware of every step I take and for giving me their enduring friendship and love.

To Jimmy, who motivated me to start this journey, and to Adrian, for always lending an ear to my craze ideas. Moreover, I am grateful to everyone I met during this time which made me feel happy despite being away from home.

For every moment, always grateful.

ABSTRACT

Villamil, A. (2023). **Evaluation of artificial neural network to predict sand-geomembrane interface shear strength**. Master's dissertation, University of Brasilia, Faculty of Technology, Department of Civil and Environmental Engineering, Brasilia DF, 96p.

The implementation of waterproofing systems during the construction of dams, landfills, and artificial channels is crucial to avoid fluid infiltration into the foundation soil, which can lead to structural damage and other potential hazards. Geomembranes are widely used in civil engineering as they offer excellent waterproofing capabilities, low permeability, and favourable mechanical properties. Like other construction materials, evaluating the strength at the interface between geosynthetics and in-contact material is necessary to ensure enough resistance to potential failures.

Various laboratory tests can be conducted to ensure adequate interface resistance, such as direct shear, ring shear, and inclined plane. These tests determine the friction angle, a critical factor in determining the interface shear strength between granular soil and geosynthetics. However, these tests can be time-consuming and expensive and may only sometimes be feasible in project planning. Therefore, finding alternative methods to obtain the necessary information is essential. One possible solution is to use reference results from other research. In this way, a database of previous results can be compiled, and a predictive model can be created to estimate the required interface strength values. This study aims to assess the effectiveness of using an Artificial Neural Network (ANN) methodology to predict the shear strength at the interface of sand and geomembrane. A Multi-Layer Perceptron (MLP) architecture was chosen to configure the ANN models, and the training process is a supervised one that involves a Back-Propagation (BP) training algorithm coupled with the Differential Evolution (DE) optimization algorithm. The input data for the models were defined from 428 laboratory tests reported in previous investigations, including 14 input parameters and sand-geomembrane interface strength results.

Four ANN models were analysed and compared, differentiated in terms of their number of inputs (9 or 14) and the number of hidden layers (1 or 2). The ANN model with the architecture 14-71-342-1 displayed the most satisfactory results for the training and testing phase in terms of the predicted values' distribution compared to the trend line (R^2: 0.919 training, R^2: 0.852 testing), a lower number of residual values outside the acceptable range (4% training, 11.6% testing), and

excellent prediction performance according to statistical metrics for both phases (RMSE: 1.92, MAE: 1.32, MAPE: 5.03% training, RMSE: 0.852, MAE: 3.36, MAPE: 7.13% training). Based on the results, the ANN technique can be defined as an effective approach for predicting sand-geomembrane interface strength values (friction angle) for the collected data.

RESUMO

Villamil, A. (2023). **Avaliação de rede neural artificial para prever a resistência ao cisalhamento da interface areia-geomembrana**. Dissertação de Mestrado, Universidade de Brasilia, Faculdade de Tecnologia, Departamento de Engenharia Civil e Ambiental, Brasilia DF, 96p.

A implementação de sistemas de impermeabilização durante a construção de barragens, aterros sanitários e canais artificiais é crucial para impedir a infiltração de fluidos no solo da fundação, o que pode levar a danos estruturais e outros perigos potenciais. Nesse contexto, as geomembranas são amplamente utilizadas na engenharia civil, pois oferecem excelentes capacidades de impermeabilização, baixa permeabilidade e propriedades mecânicas favoráveis. Assim como outros materiais de construção, avaliar a resistência na interface entre os geossintéticos e o material em contato é necessário para garantir resistência suficiente a possíveis falhas.

Para garantir a resistência adequada da interface, vários testes de laboratório podem ser realizados, como cisalhamento direto, *ring shear* e plano inclinado. No entanto, podem ser dispendiosos, e nem sempre ser viáveis no planejamento do projeto. Uma alternativa é usar resultados de outras pesquisas para criar um banco de dados e um modelo preditivo para estimar a resistência à interface. Este estudo avalia a eficácia do uso da metodologia de Redes Neurais Artificiais (RNA) para prever a resistência ao cisalhamento na interface entre areia e geomembrana. Foi escolhida uma arquitetura de Perceptron de Múltiplas Camadas (PMC) para configurar os modelos RNA, o processo de treinamento é supervisionado, envolvendo um algoritmo de treinamento de Back-Propagation (BP) combinado com o algoritmo de otimização Differential Evolution (DE). Os dados de entrada para os modelos foram definidos a partir de 428 testes de laboratório relatados em investigações anteriores, incluindo 14 parâmetros de entrada e resultados de resistência à interface entre areia e geomembrana.

Quatro modelos de RNA foram analisados e comparados, diferenciados em termos de seu número de entradas (9 ou 14) e o número de camadas ocultas (1 ou 2). O modelo de RNA com a arquitetura 14-71-342-1 mostrou os resultados mais satisfatórios para a fase de treinamento e teste em termos da distribuição dos valores previstos em comparação com a linha de tendência (R^2: 0,919 treinamento, R^2: 0,852 teste), um número menor de valores residuais fora da faixa

aceitável (4% treinamento, 11,6% teste) e excelente desempenho de previsão de acordo com as métricas estatísticas (RMSE: 1,92, MAE: 1,32, MAPE: 5,03% treinamento, RMSE: 0,852, MAE: 3,36, MAPE: 7,13% treinamento). Com base nos resultados, o algoritmo de RNA pode ser definido como uma abordagem eficaz para prever valores de resistência à interface entre areia e geomembrana (ângulo de atrito) para os dados coletados.

TABLE OF CONTENTS

LIST OF FIGURES

LIST OF TABLES

ACRONYMS

AI	Artificial Intelligence
ANN	Artificial Neural Networks
BP	Back-Propagation algorithm
CA	Contact Area
CDS	Conventional Direct Shear test
CV	Coefficient of variation
DE	Differential Evolution algorithm
EPS	Expanded polystyrene
EPDM	Ethylene propylene diene termoplymer
FML	Flexible Membrane Liner
GCE	Geocell
GDP	Drainage pipe
GGR	Geogrid
GM	Geomembrane(s)
GMA	Geomat
GNT	Geonet
GTX-K	Non-woven Geotextile
GTX-NW	Knitted Geotextile
GTX-W	Woven Geotextile
HDPE	High-density polyethylene
HPO	Hyperparameter Optimisation
IP	Inclined Plane test
LLDPE	Linear low-density polyethylene
LSA	Local Sensitivity Analysis
MAE	Mean Absolute Error
MAPE	Mean Absolute Percentage Error
MDS	Medium Direct Shear test
ML	Machine Learning
MLP	Multi-Layer Perceptron
MSE	Mean Squared Error
PP	Polypropylene
PVC	Polyvinyl chloride

ReLU	Rectified Linear Unit function
RF	Random Forest
RMSE	Root Mean Squared Error
SVM	Support Vector Machine

SYMBOLS

a'	Adhesion intercept
τ_f	Shear strength of the interface
σ'_f	Effective normal stress acting on the interface
δ'	Angle of sharing resistance of the interface [°]
ϕs	Friction angle of soil [°]
Cc	Coefficient of curvature
Cu	Uniformity coefficient
D50	Mean soil diameter [mm]
D_r	Displacement rate [mm/min]
A_h	GM asperity height [mm]
t	GM thickness [mm]
τ	Normal Stress [kPa]
ρ	Soil unit weight [g/cm³]
ρ_r	Pearson correlation coefficient
I_d	Sand relative density [%]
f	ANN activation function
i, j, k	ANN nodes/neuron
l	ANN layer
θ_o	ANN bias
X_i	ANN input value
X_{norm}	ANN input normalised value
$\hat{y}_{i,j}$	ANN output value
y_i	Actual value
E	ANN model prediction error
w_{ij}	ANN synaptic weight

d	BP desired response
e	BP error sinal
ξ	BP error energy
ξ_{av}	BP average error energy
t	BP iteration
N	BP total iterations
m	BP number of input values
η	BP learning rate
μ	BP momentum coefficient
Δw_{ji}	BP synaptic weight correction
δ_j	BP local gradient for hidden neuron j
δ_k	BP local gradient for output neuron k
G	DE generation
U_j^G	DE test vector
V_j^G	DE mutated population vector
X_j^G	DE initial vector
X_j^{G+1}	DE selection vector
n	Total number of samples
k, k'	Slope of trend line for actual vs predicted values, or vice versa
R^2	Coefficient of determination
${R_o}^2$,${R_o}'^2$	Coefficient of determination for actual vs predicted values, or vice versa
${R_s}^2$	External validation stabilization criterion
$\bar{y}$	Mean of the actual values
$\bar{\hat{y}}$	Mean of the predicted values

1 INTRODUCTION

1.1 MOTIVATION

Geosynthetics, including geomembranes (GM), have gained popularity in civil engineering as a versatile solution for various geotechnical challenges. Specifically, GM offers an excellent solution for dams, landfills, and artificial channels due to waterproofing capabilities, low permeability, and favourable mechanical properties (Koerner, 2012), managing liquids and preventing infiltration into the underlying soil materials. The strength at the interface between geosynthetics and in-contact material, such as soil, is crucial to ensure enough resistance to potential failures (Moraci et al., 2014). The friction angle determines the interface shear strength between granular soil and geosynthetic and can be determined by various laboratory tests (Palmeira, 2009; Moraci et al., 2014; Cen et al., 2018).

Various researchers have conducted multiple studies to investigate the interface resistance between soil and geomembranes. These studies have shown that factors other than the testing methods impact the strength parameters, including the geomembrane characteristics, soil properties, and external conditions such as applied stresses and contact area (Izgin, 1997; Wasti & Özdüzgün, 2001; Palmeira et al., 2002; Rebelo, 2003; Aguiar, 2008; Pitanga et al., 2009; Moraci et al., 2014; Alzahrani, 2017; Sánchez, 2018; Lashkari & Jamali, 2021; Araújo et al., 2022; Khan & Latha, 2023; Costa Junior et al., 2023)

During the early stages of a project, it is imperative to determine the shear strength of the soil-geomembrane interface but performing lab tests to obtain this information can be expensive and time-consuming. As a result, designers may choose to use reference parameters from previous research with similar specifications. Machine learning (ML) is a computational technique that uses algorithms and statistical calculations to analyse and learn from data, enabling it to predict or categorise outcomes without requiring extensive programming. According to Ebid (2021), Phoon & Zhang (2022) and Baghbani et al. (2022), many authors have applied different ML models for evaluating and resolving geotechnical issues. However, the assessment of geosynthetics' behaviour by ML is rare in comparison to other subjects (Chao et al., 2021).

This study presents the application of a Multi-Layer Perceptron (MLP) ANN with a Back-Propagation (BP) learning algorithm coupled with a Differential Evolution (DE) optimisation algorithm to predict the strength parameter at the sand-GM interface (friction angle) based on 428 laboratory results obtained from previous studies. The training algorithm was conducted using the Machine Learning module of the Tyche software (2020) from the University of Brasilia, with was implemented in the Python® language.

1.2 OBJECTIVES

The overall objective of this study is to assess the accuracy of the Multi-Layer Perceptron-Artificial Neural Network technique, utilising BP-DE algorithms, for predicting the behaviour of interface shear strength between sand and geomembrane (represented by the friction angle). The following specific objectives have been itemized:

- Gather and examine data on factors that influence the shear strength of the interface between sand and geomembrane from laboratory tests conducted by companies and published literature.
- Conduct statistical analysis on the established database to determine the linear relationship between different parameters and the interface friction angle.
- Create ANN models based on input parameters, the number of hidden layers, and the optimal architecture.
- Conduct training and testing analyses for each established ANN model to predict the interface friction angle values.
- Evaluate the accuracy of the ANN models by comparing predicted values to laboratory test results and identifying the most precise model.

1.3 THESIS OUTLINE

The study is divided into five chapters. Chapter 1 briefly introduces the research's initial considerations, motivation, and objective. Chapter 2 focuses on the literature review, presenting geosynthetics' key characteristics and applications, their behaviour at the interface with soil, and fundamental definitions and uses of Machine Learning in civil engineering and geotechnics.

Chapter 3 details the methodology and techniques used to develop, implement, process, and assess the ANN model to predict the interface strength. This chapter outlines the step-by-step

process to create the ANN model, including selecting input parameters and determining the optimal architecture.

Chapter 4 presents the results of the applied methodology for predicting the sand-geomembrane interface strength. The collected data is interpreted and correlated, and the characteristics of the implemented models are described in detail, along with their evaluation. The final developed models are evaluated to determine their accuracy compared to the laboratory results collected. Ultimately, the most accurate model was identified and selected based on its precision in predicting the interface strength.

Finally, Chapter 5 provides a comprehensive overview of the findings and highlights the main conclusions drawn from the study. It also outlines the limitations of the research and provides recommendations for future work.

The literature references used in this study are presented after the last Chapter.

2 LITERATURE REVIEW

2.1 GEOSYNTHETICS

Over time, the search for solutions to the diverse civil construction challenges has led to the development of engineering design practices, e.g. geosynthetics which is now established as a widely used option for geotechnical recommendations. In 1926, the South Carolina Highway Department (SCHD), developed several experiments using cotton fabric as a reinforcement system for asphalt pavement with successful results in improving the pavement's lifetime. This experiment increased interest in implementing geosynthetics to reinforce structures (Koerner & Soong, 1997).

Geosynthetics became more relevant in geotechnical engineering in 1977 when the first geosynthetic conference occurred in Paris. Factors such as product quality control, easy installation, high resistance to biological and chemical degradation, long-term durability in contact with soil, and easy storage and transport (Shukla & Yin, 2006; Koerner, 2012), established the use of geosynthetics as a high effective alternative material.

ASTM D4439-20 technically defines geosynthetics as "*a planar product manufactured from polymeric material used with soil, rock, earth, or other geotechnical engineering related material as an integral part of a man-made project, structure, or system*". The ISO 10318-1 standard states that it is a product in which at least one of its components is made from a synthetic or natural polymer.

Polymers are commonly characterized as "plastics" made from natural products such as petroleum and their derivatives (Koerner, 2012). The author points out that the most commonly used polymers for the manufacture of geosynthetics include: High-density polyethylene (HDPE), Linear low-density polyethylene (LLDPE), Polypropylene (PP), Polyvinyl chloride (PVC), Polyester, Expanded polystyrene (EPS), classified as thermoplastics (have the property of modifying their shape after a heating and cooling process without altering their characteristics), and Ethylene propylene diene termoplymer (EPDM) which belongs to the thermosets (do not possess the property of modifying their shape).

2.2 FUNCTION AND TYPES

According to Koerner (2012), geosynthetics are mainly used because they provide better performance and economy in comparison to other conventional materials utilized in engineering projects. In addition, as they are manufactured with synthetic or natural materials (cotton fibres, jute, coir, wool, among others), they offer greater ease and versatility in construction for geotechnical, environmental, hydraulic and transport purposes; for instance, foundation reinforcement, dike construction or soil-reinforced retaining walls, embankments, erosion control on slopes and riverbanks, hydraulic control, canal lining, rockfall control, subgrade reinforcement, asphalt layers and granular base, among others. Figure 2.1 shows some different civil construction applications using geosynthetics.

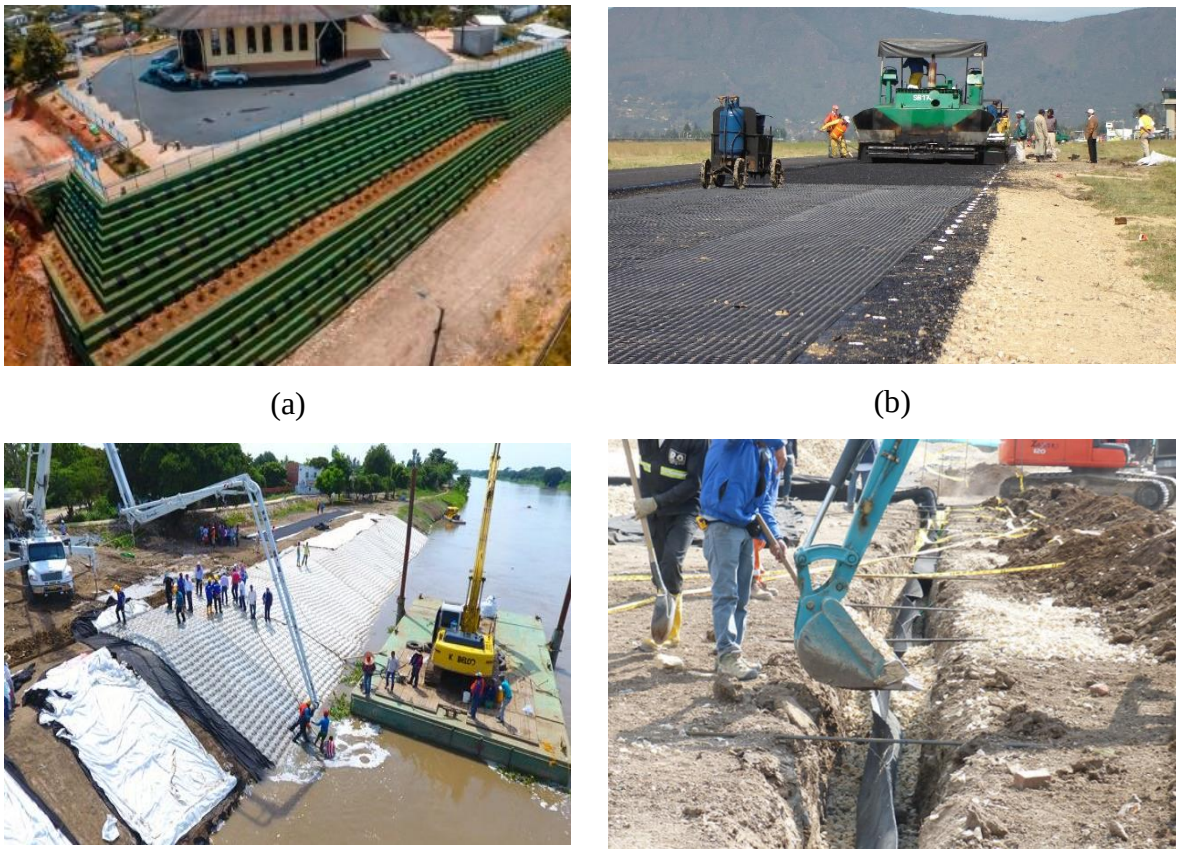

(a) (b)

(c) (d)

Figure 2.1 – Use of geosynthetics in construction projects: (a) Earth retaining wall, (b) Asphalt reinforcement, (c) River bank control, (d) Hydraulic control (Geomatrix Colombia, 2023).

The Brazilian standard ISO 10318-1 outlines seven main functions of geosynthetics: surface erosion control, drainage, filtration, barrier, protection, reinforcement and separation. Multiple

geosynthetic products are differentiated predominantly by their manufacturing process (IGS, 2015a), which establishes their functionality and application. Table 2.1 briefly describes each of the seven main functions mentioned previously and the most suitable type of geosynthetic; the same geosynthetic can be found in different applications.

Table 2.1 - Geosynthetics functions (Modified from ISO 10318-1).

Function	Description	Geosynthetic type
Surface erosion control	Prevent or reduce the movement of soil or other superficial particles caused by rainfall or surface water runoff.	GTX (W, K or NW), GMA, GCE
Drainage	Collecting and transporting of precipitation, groundwater and other fluids using a geosynthetic material, which acts as a drain that transports the fluid through lower permeability soils.	GTX (W, K or NW), GDP
Filtration	Retention of soil or other particles subjected to hydrodynamic forces, allowing the passage of fluids into or across a geosynthetic material.	GTX (N, K o W)
Barrier	Application of a geosynthetic to prevent or restrict the migration of fluids (waterproofing).	GM
Protection	Preventing or limiting of local damage to a given element or material by the use of a geosynthetic material	GTX (W or NW), GNT
Refoircement	Use of the stress-strain behaviour of a geosynthetic material to improve the mechanical properties of soil or other construction materials.	GTX (N, K o W), GGR, GCE
Separation	Prevention from intermixing of adjacent dissimilar soils and/or fill materials by the use of a geosynthetic material.	GTX (N, K o W), GM

Nomenclature taken from ISO 10318-1: GTX= Geotextile (W= Woven, K= Knitted, NW= Non-woven), GMA= Geomat, GCE= Geocell, GDP= Drainage pipe, GM = Geomembrane, GNT= Geonet, GGR= Geogrid.

Below it is given a brief description of the different geosynthetics referred previously according to the terminology established by the standard ISO 10318-1, and an image example is presented in Figure 2.2.

- *Geotextile – GTX (N, K, W)*: planar, permeable, polymeric (synthetic or natural) textile material, which may be nonwoven, knitted, or woven, used in contact with soil and/or other materials in geotechnical and civil engineering applications.

- *Geomat – GMA*: three-dimensional, permeable structure, made of polymeric monofilaments, and/or other elements (synthetic or natural), mechanically and/or thermally and/or chemically and/or otherwise bonded.
- *Geocell – GCE*: three-dimensional, permeable, polymeric (synthetic or natural) honeycomb, or similar cellular structure, made of linked strips of geosynthetics.
- *Geomembrane – GM*: also known as geosynthetic barrier – GBR, is low-permeability geosynthetic material, used in geotechnical and civil engineering applications with the purpose of reducing or preventing the flow of fluid through the construction.
- *Geonet – GNT*: geosynthetic consisting of parallel sets of ribs overlying and integrally connected with similar sets at various angles.
- *Geogrid – GGR*: planar, polymeric structure consisting of a regular open network of integrally connected, tensile elements, which may be linked by extrusion, bonding, or interlooping or interlacing, whose openings are larger than the constituents.
- *Geocomposite – GCO*: manufactured, assembled material using at least one geo-synthetic product among the components.

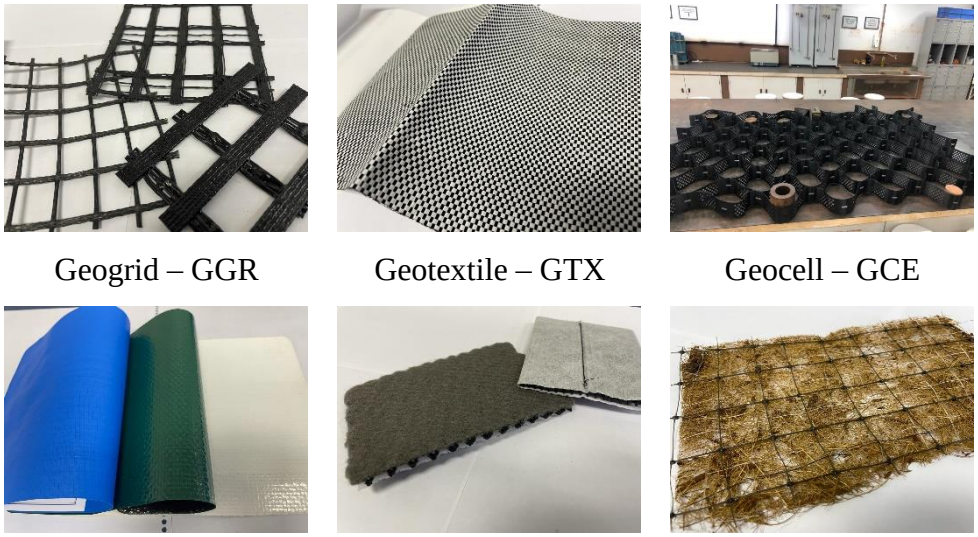

Geogrid – GGR | Geotextile – GTX | Geocell – GCE

Barrier – GBR | Geocomposite – GCO | Geomat – GMA

Figure 2.2 – Geosynthetic photographic sample.

2.3 GEOMEMBRANE AND CIVIL WORKS APPLICATIONS

Shukla & Yin (2006) describe GM as a flexible membrane liner (FML) with permeability values ranging from $0.5x10^{-12}$ to $0.5x10^{-15}$ m/s being up to 10^6 times lower in permeability than compacted clay. GM can be used as a barrier inside an earth mass or as a liner when used as an

interface. The GM can be manufactured with different characteristics such as thickness, roughness (smooth or textured), material (PVC or HDPE), among others, depending on the specific needs of the site.

A minimum thickness of 0.75 mm is recommended for all geomembrane, except for HDPE type, which should have a minimum thickness of 1.5 mm considering its manufacturing process. The most commonly used geomembrane type is HDPE. However, if greater flexibility is required, it is possible to use LLDPE (linear low-density polyethylene) geomembrane.

GM has waterproofing properties suitable for hydraulic control in construction sites. In landfills, GM is implemented on bottom, top (landfill closure) and lateral slopes, developing a system that prevents leachate infiltration (fluid generated by the runoff of water through the waste) into the ground (leading to a collection and discharge point), ensuring no soil contamination.

For hydraulic structures such as ponds, reservoirs or canals, GM offers effective infiltration control, constructability and/or lower cost than other materials such as concrete or soil (which can be affected by cracking or erosion). Other applications of GM as complementary elements are implemented in earth dams, retaining walls and tunnels (Shukla and Yin, 2006). Geotextiles are often installed on top of the GM to protect from damage by building materials or ultraviolet radiation (IGS, 2015b). Figure 2.3 shows a photographic sample for smooth and textured geomembrane.

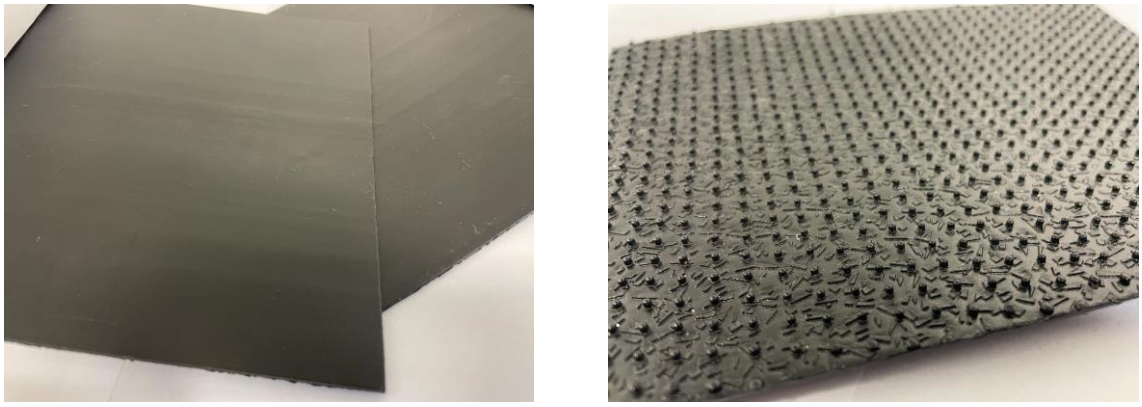

(a) (b)

Figure 2.3 – Geomembrane photographic sample: (a) Smooth, (b) Textured.

It is possible to find simple waterproofing systems composed of a single liner of geomembrane or in contact to a low permeability soil (composite liner). A composite liner combines two or more different materials with low-permeability components giving a better behaviour due to its different hydraulic, physical and resistance characteristics. There are also double liner systems characterised by two liners and a draining layer for detecting, collecting and removing liquids (Giroud & Bonaparte, 1989). Figure 2.4 illustrates fives examples of lining systems.

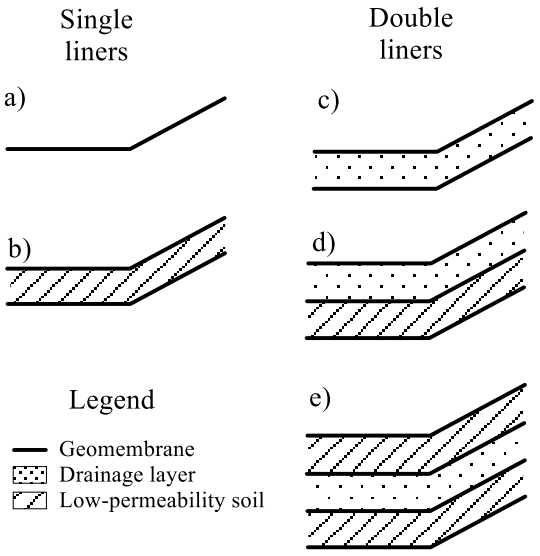

a) single geomembrane liner; b) single composite liner
c) double geomembrane liner; d) double liner with geomembrane top (or primary) liner and composite bottom (or secundary) liner; e) double composite liner

Figure 2.4 – Some examples of lining systems (after Giroud and Bonaparte, 1989).

2.4 SOIL/GEOSYNTHETIC INTERFACE SHEAR STRENGTH

In civil engineering constructions using geosynthetics, it is important to evaluate their properties and establish an appropriate design to avoid any damage that reduce the operability and integrity of the structure. In this context, enough interface strength between the geosynthetic and the adjacent material is essential to prevent potential failures. In the case of interaction with soil, suitable interface strength will prevent the sliding of the soil mass or "pulling out" of the geosynthetic (Costa e Lopes, 2001).

The Mohr-Coulomb rupture criterion is used to define the interface strength with geosynthetics by replacing the soil friction angle by the interface strength angle and the cohesion by the adhesion between the involved materials (Eq. (2.1)) (Izgin, 1997).

$$\tau_f = a' + \sigma'_f \tan \delta' \qquad \text{Eq. (2.1)}$$

Where:

τ_f: Shear strength of the interface.

a': Adhesion intercept.

σ'_f: Effective normal stress acting on the interface.

δ': Angle of sharing resistance of the interface.

In order to measure the strength parameters, laboratory tests are carried out to obtain the shear stress-displacement curve for different loading, thus determining the strength envelope (Costa Junior, 2020). For granular soil-geosynthetic interface is typical to neglect the influence by adhesion parameter (Markou & Evangelou, 2018).

According to Wu & Shu (2012), stress-displacement curves have three stages known as pre-peak, softening and residual, as shown in Figure 2.5. The maximum (peak) shear stress value occurs between the pre-peak stage and softening stage. Palmeira (1987) indicates that most of the friction angle between soil and a reinforcement material is smaller than the friction angle of the soil alone.

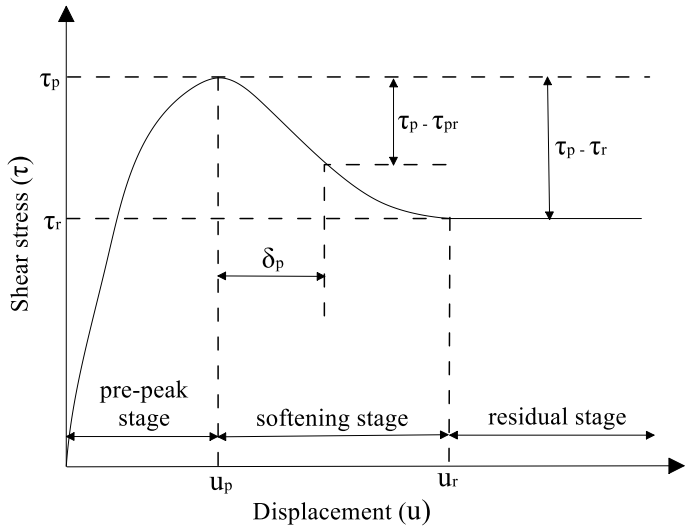

Figure 2.5 – Relationship between Shear stress and Displacement of Geomembrane Interface (Modified from Wu & Shu, 2012).

Direct Shear, Inclined Plane, Ring Shear, and Pullout tests are used as for shear strength evaluation of soil/geosynthetic interfaces. The direct shear test is the most applicable because of its ease of application and versatility (Aguiar, 2003, 2008; Rebelo, 2003; Jogi, 2005; Afonso, 2009; Alzahrani, 2017). Direct shear test and Inclined plane have their particularity and they basically are described as follows.

The Direct Shear Test is widely used in practice to evaluate material behaviour. Shear strength measurement at soil-geosynthetic interfaces (ASTM D5321-12, Procedure B) is performed by placing a geosynthetic specimen completely on a soil substrate in the lower box of the apparatus and then covering it with the upper box filled with compacted soil adjusted to the required moisture and density (ABNT NBR ISO 12957-1/ ASTM D5321-12). Subsequently, a normal load is applied, and the shear force and displacement are measured until a stable condition is achieved. The procedure is performed with a minimum of three (3) different loads on the same material to obtain the failure envelope and the interface strength parameters (interface friction angle δ' and adhesion a'). Figure 2.6 shows a typical representation of a shear-normal stress graph where the slope of the strength envelope represents the interface friction angle shearing resistance and the intercept with shear stress axis represents the apparent adhesion (Jogi, 2005).

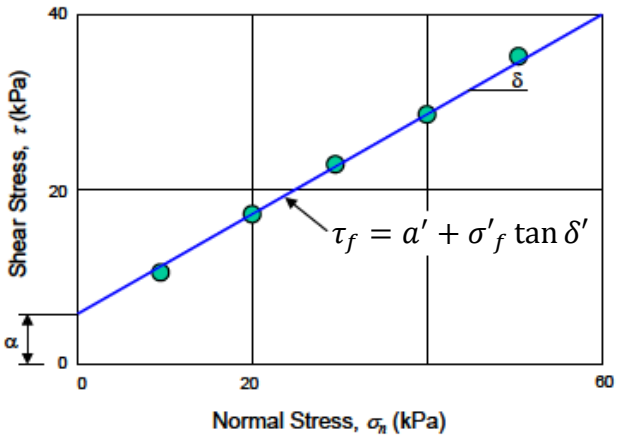

Figure 2.6 – Typical plot of shear stress vs. normal stress obtained from direct shear testing of geomembrane- soil interface (Jogi, 2005).

The box size used in the tests depends on the apparatus and procedure. The ABNT NBR ISO 12957-1/ ASTM D5321-12 standard describes the method for determining the shear strength of soil-geosynthetic interface by direct shear test, stipulating a minimum box dimension of 300 mm (12") or fifteen (15) times the d_{85} of the coarser soil used in the test and a container depth

of a minimum 50 mm (2") or six (6) times the maximum particle size of the coarser soil used. However, the standard specifies that it is possible to modify the container dimensions. For example, the Conventional Direct Shear test (CDS) employs a rounded or squared box of 60 or 100 mm dimensions, or the Medium Direct Shear test (MDS), where variations in the box size of up to 1000 mm are possible in both containers (lower and upper). Sometimes the lower container can be made with larger dimensions in case of greater deformations (Aguiar, 2003). These container dimension adjustments allow for a more extensive interface area, providing easier readings of forces and deformations (Rebelo, 2003).

There is not a single, definitive procedure for direct shear testing. Ingold (1991) specified five (5) basic methods for direct shear tests identified as fixed shear box, partially fixed shear box, free shear box, large base shear box and central base shear box, as is shown in Figure 2.7.

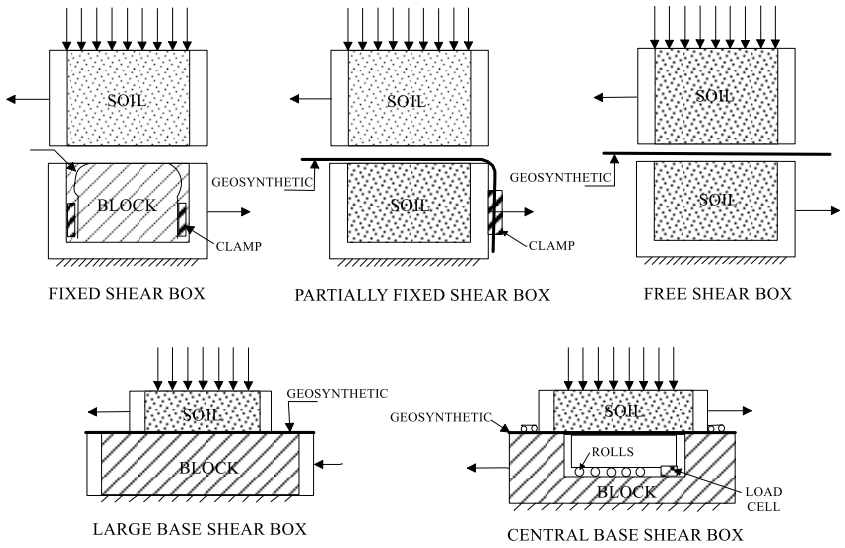

Figure 2.7 – Types of Direct Shear apparatus (After Ingold, 1991).

The Inclined Plane Test measures the friction angle values of a geosynthetic-soil interface at low normal stress using an inclining plane apparatus. The test allows the generation of inclined slope conditions for low-stress levels, which can produce errors when conventional direct shear test is used (Gourc et al., 1996).

The test quantifies the angle necessary to slide a soil box along an inclined articulated base, where the geosynthetic is fixed, at a constant speed of 3±5°/minute. The minimum box dimensions are 300x300 mm with a depth greater than 50 mm or seven (7) times the maximum

particle size of the soil used (according to ABNT NBR ISO 12957-2). Although, similar to the DS test, variations in the box dimensions are accepted and implemented. The weights must be ensured to be placed on the box to apply soil loads. Figure 2.8 shows a photograph of the inclined plane test equipment.

Figure 2.8 – IP test equipment photograph (Lima Junior, 2000).

2.4.1 FACTORS AFFECTING SAND/GEOMEMBRANE INTERFACE STRENGTH

The previous section discussed the behaviour of interface strength with geosynthetic and outlined several methods for assessing strength parameters, including two types of testing that will be referred to later in the methodology. Many authors have conducted studies evaluating the sand/GM interface strength using DS and IP tests. However, during the execution of the tests, various factors were observed to have influenced and affected the strength parameter values. Below are referenced some investigations of the various influencing factors related in the literature. Each factor is presented independently, starting with external conditions and then with the material properties.

Firstly, the type of test choice for assessing material's shear strength, either DS (with modifications in the box-dimensions) or IP, will directly influence the interface shear strength. The IP test is more appropriate for applying lower normal stresses (Lima Junior, 2000; Ling et al., 2002; Viana, 2007; Moraci et al., 2014; Sánchez, 2018; Mello, 2021; Pavanello et al., 2021), while the DS test can generate errors (Girard et al., 1990). Furthermore, the configuration of

the equipment can also affect the materials' interaction behaviour and the application of loads (Palmeira, 2009).

The DS test results at the sand/geosynthetics interface developed by Lashkari & Jamali (2021) demonstrated a decrease in friction angle values with an increase in applied normal stress. A similar condition was observed by Wasti & Özdüzgün (2001) and Pitanga et al. (2009) for geomembrane/geotextile interfaces.

Afzali-Nejad et al. (2021) conducted direct simple shear tests on various types of sand, geomembrane, and woven geotextile to observe the influence of volume change on interface strength. Among the results obtained, the authors concluded that an increase in the initial normal stress and normal stiffness generated an increase in ultimate and peak strength for dense and medium-dense sand interfaces with geosynthetics (also observed by Khan & Latha, 2023). The opposite result was obtained for loose sand interfaces. Pavanello et al. (2022), concluded that any variations in the normal stress caused by the IP test, do not result in significant differences in the outcomes.

Fleming et al. (2006) state that an increase of the normal stress can modify the mechanism of interface shear failure, generating a combination of sliding and plowing. This condition is also related to the type of geomembrane and soil present at the interface, with a higher shear strength observed for more granular soils and smooth geomembranes at sufficiently high normal stress due to the embedded particles into the geomembrane. Same sliding to plowing change condition was stated by Chen et al. (2021) according to the results of finite element and discrete element method analysis for 3D interface shear test simulations between sand and smooth geomembrane.

In the study conducted by Sánchez, (2018), different interfaces with geosynthetics were evaluated using three types of tests (CDS, MDS and IP). The author found that there is no direct relationship between the strength values and the thicknesses of the geotextiles, which was also reported by Lima Junior (2000) for inclined plane tests with sand/geosynthetics. On the other hand, the author points out that a larger contact area (involving the scale of the tests) influences the shear strength response of the interfaces and reduces the influence of other material characteristics (such as density and type of matrix).

Several authors (Izgin & Wasti, 1998; Lima Junior, 2000; Wasti & Özdüzgün, 2001; Hsieh & Hsieh, 2003; Reyes Ramirez & Gourc, 2003; Gourc & Reyes Ramírez, 2004; Viana, 2007; Aguiar, 2008; Pitanga et al., 2009; Moraci et al., 2014; Sánchez, 2018) have reported variations in the interface friction angle values for different tests when using different equipment scales and test box sizes. The results indicated different conclusions for the influence of the box sizes, where some authors state that larger contact areas result in higher values of interface friction angles, and others commented the opposite. In general, it is possible to suggests that the test equipment scale influences the interface strength response.

Monteiro (2012) performed IP and CDS tests on smooth PVC and HDPE geomembranes and textured HDPE geomembranes with fine sand (varying the degree of saturation). In general, an increase in the shear strength interface was found with higher saturation degree values. In addition, lower friction angle values were observed for the interface with smooth geomembranes (HDPE and PVC) concerning the values obtained with textured HDPE geomembranes.

Costa Junior et al. (2023) carried out direct shear tests using two types of sandy silt-clay soil (SM according to USCS system) without plasticity (one of which had a larger particle diameter) and nine types of textured geomembranes with an asperity height between 0.52 to 1.0 mm, on both sides. The tests were performed using a 300x300 mm box and different load values (5 to 50 kPa) under both, dry and saturated conditions, with a displacement rate of 1.0 mm/min. The results indicated that the strength parameter values were higher for coarser soils and dry conditions, particularly for peak values.

Karademir (2011) and Karademir & Frost (2021) studied the behaviour of interface strength with geomembranes due to ambient temperature variation. The tests showed an increase in the interface strength with geosynthetics proportional to the temperature increase. For sand-geomembrane interface, Bilgin & Shah (2021) found a contrary condition in large direct shear tests where the interface shear strength was decreasing at higher temperatures. However, high temperatures can cause GM crystallization, affecting lifespan and functionality (Rowe et al., 2009). On the other hand, Paruchuri (2011) found no significant influence on the strength of

geosynthetic samples when they are in freezing and unfreezing conditions, concluding that the impact of freezing temperatures on the interface of geosynthetics is insignificant.

From the geosynthetic interfaces tests performed by Stark et al. (1996), it was noted that there is a major difference in the interface strength values for smooth and textured geomembranes, significantly higher when textured geomembranes were used. A similar condition was evidenced by Araújo et al. (2022), where the interface adherence between sand and GM depends on the geomembrane asperity; the results showed a direct influence on the interface shear strength due to the asperity height of the geomembrane.

Lopes et al. (2001) conducted inclined plane tests following the standard guidelines for two methods. Two types of sand with different grain sizes and two types of HDPE geomembranes of the same thickness (2 mm) with a different texture (smooth and textured) were employed. The results showed that the sand/GM interface strength is strongly affected by the geomembrane surface texture, being higher when the geomembrane is rough. On the other hand, they showed that the differences between the applied test methods were not significant.

Ari & Akbulut (2022) tested the interface shear strength for three types of sand and three types of geomembrane with different fractal dimensions (units of measurement for objects with irregular morphology) by direct shear tests under three different stresses (54, 109 and 163 kPa). Figure 2.9 presents the results obtained for the interface friction angle behaviour for the fractal dimension of the three types of sand used (black: beach sand, red: crushed sand with rounded edges, and blue: crushed sand with angular edges) and the geomembranes (black: smooth, red: slightly textured, and blue: heavily textured). The results showed a proportional influence on the increase of the interface shear strength with the value of the materials' fractal dimension. This allows inferring that both the soil particle size and the geomembrane's asperity height characteristics influence the interface behaviour, considering that the soil particles (due to the applied normal stress) penetrate the geosynthetic, increasing the resistance to movement.

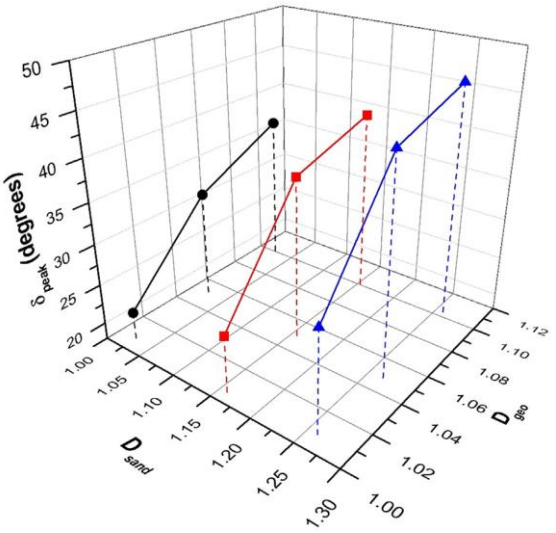

Figure 2.9 – Variation of the sand-geomembrane interface friction angle with fractal dimension (Ari & Akbulut, 2022)

The results observed by Jewell et al. (1984), Palmeira & Milligan (1989), Jewell (1990, 1996) Lopes & Lopes (1999), Costa e Lopes (2001), Aguiar (2008), Vangla & Latha (2015), Afzali-Nejad et al. (2017), have shown that soil particle size has a significant impact on the geosynthetic shear strength interface behaviour. Another influential feature is the soil density, which is directly proportional to the interface shear strength evaluated for the sand/GM interface studied by O'Rourke et al. (1990).

According to the observations presented in the different authors' research, the GM interface shear strength parameters are linked to different factors, which can be classified as showed in Figure 2.10:

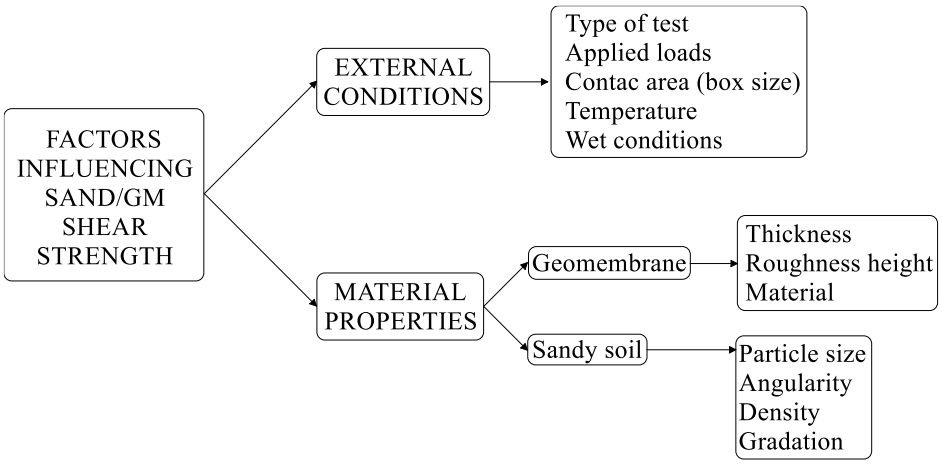

Figure 2.10 – Sand/GM interface strength influential factors.

2.5 MACHINE LEARNING (ML)

New technologies are characterised by implementing processes and methodologies that generate innovative results. However, it is possible to use novel techniques to take advantage of the vast amount of existing information produced over time to learn the expected response based on the experience already acquired. Machine Learning (ML) is a method capable of analysing and learning from previous information (data mining) to predict or classify a response using algorithms and statistical calculations without complex programming.

Arthur Samuel (1959) initially defined ML as "*the field of study that gives computers the ability to learn without being explicitly programmed"* and a newer description was given by IBM Education (2020) where ML is defined as *"...a branch of Artificial Intelligence (AI) and computer science which focuses on the use of data and algorithms to imitate the way that humans learn, gradually improving its accuracy".* As mentioned before, ML is highly related to AI, and a brief description of AI is given below.

AI is related to several disciplines (Russell et al., 2010), generating a powerful computational tool capable of developing human-like actions or responses:

- *Philosophy:* provides the component of intelligence that involves both action and reasoning.
- *Mathematics:* requires mathematical ideas based on logic, computation and probability.
- *Economics:* making rational decisions when the benefits of actions are not immediate but result from several actions taken in sequence.
- *Neuroscience:* the study of the nervous system, especially how the brain stores and interconnects information to integrate such behaviour into computers.
- *Psychology:* how computational models can use psychology regarding memory, language and logical thinking.
- *Computer engineering:* besides providing intelligence, AI requires efficient machines with modern operating systems, programming languages and tools.
- *Control and cybernetics:* allowing AI to operate under its own control.
- *Linguistics:* the relationship between language and thought, for IA related to computational language.

Although it may seem like modern 21st-century science, AI has actually existed for about 80 years since its first application. In 1943, Warren McCulloch and Walter Pitts proposed one of the first works, in which they generated an artificial model of "on/off" neurons and simulated the response to a psychological stimulus (Russell et al., 2010). Fausett (1994) noted that McCulloch and Pitts concluded that combining neurons in a network system could increase computational capacity. Consequently, other authors developed new methodologies for AI applications and improved programming tools. As a result, AI has become a widely applicable, useful and appropriate tool for solving complex problems or making decisions in many fields, such as medicine, technology, engineering, marketing, psychology, and others.

Implementing ML (or AI) for different analyses has grown due to its simple applicability using specific algorithms without incurring extensive and limited programming codes. Géron (2019) mentions the great usefulness of ML as follows:

- From a simpler code (or algorithm), it can solve problems that require more human effort or many conditioning rules.
- Seeks the best technique to find a solution to complex problems that cannot be solved by traditional methods.
- Adapts to existing information, even newly acquired.
- Obtains results from a large amount of data.

2.6 TYPES OF LEARNING IN ML

ML is based on the information available to find an answer to a problem. As mentioned above, considering that each issue has different characteristics, it is necessary to establish the best algorithm that fits the desired solution. ML can be broadly categorised into three types of analysis, mainly focused on the learning rule: Supervised Learning, Unsupervised Learning and Reinforced Learning (Abraham, 2005; Shahin et al., 2008).

2.6.1 SUPERVISED LEARNING

In supervised learning, both input and output data (desired response) are known, which allows the accuracy of the analysis to be established (based on comparison error). This type of learning is known as *learning with a teacher* (Haykin, 1999), where knowledge is represented by an input and an example output (result). Supervised learning can be divided into two types of tasks;

the first corresponds to *Classification*, where the algorithm works as a filter to define the desired output. The second task is *Prediction*, where a target value is generated from a set of input data, also known as predictors, which are trained through examples (Géron, 2019). Regression statistics establish a relationship between the independent variables (predictors) and the predicted outcome.

There are different types of supervised learning algorithms and Table 2.2 briefly describes some of the most commonly used ones.

Table 2.2 – Types of supervised learning algorithms.

Type of algorithm	**General description**
Decision Tree	The data are classified in the form of trees, where each tree represents a classification case of the information, and each branch is the assumed output value. The branch that best splits the training data becomes the root of the tree. The algorithm performs multiple splits until it finds sub-trees with the same classes at the same level (Maglogiannis, 2007).
Naïve Bayes (NB)	This algorithm corresponds to a probability-based ranking of data to predict a response. In this case, each piece of data is considered independent and therefore, it is called "naive". The analysis is performed according to Bayes' theorem (Ray, 2019).
Support Vector Machine (SVM)	The algorithm allows for classification and regression analysis. It works by generating hyperplanes that divide the data into decision boundaries (Ray, 2019).
Random Forest (RF)	It is a combination of Decision Tree and regression. From the data are generated multiple random samples generating k number of trees (Forest). Each tree generates a prediction, and the average establishes the model's final output (Pant & Ramana, 2022).
Artificial Neural Networks (ANN)*	ANN is one of the most widely used algorithms at present. Its main characteristic is that each input is connected by a network that tries to imitate the neurological characteristics of the human body (Fausett, 1994). This type of network corresponds to units (neurons) organised in layers or groups with hidden layers between the input data and the output signal. The network generates a nonlinear regression analysis, where each output value of the preceding neuron is affected by a weight (Haykin, 1999).

*: a more detailed description is presented in the following chapter to better understand the methodology used in this study.

2.6.2 UNSUPERVISED LEARNING

Unlike the previous type of learning, in this method, there are no predefined output values, so results are generated based on the analysis of the input data. The implemented algorithms learn from existing data independently, i.e. *without a teacher* (Mahesh, 2020). Like supervised learning, there are different task and performance algorithms, as presented in Table 2.3.

Table 2.3 – Types of unsupervised learning (Géron, 2019).

Type	General description	Type of algorithm sample
Clustering	Allows to establish groups of existing data based on similar characteristics of all samples.	K-means, DBSCAN, Hierarchical Cluster Analysis (HCA)
Anomaly detection and novelty detection	Defines values out of the common ranges in the input data (outliers).	One-clas SVM, Isolation Forest
Visualization and dimensionality reduction	Visualisation: allows finding and visualising specific values or data within an organised group of data (clustering). Dimensionality reduction: reduces or combines parameters with similar characteristics, generating fewer data for analysis.	Principal Component Analysis (PCA), Kernel PCA, Locally-Linear Embedding (LLE), t-distributed Stochastic Neighbor Embedding (t-SNE)
Association rule learning	Establishes relationships between the input data to show some interest characteristics.	Apriort, Eclat

2.6.3 REINFORCEMENT LEARNING

This learning algorithm is based on positive or negative reward classes. It uses a value *X* as an agent in the middle of the data (environment) to find different actions and learn from each result until it finds the most successful output according to the most favourable rewards (Géron, 2019). Figure 2.11 represents the reinforcement learning method in which a final decision is made based on learning.

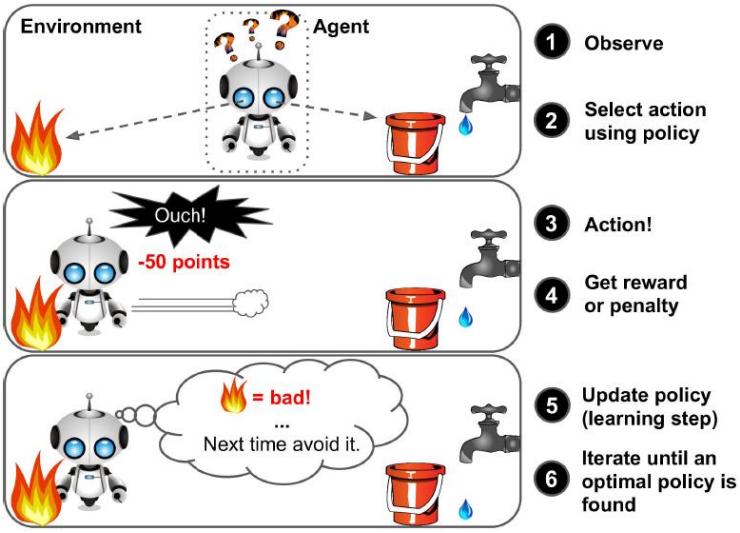

Figure 2.11 – Reinforcement learning scheme (Géron, 2019).

2.7 ARTIFICIAL NEURAL NETWORK (ANN)

Several methodologies are inspired by characteristics of living beings, such as animals, microorganisms, and even humans, due to their behaviour and decision-making processes. One of these methods is Artificial Neural Network (ANN), which is a type of ML that attempts to mimic the behaviour of the human brain using mathematical algorithms (Fausett, 1994; Basheer & Hajmeer, 2000; Shahin et al., 2009). The human brain presents one of the most complex structures known; composed of neurons that are connected to each other via axons and synapses to transmit signals and product reactions. A biological neuronal network consists of millions of neurons interconnected in an organised way (Géron, 2019).

ANNs are also structures as units (neurons) that hold analysis information and are connected by links (known as weights) which act as synapses up to an output neuron producing the desired outcome (Jain et al., 1996; Haykin, 1999; Abraham, 2005).

The use of ANNs can be traced back to 1943 when McCulloch and Pitts developed an artificial binary model of a neuron. They later realised that it was possible to create a network of multiple neurons, allowing for computational logic to be performed (Géron, 2019). Since then, the application of ANN has grown and can be found in many different areas of study due to their versatility, adaptability and potential to solve large and complex tasks (both linear and non-linear) by learning from existing information (Basheer & Hajmeer, 2000).

ANN's application can be categorised into five main categories, including prediction, classification, data association, data conceptualisation and data filtering. These categories are determined based on existing data from statistical analysis developed by algorithms (Anderson & McNeill, 1992). ANN analyse information through neurons connected by links that generates signals activated by a function (usually non-linear) until the output signal is determined (Fausett, 1994). The author also mentions that an ANN is characterised by three main elements, the network architecture (which determines how neurons are organised), the training algorithm (how the synaptic weights are determined) and the activation function.

2.7.1 NETWORK ARCHITECTURE – MULTILAYER PERCEPTRON (MLP)

As in civil projects, architecture defines the organisation and interaction of the structure's elements. The architecture of the ANN determines the network size and how the neurons are organised. Network architecture can be divided into feed-forward or recurrent categories (Jain et al., 1996).

The network architecture is designed in layers, which can be monolayer when the input and output neurons are directly connected, or multilayer when there are one or more intermediate *hidden layers* (see Figure 2.12) —ANNs process in a unidirectional (feedforward) manner in the direction of the output layer (Zurada, 1992).

The ANN process starts at an initial layer containing the input values set in n-neurons (X_i). The process then passes through the hidden layers via "*links*" or synaptic weights (w_i), generating a signal that is transmitted to the next neuron ($X_i + 1$). Each layer converts the preceding information into a number by using an activation function (f). This process continues until the last layer, where the final value of the model (output, y) is obtained. To avoid null option in each neuron, it is possible to include values known as "*bias*" (θ_o) between each layer transformation (Haykin, 1999; Shahin et al., 2009). Eq. (2.2) summarizes the aforementioned process.

$$y = f\left(\sum_{i=1}^{n} X_i w_i + \theta_o\right) \qquad \text{Eq. (2.2)}$$

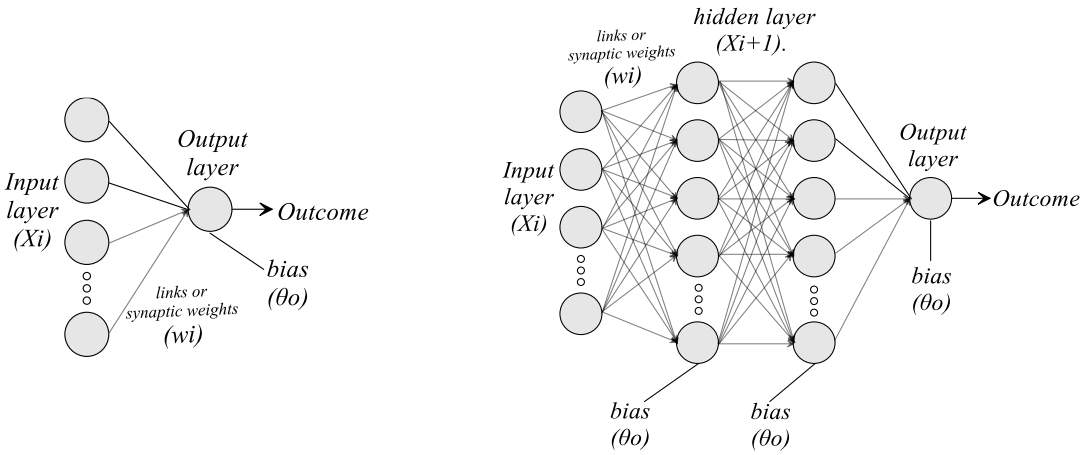

(a) (b)

Figure 2.12 – (a): single layer network and (b): Multilayer network.

The perceptron is the simplest form of the artificial neural network. It consists of a single layer and an artificial neuron. Developed by Rosenblatt in 1958, the neuron receives the input signals (which are affected by synaptic weights), processes the information, and generates the output result (Silva et al., 2016). Figure 2.13 illustrates the configuration of a perceptron and its mathematical expression.

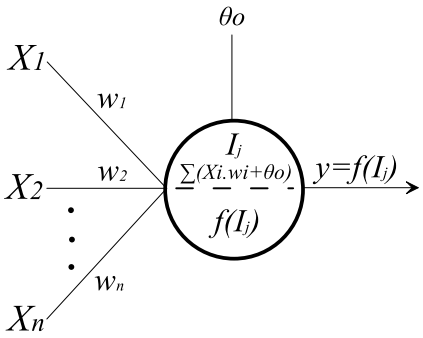

Figure 2.13 – Single perceptron scheme.

In summary, a Multilayer Perceptron (MLP) network refers to a network architecture composed of multiple layers and perceptrons.

2.7.2 TRAINING ALGORITHM – BACKPROPAGATION (BP)

ANN employs a supervised learning method, i.e. there is control over the outcomes obtained from already-known results. The learning process in ANN improves the fitting parameters (synaptic weights and bias) until the result with the lowest possible error is achieved, which means training the network (done through algorithms).

Different types of neural networks exist depending on the training algorithm used (how the weights and bias are adjusted). In the case of MLP-ANN, the most widely applied training algorithm is BackPropagation (BP) developed by David Rumelhart, Geoffrey Hinton and Ronald Williams in 1986 which is based on first-order gradient descent (Basheer & Hajmeer, 2000; Soleimanbeigi & Hataf, 2006).

The BP algorithm works in two phases. The first phase corresponds to the initial analysis of the input data up to the network output, which defines initial values for synaptic weights and bias (forward phase). The second phase consists of comparing the obtained results with the actual values, calculating the respective error (Eq. (2.3)), and determining the need for a backward analysis. Each forward and backward phase is repeated until the smallest possible error gradient is found (Silva et al., 2016). These iterative processes are known as epochs, where the algorithm is adjusted by reducing the existing error (E) between the output values obtained by the network ($\hat{y}_i$) and the actual ones (y_i). In each epoch, the values of the synaptic weights and biases are updated (Camarena-Martinez et al., 2021).

$$E = \frac{1}{n}\sum_{i=1}^{n}(\hat{y}_i - y_i)^2 \qquad \text{Eq. (2.3)}$$

The algorithm starts with randomly assigned values for the synaptic weights and bias. Each iteration involves adjusting the previous synaptic weight value by adding a variable increment, which can be positive or negative, determined by the delta rule (Zupan & Gasteiger, 1993; Abraham, 2005), as expressed in Eq. (2.4):

$$w_{ji}^{l}(t) = w_{ji}^{l}(t-1) + \Delta w_{ji}^{l}(t); \qquad \Delta w_{ji}^{l}(t) = \eta\frac{\partial E}{\partial w_{ji}} + \mu\Delta w_{ji}^{l(previous)} \qquad \text{Eq. (2.4)}$$

Where t represents each iteration, j, i are the nodes of each layer l, w_{ji}^{l} the synaptic weight, E the average of total squared errors, η is the learning rate and μ the momentum coefficient. The learning rate determines the step magnitude during weight adjustment; a high learning rate value causes oscillations and slow convergence and conversely, if the learning rate is too low, it necessitates a large number of iterations. The momentum coefficient modifies the weight value of the previous iteration to decrease the error of the current value; a large momentum

value increases the probability of overshooting the intended solution, while a very small value results in sluggish training. A properly value of η and μ aims to obtain a successful training and speed learning of the neural network (Abraham, 2005) The same procedure is applied to the bias values.

As an analysis is performed at each epoch, the activation function plays a crucial role in estimating the results. The function modifies the combined weighted sum of all incoming signals to a neuron in order to determine the intensity of its firing (Basheer & Hajmeer, 2000). Different activation functions are available, such as the sigmoidal logistic function, the hyperbolic tangential function, or the Rectified Linear Unit function (ReLU) (refer to Figure 2.14). While the first two functions are widely applicable, they lack symmetry with the central coordinate axis (zero axis). Glorot et al. (2011) suggest that the ReLU function is preferred as it is one-side antisymmetric, leading to zero response for an opposite real input.

Sigmoidal logistic function

$$f_1(x) = \frac{1}{1 + \exp(-x)}$$

Hyperbolic tangential function

$$\tanh(x) = 2\sigma(2z) - 1$$

ReLU function

$$g(z) = \max\{0, z\}$$

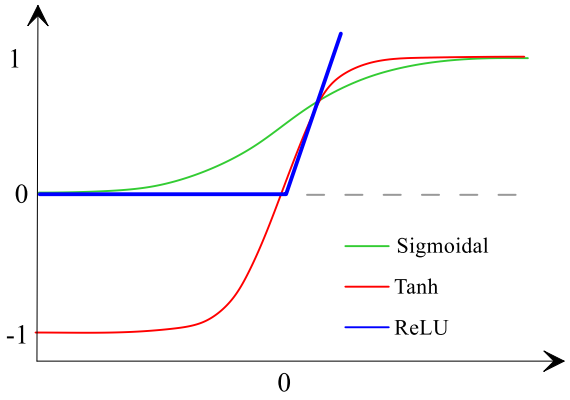

Figure 2.14 – Activation function representation and formulation.

2.7.3 PROBLEMS AND OPTIMISATION

As described above, the training phase of the network allows the model to be calibrated to obtain the smallest possible error between the actual and predicted values by adjusting its statistical parameters. It is possible to obtain good results in the training phase for a given amount of data. However, the result may be limited to only that information, generating errors when values different from those already generalised or memorised are introduced; this type of error is known as *overfitting*. In the opposite case, *underfitting* when there is not enough information to correlate the data (Haykin, 1999; Shahin et al., 2008; Géron, 2019).

The developed model needs to be checked for generalisation errors. To achieve this, a testing phase is included, therefore, the ANN analysis process is based on two phases. The first phase corresponds to the learning or training of the network, and the second phase involves checking the model. The final values of synaptic weights and bias defined during training are used in the testing phase. To perform the analysis, the data needs to be split into training and testing sets. A commonly used training/test ratio is 70/30% or 80/20%, respectively (Jeremiah et al., 2021), but it is necessary to verify the size of the database to determine the appropriate ratio (Géron, 2019).

The training phase can be further subdivided into estimation and validation, which is known as *cross-validation* in statistics. Various combinations of validated estimation models are developed to choose the best-performing one. During the cross-validation technique, the error value generated by the model can be assessed. The best model selection will occur when the validation set error starts to increase, as represented in Figure 2.15 (*Early Stopping Method*) (Haykin, 1999; Silva et al., 2016).

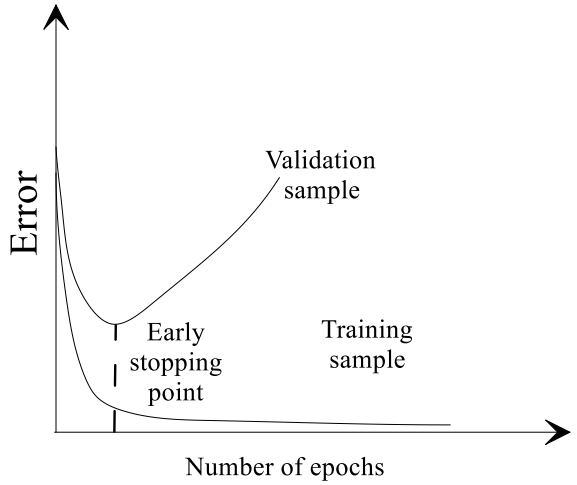

Figure 2.15 – Early stopping rule based on cross-validation (Haykin, 1999).

Another way to control the probability of overfitting in the model is to perform hyperparameter regularisation. In ML, the input parameters used during training control part of the learning, analysis and the outcome to be predicted. However, certain algorithm parameters remain constant during the training phase. These parameters are known as hyperparameters, which can be optimised to reduce effort and improve the performance of the applied algorithm (Hutter et

al., 2019). Optimisation allows for finding the parameter(s) that help to minimise a desired function (Das & Suganthan, 2011).

According to Bilal et al. (2020), optimisation algorithms are related to metaheuristics and can be separated into two categories. These algorithms may resolve complex problems that classical gradient-based methods cannot solve and are listed as follows.

- *Neighbourhood-based Algorithms*: algorithms based on the search for target improvement using neighbouring solutions. The most well-known algorithms are Simulated Annealing and Tabu Search.
- *Population-based Algorithms*: These are algorithms based on solutions inspired by natural population behaviour. Within this category, there are two subcategories known as Swarm Intelligence (SI), where the socio-cooperative behaviour of insects and other animals defines the analysis actions; the algorithms Ant Colony Optimization, Particle Swarm Optimization (PSO), Artificial Bee Colony Optimization, Firefly Algorithm and Cuckoo Search, correspond to examples of this group. Evolutionary Algorithms (EA) correspond to techniques based on the theory of the evolution of species; it is possible to find algorithms such as Evolutionary Programming, Genetic Algorithm (GA), Genetic Programming, Evolutionary Strategies and Differential Evolution (DE).

2.8 ANN IN CIVIL ENGINEERING

This section shows a brief compilation of papers that focused on the application of AI in Civil Engineering (specifically ANN), highlighting its use in Geotechnical Engineering and geosynthetics behaviour.

AI has attracted interest in many professional fields due to its versatility, simplicity of application and ability to solve complex problems from existing data results. One of the first authors to compile publication records on AI in Civil Engineering was Sriram in 1984, who presented a series of titles related to architecture, civil engineering and geology using the Knowledge-Based Expert Systems (KBES) methodology. Afterwards, other authors published state-of-the-art research compiling the application of IA in civil engineering, showing a high interest in analysis and problem-solving (Reich, 1997; Adeli, 2001; Lu et al., 2012; Shahin,

2013; Salehi & Burgueño, 2018; Dede et al., 2019; Huang et al., 2019; Lagaros & Plevris, 2022).

2.8.1 ANN IN STRUCTURAL ENGINEERING

One of the main phases prior to construction is good structural analysis and design. For this reason, ANNs have been used to predict the behaviour of structural elements and materials. For instance, Vanluchene & Sun (1990) implemented a BP-ANN to solve three types of complex problems, the establishment of recognition patterns for load location problems, the definition of the cross-section of reinforced concrete beams and the analysis of bearing plates.

ANN has been used in different solutions, such as defining the design of structural element sections (Messner et al., 1994; Kim et al., 2000), damage and crack detection (Theocaris & Panagiotopoulos, 1993; Yeh et al., 1993; Hegazy et al., 1998; Chatterjee et al., 2017), structural element and material behaviour prediction (Abdalla & Stavroulakis, 1995; Anderson et al., 1997; Mukherjee et al., 1996; Yun & Bahng, 2000; Cascardi et al., 2017; Yan et al., 2017; Naderpour et al., 2018; Barbosa & Evangelista Jr, 2020; Chaves, 2021), assessment of dynamic response (Masri et al., 1993; Adeli & Park, 1995; Huang & Loh, 2001), computational tools for structural analysis like finite elements and BIM (Manevitz et al., 1997; Pain et al., 1999; García-Segura et al., 2017).

Other studies related to construction engineering are presented by Adeli (2001) and Huang et al. (2019).

2.8.2 ANN IN ENVIRONMENTAL ENGINEERING AND WATER RESOURCES

ANNs have also been used to predict and classify features related to environmental conditions and water sources' behaviour. For example, Karunanithi et al. (1994) applied ANNs to predict river streamflow of the Huron River at the Dexter sampling station, showing that ANN model leads to describes the changes in the flow history. Other related applications include predicting pollution and production of toxic waste, presented by Grubert (1995), Kao & Liao (1996), Crespo & Mora (1995), and Shang et al. (2004). Additional studies on hydrological phenomena using ANN are presented by Deo & Rao (1997), Gangopadhyay et al. (1999), Liong et al. (2000), Govindaraju & Rao (2000), Guo (2001).

2.8.3 ANN IN TRANSPORT ENGINEERING

Traffic studies and road design (including paving) are necessary to build highways. ANN has also been widely used in analysing these types of studies. In traffic studies, for example, Cheu & Ritchie (1995) used three types of ANN to identify incident patterns in traffic data, and Lingras & Adamo (1996) successfully estimated average and peak hour traffic volumes using ANN.

ANN has also been applied for road design and paving, including pavement condition assessment (Owusu-Ababio, 1998; Attoh- Okine, 2001; Zaman et al., 2010; Sadrossadat et al., 2016; Hanandeh et al., 2020).

2.8.4 ANN IN GEOTECHNICS

A geotechnical study involves various exogenous and endogenous conditions of earth materials with physical, mechanical and chemical characteristics of greater complexity than other construction materials (Baghbani et al., 2022). AI techniques have established themselves as valuable tools for solving geotechnical problems. As shown previously, various AI techniques are based on the type of output required. However, ANN remains the most widely used methodology in different investigations.

Phoon & Zhang (2022) presented the results of a survey conducted in 2021 by ISSMGE TC304/309 on 444 papers using ML for different geotechnical applications. The survey results showed that 43% of the papers were developed using supervised training, where the ANN algorithm had been the most applied (120 of the 444 papers). Site characterisation and slope stability were the most researched topics. Figure 2.16 shows graphically the results obtained in the survey.

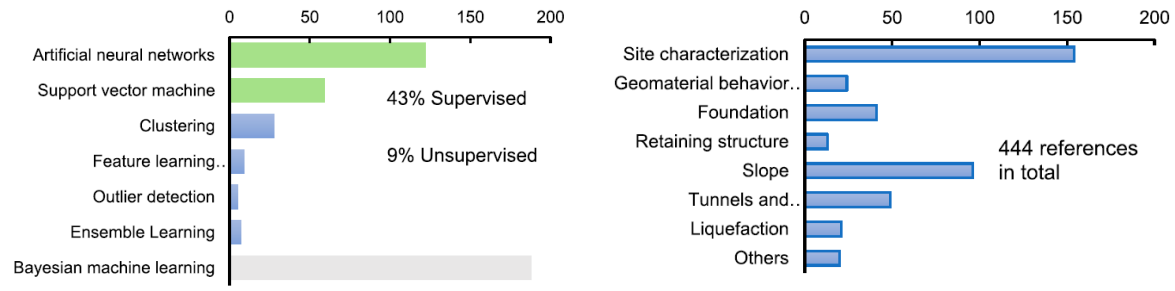

Figure 2.16 – ML algorithms (left) and applications in geotechnics (right) surveyed by ISSMGE TC304/309 (Phoon & Zhang, 2022).

In the study entitled "35 Years of (AI) in Geotechnical Engineering: State of Art" by Ebid (2021), 626 papers published from 1984 to May-2019 on the application of AI to the evaluation of geotechnical techniques were collected. The author concluded that soil properties were the major interest topic among the compiled papers. In addition, the authors found that ANN was the most widely used methodology within the AI techniques (approximately 48%). Figure 2.17 shows the relationship between the geotechnical characteristics and the AI technique used in the articles.

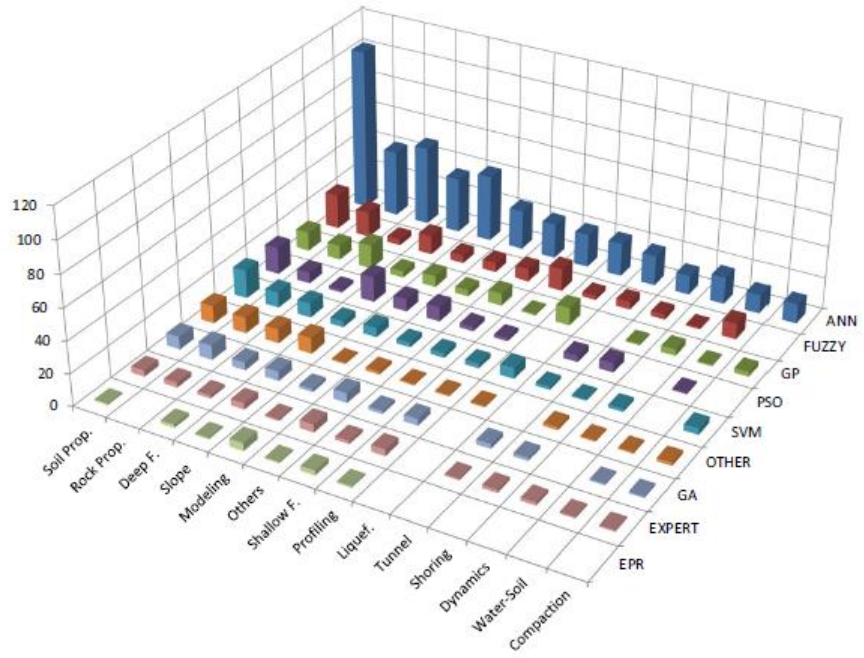

Figure 2.17 – Number of researches classified by Subject and AI Technique (Ebid, 2021).

Baghbani et al. (2022) surveyed a review of articles published in journals and books prior to 2021, in which IA methods were applied in 9 geotechnical categories (frozen soils and thermal soil properties, rock mechanics, subgrade and pavement soil, landslides and liquefaction, slope stability, shallow and deep foundations, tunnels and tunnel boring machines (TMB), dams, and unsaturated soils). The statistical analysis of the collected data showed that among the nine topics mentioned, the study of mechanical rock properties, landslides and liquefaction, and TMB were the most investigated, as seen in Figure 2.18. The results also showed that the most widely implemented technique is ANN compared to other AI techniques. However, in recent years there has been most interest in other types of algorithms (see Table 2.4), where the percentage of ANN applications has decreased.

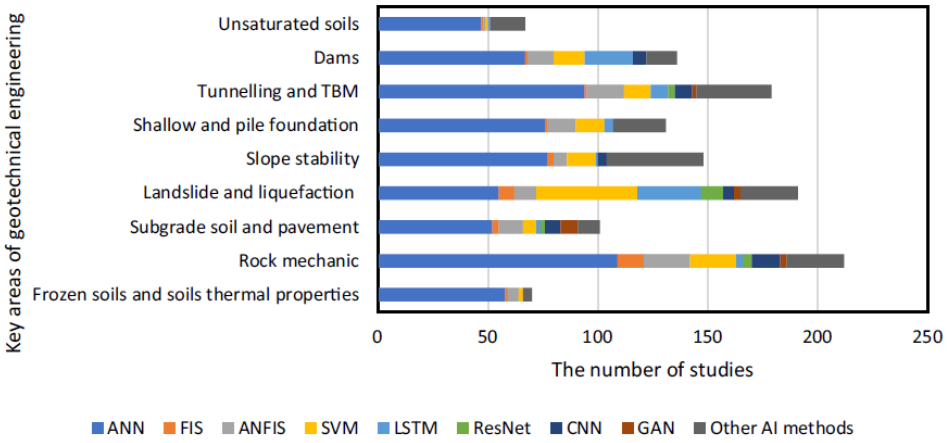

Figure 2.18 – Distribution of IA use in 9 categories in geotechnics (Baghbani et al., 2022).

Table 2.4 – ANN application percentage in different periods (Baghbani et al., 2022).

Time period	Application of artificial neural network (ANN) (%)								
	Pavement & subgrade soil	Frozen soils	Slope stability	Landslide & liquefaction	Foundation Shallow & Piles	Dam	Rock mechanic	Tunneling &TBM	Unsaturated soils
Till 2010	60.00	62.50	63.33	69.57	75.00	73.68	74.07	88.24	84.21
2011-2015	53.85	69.23	34.15	51.43	50.00	70.83	45.45	64.10	62.50
2016-2020	48.94	77.14	46.25	28.89	56.06	57.50	54.17	40.66	54.29

As shown above, ANNs have been adequately used for geotechnical engineering problems, where soil characterisation is the topic of major interest (Cal, 1995; Basheer et al., 1996; Chang, 2000; Caglar & Arman, 2007; Boadu et al., 2013; Jeremiah et al., 2021). Table 2.5 shows other interesting topics in geotechnical engineering where ANN models were implemented.

Table 2.5 – Geotechnical engineering topics with ANN application.

Topic	**Authors**
Load and capacity behaviour in foundations	(Kiefa, 1998; Rahman et al., 2001; Hanna et al., 2004; Ahmad et al., 2007; Kalinli et al., 2011; Shahin, 2016; Pooya Nejad & Jaksa, 2017; Alzo'ubi & Ibrahim, 2019; Alzo'Ubi & Ibrahim, 2021; Bagińska & Srokosz, 2019; Pham et al., 2020)
Retaining structures	(Goh et al., 1995; Shahin & Jaksa, 2005; Kung et al., 2007; Bekdaş & Temür, 2018; Ghaleini et al., 2019)
Prediction of liquefaction effects in soil	(Young-Su & Byung-Tak, 2006; Hanna et al., 2007; V. Kumar et al., 2012; Erzin & Ecemis, 2015)

Table 2.6 – Geotechnical engineering topics with ANN application (Continued).

Topic	**Authors**
Prediction of foundation settlement	(Shahin et al., 2002, 2005; Soleimanbeigi & Hataf, 2006; Hasanipanah et al., 2016; Chen et al., 2019)
Application in expansive soils	(Erzin, 2007; Ikizler et al., 2010; S. K. Das et al., 2010; Bekhor & Livneh, 2014; Salahudeen et al., 2020)
Slope stability	(Mayoraz & Vulliet, 2002; Ermini et al., 2005; Ferentinou & Sakellariou, 2007; Chauhan et al., 2010; Aleshin & Torgoev, 2013; J. A. Abdalla et al., 2015; Aghajani et al., 2015; Yi et al., 2022)
Rock mechanics	(Lee & Sterling, 1992; Bahrami et al., 2011; Enayatollahi et al., 2014; Leite, 2019)
GIS in geotechnics	(Lee et al., 2003, 2006; Bhardwaj & Venkatachalam, 2014; Aditian et al., 2018)

Nonetheless, the different literature studies do not refer to the application of ANN to evaluate geosynthetic behaviour. Therefore, some of the research carried out in this field is mentioned below.

Abuel-Naga & Bouazza (2014) derived empirical equations from a General Method of Data Handling (GMDH) ANN to predict the liquid leakage rate across the GM/GCL interface with a circular and longitudinal defect in the GM and free drainage. Data for network analysis were obtained from numerical methods. The results achieved from the proposed equations were satisfactory when compared to both numerical outcomes and other practical equations.

Similarly, Kumari & Dutta (2019) used an ANN (4-3-1 architecture) for leakage rate prediction in a barrier composed of compacted clay and defective geomembrane (in three types of shapes: square, rectangular and circular). One hundred sixty-five (165) literature data were used for training and testing the network. The authors applied different activation functions, finding that the best prediction was achieved with the sigmoidal one. From the ANN, they established an equation with better results than other models presented in the literature. Figure 2.19 compares ANN results concerning other empirical equations reported by Giroud et al. (1992) and Giroud and Bonaparte (1989). In both comparison cases, the R^2 values of ANN are significantly

different from those obtained by the empirical equations, with the results obtained by the ANN model being more accurate.

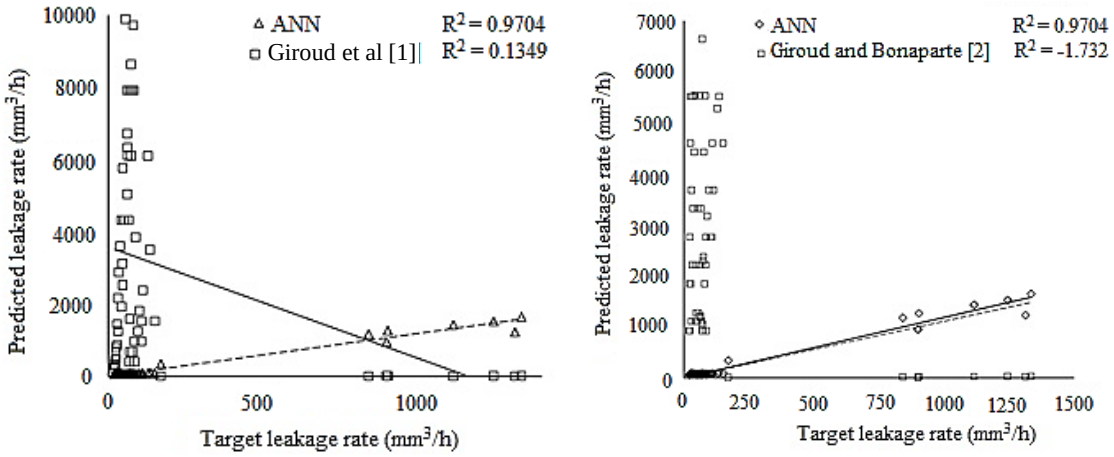

Figure 2.19 – Comparison of ANN and empirical models reported by Giroud et al (1992) and Giroud and Bonaparte (1989) (Kumari & Dutta, 2019).

Qadir et al. (2020) used ANNs to predict the behaviour of geosynthetics as reinforced for asphalt concrete pavements. A multilayer network (MLFNN) and radial-based network (RBNN) were utilised to predict flexural stiffness and rutting depth values of reinforced asphalt pavements using Marshall test design and rut depth parameters, respectively. Both models achieved a good accuracy for parameter estimation despite the small samples quantity. The results were employed for designing purposes without carrying out high-tech testes.

Raja & Shukla (2021) used an artificial neural network (ANN) along with the grey wolf optimisation (GWO) algorithm to forecast soil settlement in foundations reinforced with geosynthetics. They used a dataset of 475 samples with 9 input parameters derived from a 3D finite element model. The predicted values were compared to reference studies and assessed using statistical metrics such as RMSE, MAE, MAPE%, R^2, and refined Willmott index. Due to the high precision of the predicted values, they derived a final equation to estimate the maximum settlement value in reinforced soil foundations supporting service loads.

The prediction for the pullout coefficient in geogrids was studied by Pant & Ramana (2022) using four different ML techniques including RF, Multivariate Adaptive Regression Splines, MLP and Decision Tree. A dataset of 198 samples from the literature was implemented in the different models, which were split into training and testing phases in an 80/20 ratio. The

accuracy of the models was evaluated using statistical metrics (R^2, MSE and MAPD%), finding the RF as the most precise algorithm and recommended for practical use.

Raja et al. (2022) compared the results of eight ML methodologies (including ANN) used to predict CBR values in geosynthetic reinforced soil subgrade (GRS) based on 97 data obtained from the literature with 11 parameters of each sample. The dataset was divided into 60% for training and 40% for testing. The models were evaluated using R^2, RMSE, Scatter index, Index of agreement, MAE and external validation, where Lazy K-star (LKS) and ANN were the most accurate models. Considering the high accuracy of the ANN results, an equation for CBR estimation was implemented.

Amjad Raja et al. (2023) employed artificial intelligence (AI) techniques to predict the load-settlement behavior of geosynthetic-reinforced soil. The researchers utilized the Harry Hawk optimization (HHO) algorithm to optimize artificial neural network (ANN) models and compared the results with other regression methods such as SVR, Gaussian process regression, relevance vector machine, sequential minimal optimization regression, and least-median square regression. The dataset used for training and testing consisted of 354 data points obtained from finite difference modelling (FDM). The ANN architecture included a 9-input layer, one hidden layer with four neurons, and a one-output layer. Six statistical indexes were used to evaluate the accuracy of the models, and the ANN-HHO model was found to be the most precise for both training and testing phases. Finally, the model outcomes were transformed into a simple mathematical equation, which can be easily utilized in the initial design of geosynthetic-reinforced soil (GRS) abutments.

The following research works are presented, utilizing ANN to forecast the behavior of interface strength with geosynthetics.

Debnath & Dey (2017) used an MLP-type neural network model with a hidden layer to predict clay-geosynthetic interface behaviour. Three different numbers of hidden layer neurons (4, 10 and 15) were selected according to the mean squared error (MSE) as presented in Figure 2.20.

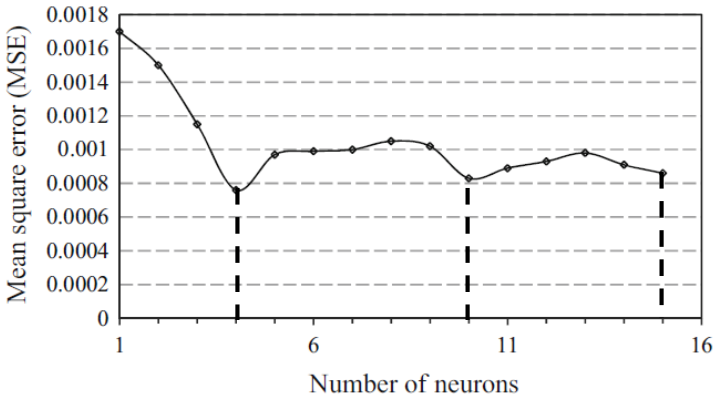

Figure 2.20 – Relationship between the number of neurons and MSE (Debnath & Dey, 2017).

The database was obtained from literature references for six influencing factors (input parameters). The data were split in a 70/30% ratio for training/testing. Three learning algorithms (Bayesian regularization, Levenberg-Marquardt and Scaled conjugate gradient) were compared. Five statistical evaluation criteria were employed to assess model performance (R^2, MSE, MAPE, MEDAE and VARE). The results showed a good accuracy of the implemented ANN models for resistance prediction. The 4-neuron network with Bayesian Regularization type algorithm was the most accurate model, as shown in Table 2.6.

Table 2.6 – Statistical errors of different models for predicting PSS (Debnath & Dey (2017).

ANN model		**Statistical errors**				
Learning algorithms	**No. of hidden nodes**	**R^2**	**MSE**	**MAPE**	**VARE**	**MEDAE**
Bayesian regularization	4	0.988	1.48	3.31	1.27	0.60
	10	0.986	2.21	3.81	1.81	0.602
	15	0.984	2.45	3.82	2.35	0.606
Levenberg-Marquardt	4	0.964	5.46	7.31	5.52	1.42
	10	0.960	7.48	8.00	6.21	1.73
	15	0.871	23.52	11.72	10.72	2.34
Scaled conjugate gradient	4	0.977	6.47	3.88	2.09	0.64
	10	0.954	7.73	8.21	6.42	1.49
	15	0.973	3.58	6.18	5.18	1.31

Chao et al. (2021) used five ML techniques to evaluate peak shear strength between soil-geocomposite interfaces (GDL). The models utilized were the Back Propagation Artificial Neural Network (BPANN), the Support Vector Machine (SVM) optimized by Particle Swarm Optimisation (PSO) and Genetic Algorithm (GA) algorithms, respectively, and Extreme Learning Machine (ELM) optimized with Exhaustive Method algorithm. The database was

obtained from 209 direct shear test results. Five statistical criteria were used to define the accuracy of the models, with the BPANN-PSO algorithm being the most accurate, as shown in Table 2.7. According to the sensitivity analysis results, normal stress had the greatest impact among the nine influence factors, with a 17.91% of influence (see Figure 2.21).

Table 2.7 – R^2 values of the models for training and testing dataset (Chao et al. (2021).

Phase	**GA-BPANN**	**PSO-BPANN**	**GA-SVM**	**PSO-SVM**	**ELM**
Training	0.95	0.95	0.90	0.92	0.90
Testing	0.87	0.93	0.86	0.86	0.79

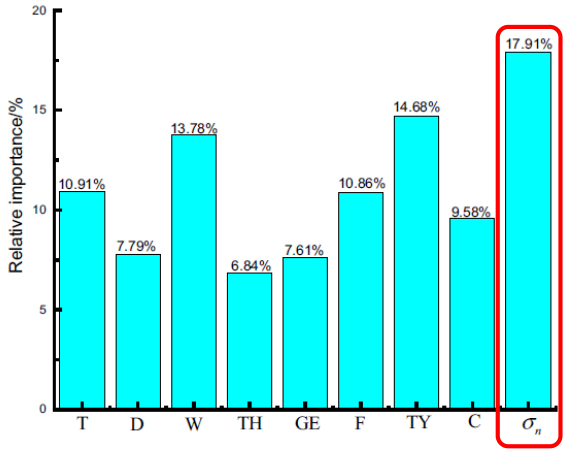

Figure 2.21 – Relative importance of the input parameters (Chao et al. (2021).

Chao et al. (2023) coupled a model using Mind Evolutionary (MEA) methodology and the Adaptive Boosting – Back Propagation Algorithm (ADA-BPANN) for shear strength prediction at clay-geomembrane interfaces, obtaining high accuracy. The method was compared with 4 ML techniques (PSO-ADABPANN, GA-ADABPANN, MEA-SVM and Random Forest - RF), validating that its results were better than the other techniques as shown in Figure 2.22, where the ADA-BPANN has the lowest RMSE values for training and testing dataset. A total of 623 direct shear laboratory test results at clay-geomembrane interfaces were used for the analysis. As in the previous work, the sensitivity analysis showed that the normal stress corresponds to the factor with the highest impact within the five input parameters.

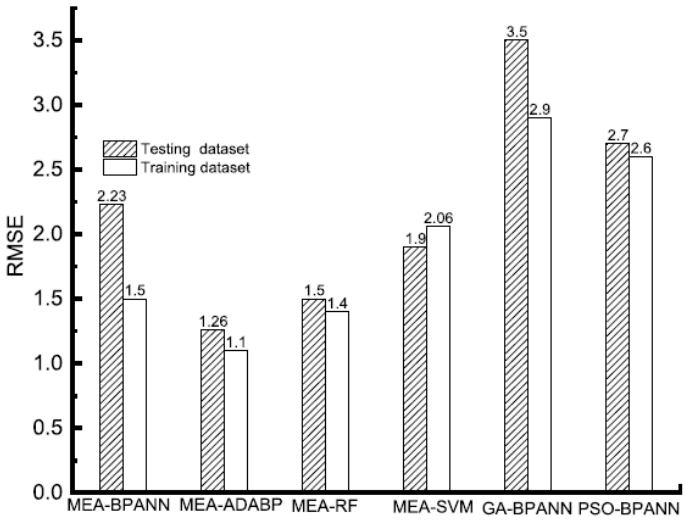

Figure 2.22 – RMSE value of the models (Chao et al. (2023).

3 METHODS

In this study, the methodology to evaluate the use of ANN as a sand/GM interface strength prediction tool consists of three stages, (i) data collection, (ii) definition of the ANN model and (iii) evaluation of the model, as shown in Figure 3.1. The model's performance depends on the amount and the limit values of the collected data and the category of use (in this case, prediction). Statistical analysis is also used to validate the results by comparing the actual values to those predicted by the model. The Python® programming language, developed by the Python Software Foundation, was used to implement the analysis algorithm codes. These codes were executed in the *Machine Learning* module available in the software produced by Tyche (2020) from the University of Brasilia. The module was successfully utilized in another studies for prediction purposes (Chaves, 2021; Tanga, 2022; Chaves et al., 2023; Lima et al., 2023).

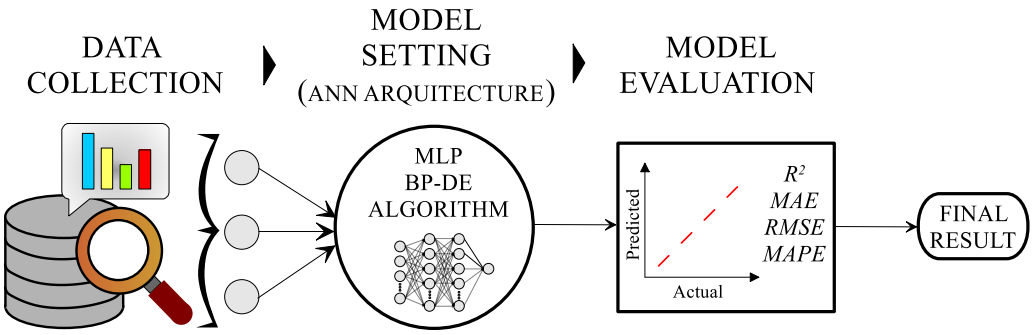

Figure 3.1 – Methodology outline.

3.1 DATA COLLECTION

Applying ANN is profitable for solving problems based on learning input and output data (Shahin, 2013). The larger the number of input variables, the larger the size of the network and, consequently, the longer the processing time required (Lachtermacher & Fuller, 1994). However, many variables can also improve network performance (Shahin et al., 2008). In this investigation, an MLP-ANN is used to predict sand/GM interface strength parameter (friction angle).

The first stage consisted of a search for laboratory test results to evaluate the interface shear strength between the sand and geomembranes from the literature, published in international journal articles, thesis and dissertations. For each collected study, the description of the interface friction angle, the characteristics of the test type and materials used were verified to

establish the input parameters and output values (supervised training). In total, 453 data were collected from the literature. In addition, a Brazilian manufacturer company provided more 35 data, resulting in a total of 488 samples for training and validation of the ANN model. Table 3.1 presents the general information for each study used as input data.

Table 3.1 – General input data information.

Study/Paper title	**Author(s)**	**No. collected data**	**General description**	**Country**
Shear Strength characteristics of sand-polymer interfaces	O'Rourke et al., 1990	12	CDS test: smooth HDPE and PVC GM type with Ottawa sand	USA
Interfacial friction study of cap and liner components for landfill design	Koutsourais et al., 1991	20	MDS test: 5 types of GM with Chatahooche river medium sand	USA
Geomembrane - sand interface friction	Izgin, 1997	195	CDS test: rough and smooth GM with crushed stone and Ottawa sand IP test: four types of GM with two types of crushed stone sand and Ottawa sand	Turkey
Study of soil-geosynthetic interaction in environmental protection works using an inclined plane equipment (in Portuguese)	Lima Junior, 2000	12	IP test: two types of GM with coarse grained sand	Brazil
Study of soil-geosynthetic interaction in waste disposal slope works (in Portuguese)	Mello, 2001	15	IP test: three types of GM with fine grained sand	Brazil
Study of soil-geosynthetic interaction through inclined plane shear tests (in Portuguese)	Costa e Lopes, 2001	6	IP test: smooth and rough GM with two types of sand	Portugal

Table 3.1 – General input data information (Continued).

Study/Paper title	Author(s)	No. collected data	General description	Country
Interaction between soils and geosynthetic layers in large-scale ramp tests	Palmeira et al., 2002	15	IP test: three types of GM with fine and coarse grained sand	Brazil
Interface strength between geomembranes and soils through Ring Shear test (in Portuguese)	Rebelo, 2003	15	MDS test: 5 types of GM with coarse to medium grained sand	Brazil
Study of stability and hydraulic conductivity of conventional and alternative lining systems for waste disposal sites (in Portuguese)	Viana, 2007	9	IP test: smooth and textured GM with coarse and fine to medium grained sand	Brazil
Microscale Geomembrane-Granular Material Interactions	David Frost et al., 2012	17	CDS test: one smooth and two textured GM types, with Ottawa 20/30 and blasting sand	USA
Frictional behaviour of three critical geosynthetic interfaces	Bacas et al., 2015	6	MDS test: two textured GM with fine grained sand	Spain
Shear behavior of sand-smooth geomembrane interfaces through micro-topographical analysis	Vangla & Gali, 2016	15	MDS test: smooth GM with 5 type of sand	India
Effect of time on soil-geommebrane interface shear strength	Alzahrani, 2017	6	MDS test: smooth and textured GM with Ottawa 20/30 sand	USA
Study of some aspects that influence the adhesion between geosynthetics and different materials (in Portuguese)	Sánchez, 2018	45	CDS, MDS and IP test: 4 types of textured GM and 1 type of smooth GM, with medium-grained sand	Brazil
Laboratory investigation of shear behavior of High-Density Polyethylene Geomembrane interfaces	Cen et al., 2018	16	MDS test: smooth and textured GM with fine sand and sandy gravel	China

Table 3.1 – General input data information (Continued).

Study/Paper title	Author(s)	No. collected data	General description	Country
Global and local sand–geosynthetic interface behavior	Lashkari & Jamali, 2021	49	CDS test: one type of GM with six types of sand	Iran
Company laboratory test results	Manufacturer company	35	MDS test: one type of GM with remolded and silty sand	USA

The samples were chosen based on similar influencing factors, and a set of twelve (12) parameters were selected to describe them: displacement rate, applied normal stress, contact area, GM thickness, GM asperity height, sand density index, sand unit mass, coefficient of curvature, uniformity coefficient, median grain size, soil friction angle and type of test implemented (CDS, MDS or IP). Table 3.2 shows the relationship between the input and output parameters, as well as the corresponding amount of collected data.

Table 3.2 – Data quantity on influence parameters.

Sym.	Parameter	Data quantity	Sym.	Parameter	Data quantity
Input					
D_r	Displac. rate (mm/min)	437	ρ	Unit soil mass (g/cm³)	401
τ	Normal stress (kPa)	488	*Cc*	Coefficient of curvature	372
C.A.	Contact area (cm²)	488	*Cu*	Uniformity coefficient	447
t	GM thickness (mm)	451	D_{50}	Median grain size (mm)	422
A_h	GM asperity h (mm)	291	ϕs	Friction angle of soil (°)	431
I_d	Sand density index (%)	253		Type of test	488
Output					
δ'	Friction angle interface (°)	488			

Values outside the mean of the data (outliers) were eliminated to avoid overfitting errors during the ANN training phase. A final value of 428 useful samples for the analyses was defined. The parameters with missing values were completed using the mean of the remaining data.

3.1.1 NORMALISATION

Data normalisation helps to define more uniform values by decreasing the probability of overriding smaller ones, and avoiding information saturation at the network nodes (Basheer & Hajmeer, 2000). There is no specific equation to develop a normalisation process. However, in this study a max-min normalisation was used as expressed by the Eq. (3.1).

$$X_{norm} = \frac{X_i - X_{min}}{X_{max} - X_{min}} \qquad \text{Eq. (3.1)}$$

Where X_{norm} is the normalised value of X_i, and X_{min} and X_{max} are the minimum and maximum values of X_i in the database.

3.1.2 DATA CORRELATION - PEARSON'S CORRELATION COEFFICIENT (ρ_r)

Pearson's correlation coefficient was used to establish both relationship and influence of the input parameters in relation to the output value. The ρ_r, discovered by Bravais in 1846 but described by Karl Pearson fifty years later (Hauke & Kossowski, 2011), allows establishing the monotonic linear relationship between two continuous and random variables.

The coefficient between two variables can be determined according to Eq. (3.2), obtaining results ranging from -1 to 1, where values closer to ±1 show a stronger correlation (the sign represents whether the variables are inversely or directly proportional). Table 3.3 sets out some ranges of interpretation for the ρ_r.

$$\rho_r(a,b) = \frac{cov(ab)}{\sigma_a \sigma_b} \qquad \text{Eq. (3.2)}$$

Where cov represents the covariance between variables and σ the standard deviation of each variable.

Table 3.3 – Example of a conventional approach to interpreting a correlation coefficient (Schober et al., 2018).

Absolute magnitude of the observed correlation coefficient	Interpretation
0.00 – 0.10	Negligible correlation
0.10 – 0.39	Weak correlation
0.40 – 0.69	Moderate correlation
0.70 – 0.89	Strong correlation
0.90 – 1.00	Very strong correlation

3.2 ANN – MODEL SETTING

A feedforward MLP network with a backpropagation (BP) learning algorithm was implemented for the analysis. The Differential Evolution (DE) algorithm was coupled to perform hyperparameter optimisation (HPO) of the network.

3.2.1 NETWORK ARCHITECTURE

The MLP network architecture is divided into three main layers: input, hidden layer and output (Abraham, 2005). The number of neurons in the input and output layers is determined by the influential parameters and the result to be predicted, respectively. However, the definition of the number of hidden layers and neurons is more complex, and is established through trial and error based on statistical criteria (Shahin et al., 2008; Priyadarshee et al., 2020). Implementing many hidden layers allows for a better statistical analysis of the data, but it can lead to longer training times and a higher probability of overfitting. Hecht-Nielsen, (1989) suggests that a single hidden layer is sufficient, while Lapedes & Farber, (1989) points out that two hidden layers give good results in the analysis.

The present study implemented multiple combinations of one- and two-hidden layer networks with different numbers of neurons. The optimal network selection was defined using the coefficient of determination (R^2) according to the analysis results obtained in the Backpropagation - Differential Evolution (BP – DE) training and optimisation algorithm. Figure 3.2 schematically represents the implemented artificial neural network. The input layer includes the influencing parameters (the Test Type parameter encompasses three types: CDS, MDS, and IP). The hidden layers can be one or two with a variable number of neurons. The output layer represents the predicted interface friction angle.

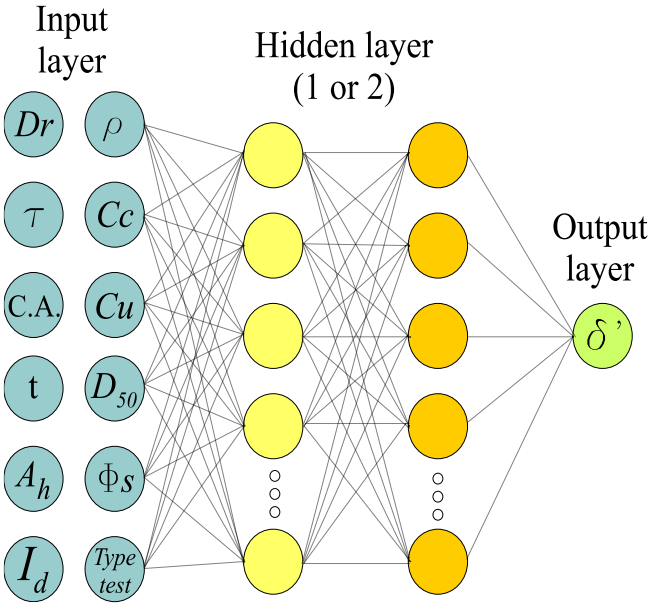

Figure 3.2 – ANN schematic model.

3.2.2 TRAINING ALGORITHM – BACK PROPAGATION

The Backpropagation learning algorithm coupled with the Differential Evolution (BP – DE) algorithm was applied for the training phase to optimise the hyperparameters.

As mentioned in the previous chapter, the BP algorithm works by iterative analysis (epochs) until the lowest error between the actual and predicted network values is found. Haykin (1999) cites the following mathematical formulation for the BP algorithm.

Eq. (3.3) is used to estimate the error signal $e_j(t)$ between the desired response $d_j(t)$ for a neuron j (output node) and the predicted output value $y_j(t)$ for the same neuron j, both at the same iteration t.

$$e_j(t) = d_j(t) - y_j(t) \qquad \text{Eq. (3.3)}$$

The error energy ξ for a neuron j can be obtained from Eq. (3.4). Therefore, the sum of all neurons in the same layer $\xi(t)$ is given by Eq. (3.5).

$$\xi(j) = \frac{1}{2} e_j(t)^2 \qquad \text{Eq. (3.4)}$$

$$\xi(t) = \frac{1}{2}\sum_{j=C} e_j(t)^2 \qquad \text{Eq. (3.5)}$$

Where C corresponds to the number of neurons in the network layers. Eq. (3.5) calculates the total error energy for an iteration n. Then, for all N iterations presented in the training phase, the average error energy ξ_{av} is determines by Eq. (3.6).

$$\xi_{av} = \frac{1}{N}\sum_{n=1}^{N} \xi(t) \qquad \text{Eq. (3.6)}$$

All the error energy is function of synaptic weights and bias levels (free parameters). Thus, the main goal of every single epoch is to find the most accurate free parameter values to reduce the average error network ξ_{av}.

For each predicted output value $y_j(t)$ of a neuron j, there is m number of input values of the previous layer output $y_i(t)$. Hence, $y_j(t)$ is evaluated by Eq. (3.7) as the total interaction between the synaptic weights w_{ji} and the input values $y_i(t)$ activated by a function f.

$$y_j(t) = f\left(\sum_{i=0}^{m} w_{ji}(t)y_i(t)\right) \Rightarrow y_j(t) = f\left(v_j(t)\right) \qquad \text{Eq. (3.7)}$$

The synaptic weight correction $\Delta w_{ji}(t)$ can be expressed as the partial derivate of $\xi(t)$ for the synaptic weight $w_{ji}(t)$ as described in Eq. (3.8).

$$\frac{\partial \xi(t)}{\partial w_{ji}(t)} = \frac{\partial \xi(t)}{\partial e_j(t)}\frac{\partial e_j(t)}{\partial y_j(t)}\frac{\partial y_j(t)}{\partial v_j(t)}\frac{\partial v_j(t)}{\partial w_{ji}(t)} \qquad \text{Eq. (3.8)}$$

Eq. (3.9) to Eq. (3.12) represents the result of each part of the derivate. Therefore, substituting each part of the derivate, Eq. (3.8) can be reduces to Eq. (3.13).

$$\frac{\partial \xi(t)}{\partial e_j(t)} = e_j(t) \qquad \text{Eq. (3.9)}$$

$$\frac{\partial e_j(t)}{\partial y_j(t)} = -1 \qquad \text{Eq. (3.10)}$$

$$\frac{\partial y_j(t)}{\partial v_j(t)} = f'\left(v_j(t)\right) \qquad \text{Eq. (3.11)}$$

$$\frac{\partial v_j(t)}{\partial w_{ji}(t)} = y_i(t) \qquad \text{Eq. (3.12)}$$

$$\frac{\partial \xi(t)}{\partial w_{ji}(t)} = -e_j(t) f'\left(v_j(t)\right)\, y_i(t) \qquad \text{Eq. (3.13)}$$

The synaptic weight correction $\Delta w_{ji}(t)$ can be also defined by the delta rule as defined in Eq. Eq. (3.14).

$$\Delta w_{ji}(t) = -\eta \frac{\partial \xi(t)}{\partial w_{ji}(t)} \qquad \text{Eq. (3.14)}$$

Substituting Eq. (3.13) in Eq. (3.14), synaptic weight correction $\Delta w_{ji}(t)$ can be rewritten as Eq. (3.15):

$$\Delta w_{ji}(t) = \eta e_j(t) f'\left(v_j(t)\right)\, y_i(t) \;\Rightarrow\; \Delta w_{ji}(t) = \eta \delta_j(t)\, y_i(t) \qquad \text{Eq. (3.15)}$$

Where, $\delta_j(t)$ represents the local gradient for neuron j and it is directly related to the error signal $e_j(t)$ (Eq. (3.3)) . However, this expression is associated with the output node. For a hidden node neuron, the error signal is determined by considering all the neurons that is directly connected to, redefining the local gradient $\delta_j(t)$ as:

$$\delta_j(t) = -\frac{\partial \xi(t)}{\partial y_j(t)} \frac{\partial y_j(t)}{\partial v_j(t)} = -\frac{\partial \xi(t)}{\partial y_j(t)} f'\left(v_j(t)\right) \qquad \text{Eq. (3.16)}$$

In Eq. (3.16) the superscript j represents a hidden node and the output node will be identified as k. The total error energy $\xi(t)$ can be defined in terms of j, k nodes as presented in Eq. (3.17).

$$\xi(t) = \frac{1}{2}\sum_{k \in C} e_k(t)^2 \qquad \text{Eq. (3.17)}$$

Eq. (3.18) defines the equivalent form of differentiating Eq. (3.17) with respect to the function signal $y_j(t)$ and applying the chain rule.

$$\frac{\partial \xi(t)}{\partial y_j(t)} = \sum_k e_k(t) \frac{\partial e_k(t)}{\partial v_k(t)} \frac{\partial v_k(t)}{\partial y_j(t)} \qquad \text{Eq. (3.18)}$$

It is possible to obtain the partial derivate in terms of the local gradient $\delta_k(t)$ of the output node k by substituting the partial derivate of the error signal $\partial e_k(t)$ for neuron k (Eq. (3.19)) and the input of the activated function $\partial v_k(t)$ for neuron k (Eq. (3.20)).

$$\frac{\partial e_k(t)}{\partial v_k(t)} = -f'_k\big(v_k(t)\big) \qquad \text{Eq. (3.19)}$$

$$\frac{\partial v_k(t)}{\partial y_j(t)} = w_{kj}(t) \qquad \text{Eq. (3.20)}$$

$$\frac{\partial \xi(t)}{\partial y_j(t)} = -\sum_k e_k(t)\, f'_k\big(v_k(t)\big)\, w_{kj}(t) = -\sum_k \delta_k(t)\, w_{kj}(t) \qquad \text{Eq. (3.21)}$$

Finally, the local gradient for a hidden node $\delta_j(t)$ can be determined by replacing Eq. (3.21) in Eq. (3.16) resulting the back-propagation formula of a hidden node j (Eq. (3.22))

$$\delta_j(t) = f'_j\Big(v_j(t)\Big)\sum_k \delta_k(t)\, w_{kj}(t) \qquad \text{Eq. (3.22)}$$

3.2.3 OPTIMISATION ALGORITHM – DIFFERENTIAL EVOLUTION

DE is a heuristic optimisation algorithm developed by Storn and Price in 1996. It is based on the theory of evolution, known as evolutionary computation or Evolutionary Algorithms (EA). Compared to other EA algorithms, DE is characterised by a greater simplicity of implementation and better performance (Vesterstrom & Thomsen, 2004; Das & Suganthan, 2011; Bilal et al., 2020). DE allows the optimisation of nonlinear and non-differentiable functions.

The DE workflow is divided into two main stages: an initialisation and an evolution stage (see Figure 3.3) (Das & Suganthan, 2011; Saleh et al., 2014; Bilal et al., 2020; Atangana Njock et al., 2021). In the initialisation stage, initial data vectors of the hyperparameter to be optimised, represented by a random population (NP), are established. For any generation G, $X_j^G = \{x_{1,j}^G, x_{2,j}^G, \dots, x_{D,j}^G\}$ describes the D-dimensional vector. In a space S^G, X_j^G can be considered uniformly random for the upper and lower bounds as follows:

$$X_j^G = X_{low} + (X_{upp} - X_{low}) * rand(0,1) \quad \text{Eq. (3.23)}$$

Once the population vector has been defined (Eq. (3.23)), the second stage, evolution, is activated. This second phase is divided into three sub-phases, Mutation, Crossover, and Selection, correlated to Eq. (3.24), Eq. (3.25) and Eq. (3.26), respectively.

(i) *Mutation*: where the initial vector is affected by a modifying factor (F) that varies from 1 to 0, generating a new population vector V_j^G.

$$V_j^G = X_{r1}^G + F * (X_{r2}^G - X_{r3}^G); \quad r1, r2, r3 \in \{1, 2, \dots, NP\} \quad \text{Eq. (3.24)}$$

(ii) *Crossover*: a test vector $U_j^G = \{u_{1,j}^G, u_{2,j}^G, \dots, u_{D,j}^G\}$ is generated between the initial vector X_j^G and the mutated vector $V_j^G = \{v_{1,j}^G, v_{2,j}^G, \dots, v_{D,j}^G\}$ using the crossover probability Cr factor.

$$u_{i,j}^G = \begin{cases} v_{i,j}^G \; if \; rand_j \leq Cr \\ x_{i,j}^G \; otherwise \end{cases}; \quad i \in \{1, 2, \dots, D\} \; and \; Cr \in [0, 1] \quad \text{Eq. (3.25)}$$

(iii) *Selection*: is selected between the initial vector X_j^G and the test vector U_j^G, the one that establishes a better performance. The resulting vector will survive for the next generation of analysis.

$$X_j^{G+1} = \begin{cases} U_j^G \; if \; f\left(U_j^G\right) \leq \left(X_j^G\right) \\ X_j^G \; otherwise \end{cases} \quad \text{Eq. (3.26)}$$

The second phase is executed as many times as necessary until the stopping criteria (maximum number of generation and/or convergence criterion) is reached.

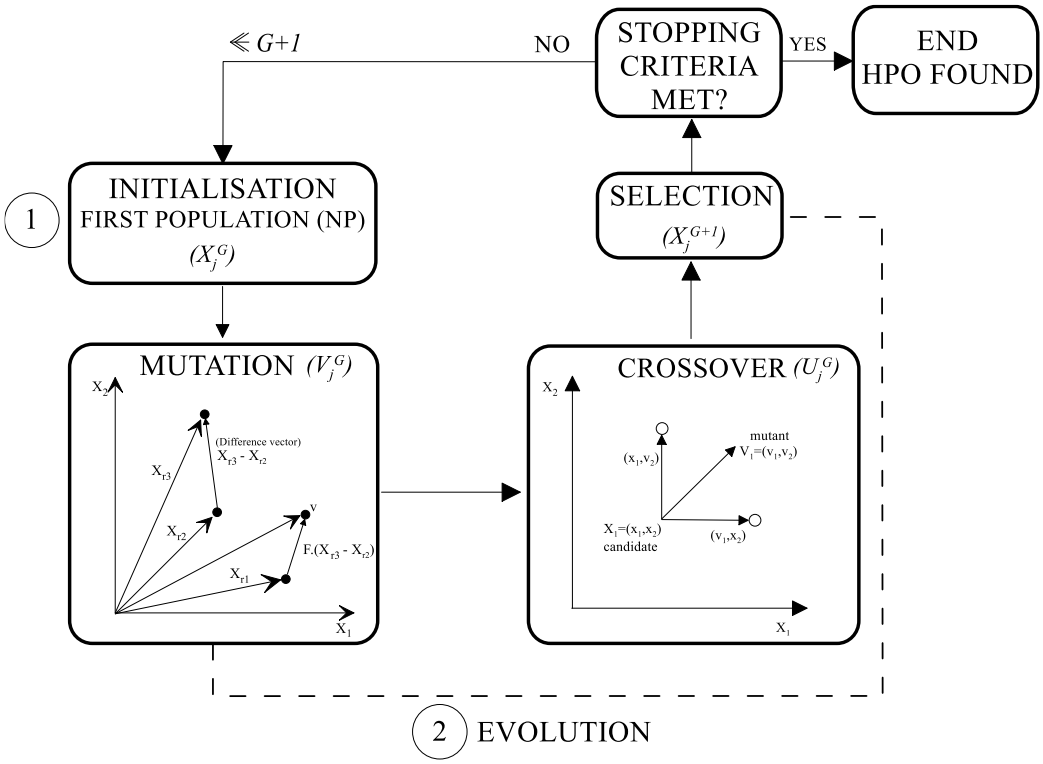

Figure 3.3 – Flowchart of DE (recreated based on Bilal et al., 2020).

The optimisation algorithm aims to find the best ANN for prediction analysis. The applied process consists of initialising the defined hyperparameter population, implementing the mutation and cross-over phases, training the network using BP and the collected data, and selecting the final HPO according to the criteria. The process is iterative until the best accuracy value is found by varying the hyperparameter population of the network. The general procedure used in the BPANN – DE algorithm model is outlined in Figure 3.4.

For the present study, the number of neurons, the type of activation function, the learning rate and the moment coefficient were established as hyperparameters (HPO) of the network. For all training cases, a maximum value of 3000 iterations (epochs) with an early stopping criterion was set.

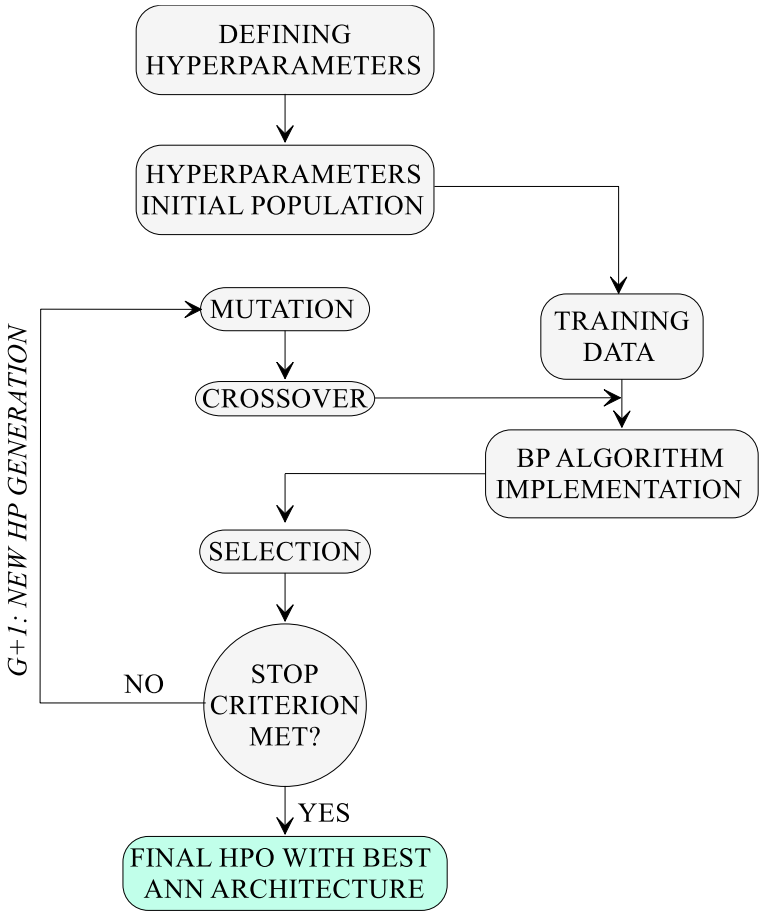

Figure 3.4 – Flowchart of BPANN – DE coupled model.

For the network training phase, 80% of the input data (342 samples) was randomly selected. The remaining 20% (86 samples) was applied to the test phase. During the training phase, the data was divided into estimation and validation subsets using the k-fold cross-validation method with a k-value equal to 3 (33.33% of the data in each subgroup). The model was then trained on the estimation subset and tested on the validation subset using different combinations of hyperparameters until the model with the lowest error was identified. This allowed for the determination of the optimal values of synaptic weights and biases that generated the lowest possible error in the model's prediction. Finally, in the testing phase, the performance of the model was evaluated using the final parameters obtained from the training phase.

3.3 EVALUATION OF THE MODEL

Once the ANN model for sand/GM interface strength prediction has been established (in each training and testing phase), the accuracy was evaluated by comparing the actual and predicted values. Figure 3.5 illustrates a graphical example of a comparison between the values predicted

by a model and the actual expected values. It is possible to establish a regression line of the data; closer values mean a minor difference between both values showing a good prediction performance of the model. A perfect model will be establishing when the best fitting line has a slope of 45° from the intercept of the graph's axes.

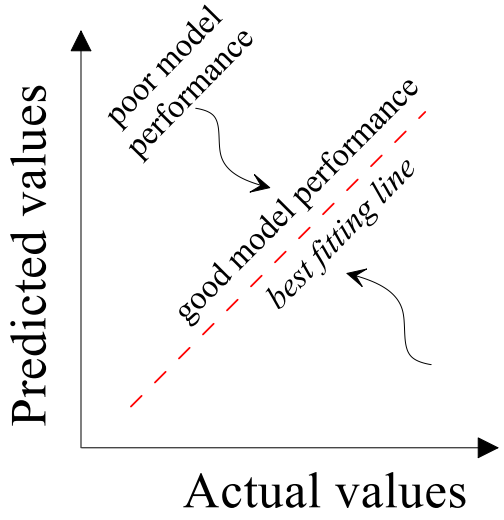

Figure 3.5 – General plot of actual vs model predicted values.

Four statistical metrics expressed in Eq. (3.27) to Eq. (3.30) were used in this study to evaluate the performance of the implemented ANN model.

(i) The coefficient of determination R-squared (R^2): allows to evaluate the goodness of fit of a regression model between an actual and an expected value.

$$R^2 = 1 - \frac{\sum_{i=1}^{n}(y_i - \hat{y}_i)^2}{\sum_{i=1}^{n}(y_i - \bar{y})^2} \quad \text{Eq. (3.27)}$$

(ii) The Root Mean Squared Error (RMSE): establishes the squared error between the predicted and actual values concerning the mean value of the data. It indicates how the data are closer to the line of best fit.

$$RMSE = \sqrt{\frac{1}{n} * \sum_{i=1}^{n}(y_i - \hat{y}_i)^2} \quad \text{Eq. (3.28)}$$

(iii) The Mean Absolute Error (MAE): measures the average absolute difference between the actual and predicted values in a dataset.

$$MAE = \frac{1}{n} * \sum_{i=1}^{n} |y_i - \hat{y}_i| \quad \text{Eq. (3.29)}$$

(iv) The Mean Absolute Percentage Error (MAPE): measures the accuracy of a prediction model in percentage terms. It is calculated as the average of the absolute differences between the actual and predicted values, divided by the actual values, and then multiplied by 100

$$MAPE = \frac{1}{n} * \sum_{i=1}^{n} \left| \left(\frac{y_i - \hat{y}_i}{y_i} \right) 100 \right| \quad \text{Eq. (3.30)}$$

In the equations, n corresponds to the total number of samples, y_i is the actual value, $\hat{y}_i$ is the value predicted by the network, and $\bar{y}$ is the mean of the actual values.

The mean error values, which include the RMSE, MAE, and MAPE, provide an indication of how well the predicted values match with the actual ones. When the error values are close to 0, it means that the predicted values are very similar to the actual, indicating a better fit of the model to the data. On the other hand, the coefficient of determination (R^2), which measures the proportion of variance in the dependent variable that is explained by the independent variables, provides a measure of how well the model fits the data. A value of R^2 close to 1 indicates a good performance of the model, meaning that it can accurately predict the dependent variable based on the independent variables. Therefore, when the mean error values are close to 0 and the R^2 value is close to 1, it suggests that the model has a good performance and can accurately predict the values of the dependent variable.

3.3.1 EXTERNAL VALIDATION

External validation corresponds to a methodology implemented by Golbraikh & Tropsha (2002) to verify the accuracy of a predictive model based on the test phase results, considering that the value of the determination coefficient R^2 obtained during training may not represent the actual accuracy of the model.

An ideal model would correspond to a trend line with a slope of 1:1 and an intercept from the origin of the coordinate axis, where all cases of predicted values would be perfectly equal to the actual values. Based on this consideration, the closer the model presents a correlation to the ideal model, the greater the precision that can be established. Graphically, it is possible to find the model's relationship by comparing the actual vs predicted values, or vice versa, thus defining that the slopes of the correlation lines would be expressed by k or k', respectively, calculated using Eq. (3.31).

$$k = \frac{\sum_{i=1}^{n} \hat{y} * y}{\sum_{i=1}^{n} \hat{y}^2}, \quad k' = \frac{\sum_{i=1}^{n} \hat{y} * y}{\sum_{i=1}^{n} y^2} \qquad \text{Eq. (3.31)}$$

And the coefficient of determination values for the trend lines passing through the origin can be estimated as expressed in Eq. (3.32) and Eq. (3.33), where ${R_o}^2$ and ${R_o}'^2$ correspond to the correlation of the actual vs predicted values or predicted vs actual values, respectively.

$${R_o}^2 = \frac{\sum_{i=1}^{n} \hat{y}(1-k)^2}{\sum_{i=1}^{n} \left(\hat{y} - \bar{\hat{y}}\right)^2} \qquad \text{Eq. (3.32)}$$

$${R_o}'^2 = \frac{\sum_{i=1}^{n} y(1-k')^2}{\sum_{i=1}^{n} (y - \bar{y})^2} \qquad \text{Eq. (3.33)}$$

A stabilization criterion proposed by Roy & Roy (2008) can be established through Eq. (3.34).

$${R_s}^2 = R^2 \left(1 - \sqrt{\left|R^2 - {R_o}^2\right|}\right) \qquad \text{Eq. (3.34)}$$

Finally, it is possible to establish the reliability of the model for the testing phase if it meets at least two of the following criteria (Golbraikh & Tropsha, 2002; Pant & Ramana, 2022):

- R^2 is greater or equal to 0.6.
- k o k' is between 0.85 and 1.15.
- $\left[\frac{R^2 - {R_o}^2}{R^2}\right] < 0.1$ or $\left[\frac{R^2 - {R_o}'^2}{R^2}\right] < 0.1$.
- ${R_s}^2$ is greater or equal to 0.5.

4 RESULTS

This chapter presents and discusses the results after applying the previously presented methodology to predict the interface shear strength between sand and geomembrane. The collected data is initially interpreted and correlated. Then a detailed description of the characteristics of the implemented models and their evaluation is made.

4.1 DATA ANALYSIS

4.1.1 DATA INTERPRETATION

As mentioned in Chapter 3.1, 488 samples were collected from the results found in 16 bibliographic publications and data provided by the manufacturer company. The samples were selected considering similar influencing factors, establishing 12 final parameters. Figure 4.1 shows the trend of missing values (represented as blank spaces) for each parameter. It is possible to observe that the relative density (I_d) and GM asperity height (A_h) correspond to the data with the least reported information in the collected studies (for A_h parameter the empty data corresponds to textured GM where the height was not specified. In the case of smooth GM, the asperity height was specified as null, meaning equal to 0 mm). In contrast, the normal stress (τ) and contact area (C.A.) represent the data with the highest amount reported in the investigations.

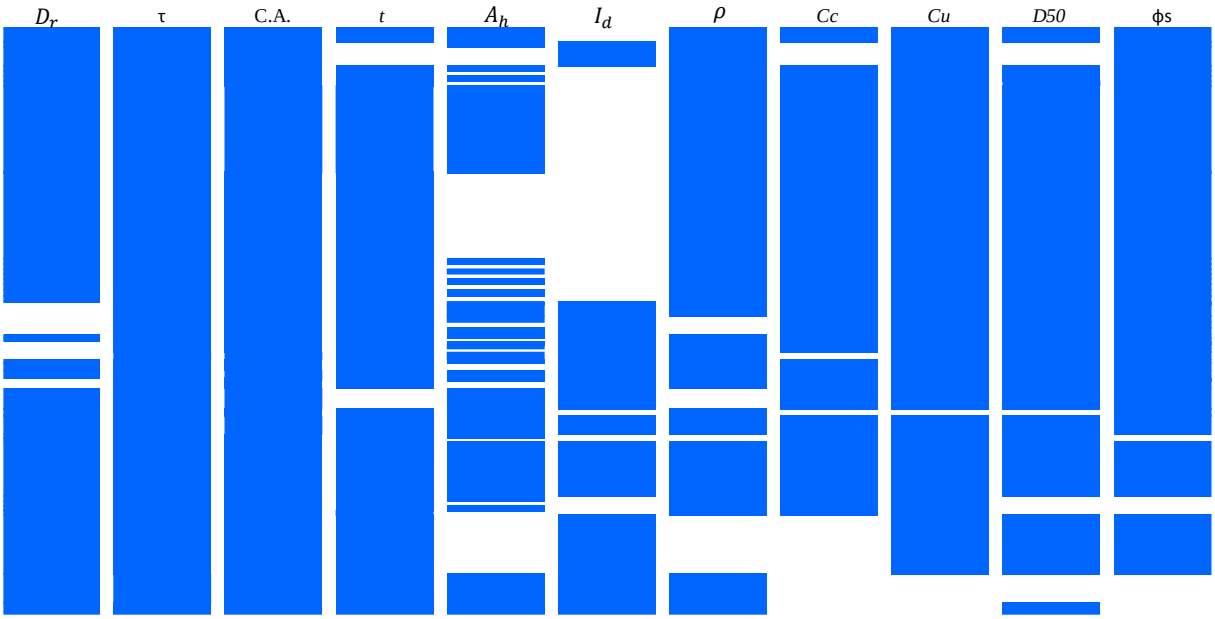

Figure 4.1 – Existing and absent values distribution of the references used data.

Note: The organization of the data was carried out chronologically according to each reference as presented in Table 3.1.

Table 4.1 shows the statistical data of the influence parameters used after the outliers data cleansing (final value of 428 useful samples). Each parameter's maximum, minimum, and mean values are calculated, along with data distribution measured by the standard deviation, coefficient of variation, and skewness coefficient. The standard deviation measures the data deviation from the average value, with a smaller value indicating a tighter concentration around the mean. On the other hand, the coefficient of variation indicates the level of homogeneity of the data, with a higher percentage suggesting greater heterogeneity. The skewness coefficient indicates the symmetry of the data distribution, with a higher value indicating more significant asymmetry and the sign representing its direction (positive: right, negative: left). For the parameter "Type of test", it is showing the amount of each test carried out.

Table 4.1 – Statistical information on influence parameters.

	Parameter	**Min**	**Max**	**Mean**	σ	**CV**	**Skewness**
	Input						
D_r	Displac. rate (mm/min)	0.10	3.00	1.20	0.64	52.8%	0.30
τ	Normal stress (kPa)	1.00	500.0	43.51	60.52	139.1%	3.82
C.A.	Contact area (cm²)	36.00	9024.00	1733.74	3169.83	182.8%	1.83
t	GM thickness (mm)	0.50	3.00	1.66	0.42	25.0%	0.48
A_h	GM asperity h (mm)	0.00	1.71	0.24	0.33	139.6%	2.08
I_d	Sand density index (%)	20.80	98.00	60.95	12.73	20.9%	0.33
ρ	Unit soil mass (g/cm³)	1.40	2.34	1.60	0.18	10.9%	1.12
Cc	Coefficient of curvature	0.80	1.68	1.02	0.15	15.0%	1.77
Cu	Uniformity coefficient	1.11	46.86	3.02	6.11	202.4%	6.94
D_{50}	Median grain size (mm)	0.20	3.08	0.59	0.31	52.9%	5.97
ϕs	Friction angle of soil (°)	29.00	49.50	38.39	4.64	12.1%	0.18
	Type of test	CDS: 57; MDS: 119; IP: 252					
	Output						
δ'	Friction angle interface (°)	16.00	58.70	27.91	6.87	24.6%	0.96

Legend: GM: Geomembrane, CDS= Conventional Direct Shear, MDS= Medium Direct Shear,

IP= Inclined plane, CV= Coefficient of variation, σ= Standard deviation.

The standard deviation of 0.64 for the displacement rate values indicates that the majority of data clusters around the mean, with a slight tendency towards higher values (skewness = 0.3). The coefficient of variation of 52.8% shows a heterogeneity in the data, with predominant values around 1.0 and 1.65 mm/min. This suggests that the displacement rate regularly used is relatively low, which helps prevent an excess of pore pressure from interfering with failure (ASTM D5321).

The stress range applied in the tests is extensive, ranging from 1 kPa to significant values of 500 kPa. The data exhibit a highly dispersed tendency (σ=60.52 and CV=139.1%) with a right-skewed distribution, indicating that the values are variable and often below the mean (43.51 kPa). This is mainly due to a significant portion of the total data (58.9%) corresponding to inclined plane tests primarily conducted at lower normal stresses (Ling et al., 2002; Moraci et al., 2014; Pavanello et al., 2021), as well as direct shear tests that start with low loads. The higher stress values are associated with larger-scale tests (MDS).

A similar condition is observed in the contact area parameter, where the data exhibits significant dispersion (σ=3169.83 and CV=182.8%) due to variations in test conditions across different investigations. There is a clear tendency towards smaller contact areas (ranging from 36 to 100 cm^2) in CDS and small-scale inclined plane tests. Intermediate contact areas are observed in MDS-type tests. The maximum contact areas (9024 cm^2) are associated with large-scale inclined plane tests, which show a higher variation in data distribution despite being less frequent.

According to the results, the geomembrane's thickness is within the nominal values commonly used in the industry, ranging from 0.5 to 3.0 mm. The data indicates a reasonably symmetric distribution (σ=0.42), where most data cluster around the mean with a slightly right-skewed tendency. Approximately 50% of the tests were conducted on geomembranes with a thickness of 1.5 mm.

Regarding GM asperity height, the data reveals that smooth geomembranes with a minimum height of 0.0 mm are used. In comparison, textured geomembranes can have heights up to 1.71

mm, which is within the industry's typical range of nominal values. However, based on the collected data, nearly 50% of the tests were conducted on smooth geomembranes (with heights less than 0.24 mm), resulting in a skewness value 2.08. Despite this, the statistics demonstrate high heterogeneity with a coefficient of variation (CV) of 139.6%, which provides valuable information related to textured conditions. Figure 4.1 illustrates that a significant amount of data is missing for this parameter in the collected studies. The missing data points were filled with the average value to address this, resulting in a more symmetrical distribution with a standard deviation of 0.33.

On the other hand, the statistical information obtained from the different research studies reveals the use of various types of sand in relation to soil properties. The sands range from fine-medium, with an average size of 0.2 mm (as reported by Mello, 2001), to coarse sand, with a size of 3.08 mm (according to Vangla & Gali, 2016). The average value of the data (D50 = 0.59 mm) indicates the presence of medium sands. The data distribution is heterogeneous, with a coefficient of variation (CV) of 52.9%, and there is a tendency for values to be lower than the average (skewness of 5.97).

The uniformity coefficient (Cu) and coefficient of curvature (Cc) reveals that most sand samples used in the tests belongs to the category of poorly-graded soil, with a few exceptions where values exceeding a Cu = 4.0 are observed due to fine and gravel materials (Cen et al., 2018). The maximum values (Cu = 46.86) are responsible for the significant dispersion of the data (CV = 202.4%).

4.1.2 DATA CORRELATION - PEARSON'S CORRELATION COEFFICIENT (ρ_r)

The Pearson coefficient can be used to establish statistically significant linear monotonic correlations that define the relationship between two variables, indicating whether there is a direct (positive value) or inversely proportional (negative value) relationship (Schober et al., 2018). Although the relationship between soil and geomembrane interface strength is not totally linear, a ρ_r can be used to stablish a linear correlation between with the input parameters and interface friction angle results in order to observe behaviour trends. Table 4.2 presents absolute values for the classification ranges of the Pearson correlation coefficient for each influential parameter, where a value close to zero indicates a weak correlation, while values closer to one show a strong relationship. On the other hand, Figure 4.2 and Figure 4.3 illustrates the

correlation between different influencing factors and the interface strength obtained from laboratory tests.

Table 4.2 –Pearson coefficient classification range between influential parameter and predict outcome.

Absolute magnitude correlation coefficient	**Parameter**
0.00 – 0.10 (Negligible correlation)	C.A., t, I_d
0.10 – 0.39 (Weak correlation)	D_r, τ, ρ, Cc, Cu, D_{50}, ϕs, *CDS*, *MDS*
0.40 – 0.69 (Moderate correlation)	A_h, *IP*
0.70 – 0.89 (Strong correlation)	
0.90 – 1.00 (Very strong correlation)	

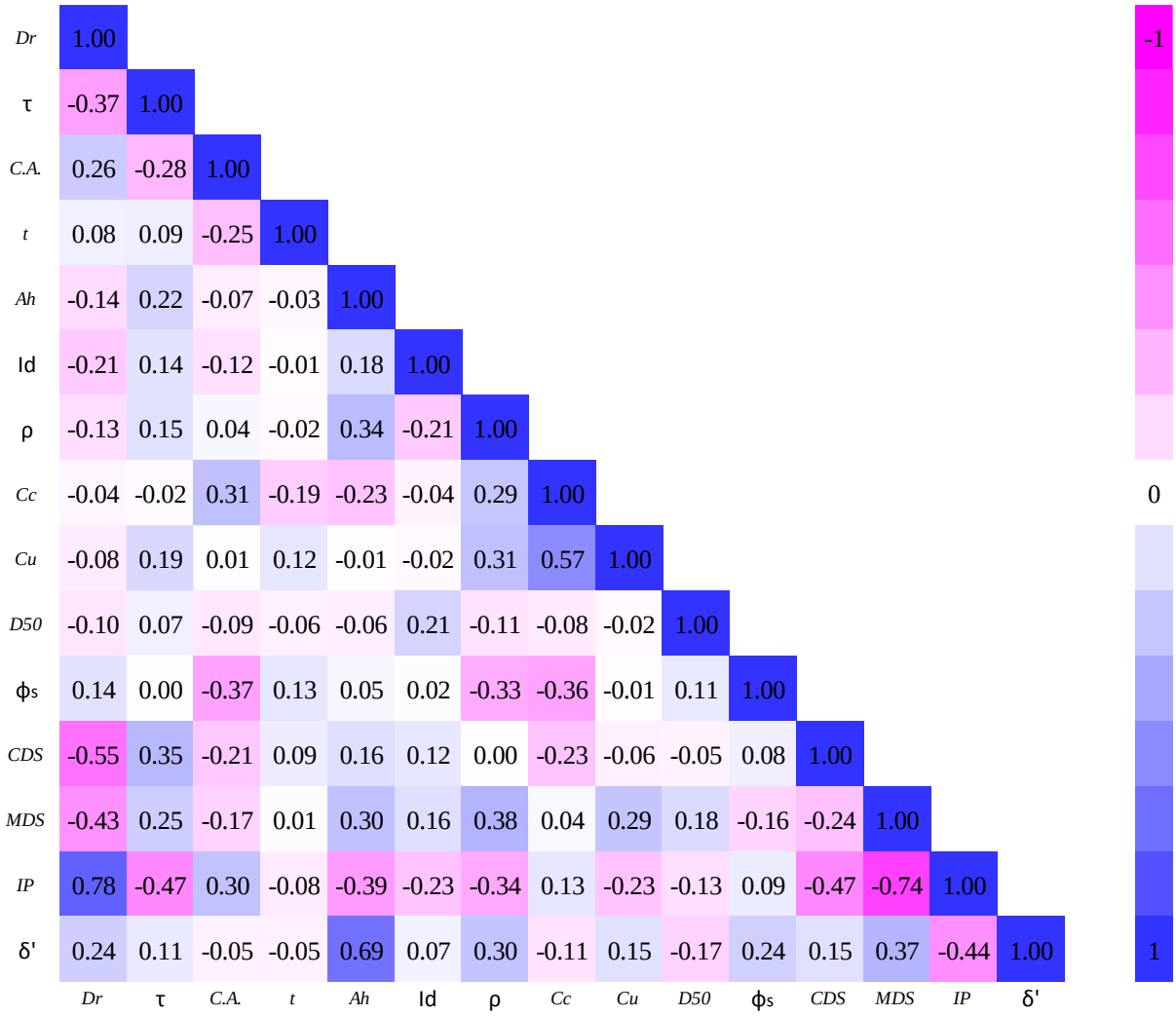

Figure 4.2 – Pearson correlation coefficient of influencing factors and the interface strength laboratory results.

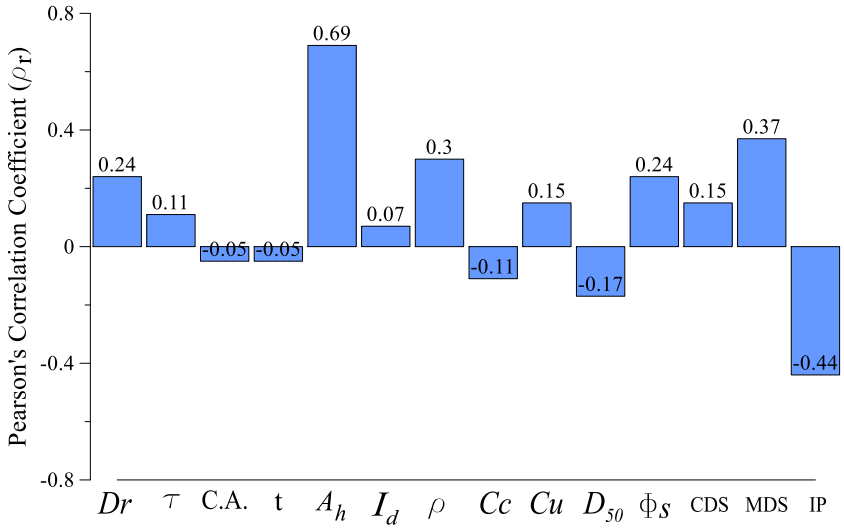

Figure 4.3 – Pearson correlation coefficient of each influential parameter.

Based on the results, it can be observed that the nominal parameter "test type" has a moderate to low correlation with the interface strength, (ρ_r of 0.15 for CDS, 0.37 for MDS, and -0.44 for IP). According to the correlation values, it can be established that the MDS test has a more significant direct influence on the determination of the interface friction angle, which can be associated with higher strength values (Hsieh et al., 2002). In the case of the IP test, despite having a high correlation value, the negative sign may indicate that lower values of the interface friction angle can be obtained when this test is executed. Monteiro (2012) observed that the interface strength values for low stresses obtained in IP tests are lower than those obtained by DS tests.

The correlation analysis of the collected data revealed that the asperity height of the geomembrane (A_h) exhibited a strong positive correlation with the interface strength (ρ_r = 0.69), which is consistent with previous study results conducted by multiple authors such as Stark et al. (1996), Lopes et al. (2001), Frost et al. (2012), Araújo et al. (2022) and Junior et al. (2023), where in all cases there was an increment in the interface friction angle values for textured GM comparing with smooth GM. The soil unit weight was the second parameter with the highest correlation (ρ_r = 0.3), and it also had a direct proportional relationship with the interface strength showing that its increase implies in a higher interface shear strength, which is linked to the soil density as indicated by O'Rourke et al. (1990), Gomes (1993) and Lima Junior (2000).

The sand properties have a minor influence on the interface shear strength, with the friction angle being the parameter most strongly correlated (ρ_r = 0.24), followed by the mean particle diameter D_{50} (ρ_r = -0.17), the coefficient of uniformity C_u (ρ_r = 0.15), and finally the coefficient of curvature C_c (ρ_r = -0.11). In each PCC value, the sign represents whether the variables are inversely (negative) or directly proportional (positive) to the interface shear strength result. The results are not consistent for the D_{50} and C_c parameters considering that researchers have investigated the effects of various soil properties, such as particle size, gradation, and angularity, on the interface strength finding a direct relationship with the interface friction angles (Izgin & Wasti, 1998; Lopes & Lopes, 1999; Costa e Lopes, 2001; Afonso, 2009; Choudhary & Krishna, 2016; Markou & Evangelou, 2018; Cen et al., 2018).

The displacement rate presents a correlation coefficient of 0.24, establishing a weak directly proportional influence on the interface strength. This implies that the rate of shear displacement (Alzahrani, 2017) or plane inclination rate (Briançon et al., 2011) has minimal proportional impact on the interface friction angle.

Thickness of the geomembrane (t) and contact area of the test (C.A.) are the parameters with the least correlation for the provided data, with ρ_r values equal to 0.05. Similar relationship was obtained by Lima Junior (2000) and Sánchez (2018) where the laboratory results showed no direct influence between geosynthethics thickness and interface shear strength. However, several authors found a variable behaviour of interface friction angle for different box sizes, establishing the contact area as influential factor (Izgin & Wasti, 1998; Wasti & Özdüzgün, 2001; Hsieh & Hsieh, 2003; Reyes Ramirez & Gourc, 2003; Gourc & Reyes Ramírez, 2004; Aguiar, 2008; Pitanga et al., 2009; Moraci et al., 2014).

4.2 ANN MODEL ANALYSIS

4.2.1 ANN ARCHITECTURE

Before the neural network's training, its architecture needs to be defined. The analysis type utilized for the network is Multi-Layer Perceptron (MLP), which implies the presence of at least one hidden layer between the input and output layers (Haykin, 1999). Each layer is comprised of interconnected neurons that transmit transformed analysis information. In terms of the input and output layers, the number of neurons is determined by the input and outcome parameters, respectively. All the analyses were developed using the Machine Learning module available in

the Tyche software (2020) from the University of Brasilia.

Initially, two models were developed – one with a single hidden layer and another with two hidden layers, where the maximum number of neurons was limited to 100 for both. The type of test (a nominal variable) and parameters of lesser influence according to the data correlation (contact area and thickness of the geomembrane) were not considered, resulting in a total of nine input parameters. The number of neurons for each layer was determined based on the highest coefficient of determination (R^2) obtained from different combinations through a trial-and-error method, which was performed using the optimization Differential Evolution algorithm (DE) coupled with the Back-Propagation algorithm described in Chapter 3. The number of hidden neurons, the type of activation function (including the logistic sigmoid, hyperbolic tangent, and ReLU function), learning rate, and momentum coefficient, were defined as the initial hyperparameter population. Each analysis also established the number of epochs (3000) and early stopping criterion as constant. The algorithm identified the ReLU function as the most effective among the three activation functions analyzed (Glorot et al., 2011).

The optimal architecture for the single-layer model was 9-60-1 (the sequence represents the number of neurons established for input layer (9), number of neurons in the hidden layer (60) and neurons in the output layer (1), respectively); the optimal learning rate was 9.25, and a momentum coefficient of 0.7 for the best performance.

On the other hand, the optimal architecture for the two-layer model was 9-44-42-1 (the sequence represents the number of neurons established for input layer (9), number of neurons in the hidden layers (44 and 42) and neurons in the output layer (1), respectively). In this case, the optimal learning rate was 61.89, and a momentum coefficient was 0.5. The R^2 values for the different combinations of hidden neurons in the single-layer and two-layer models are shown in Figure 4.4 and Figure 4.5, respectively. Figure 4.5 also displays a 2D representation corresponding to the sum of neurons in each hidden layer, enabling a clearer visualization.

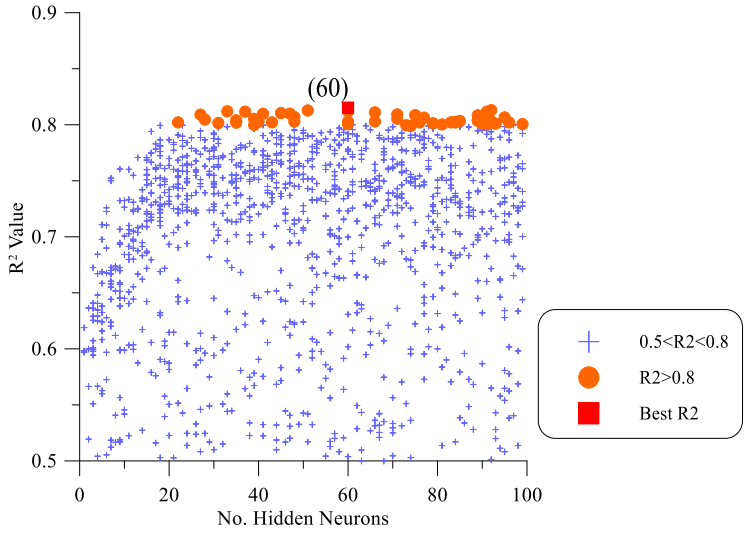

Figure 4.4 – Relationship between number of neurons and R^2 value, 1-layer model with 9 inputs.

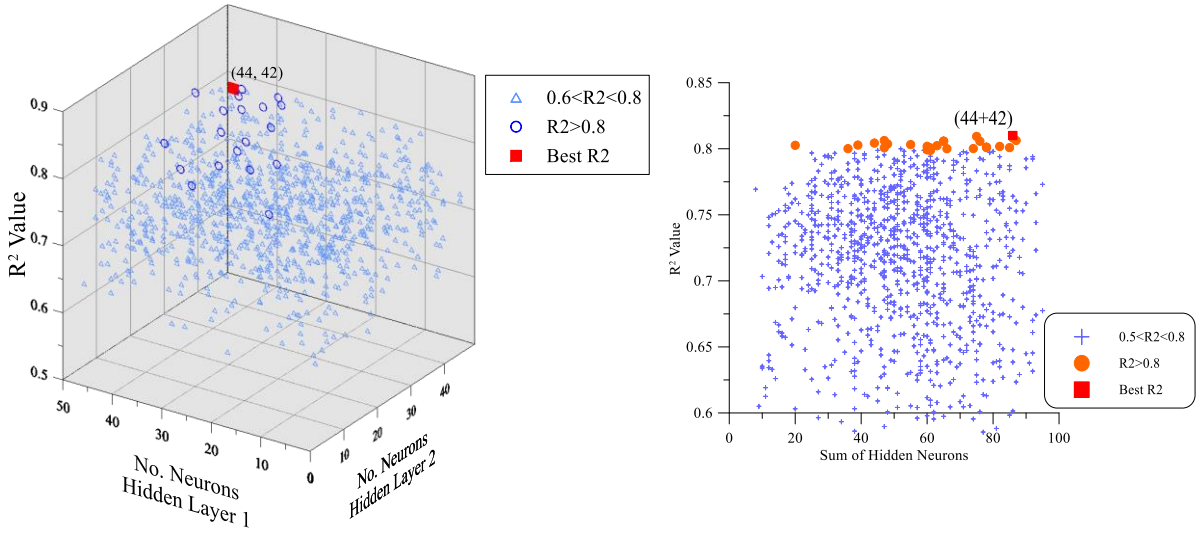

Figure 4.5 – Relationship between number of neurons and R^2 value, 2-layer model with 9 inputs.

A model with a single hidden layer was subsequently created considering the total of input parameters. In this case, a number of 3000 epochs, an early stopping criterion, and a ReLU activation function were defined as constant hyperparameters of the model. The optimal architecture for the model was 14-30-1 (the sequence represents the number of neurons established for input layer (14), number of neurons in the hidden layer (30) and neurons in the output layer (1), respectively). For the best network performance, the optimal learning rate was 0.003, and momentum coefficient was 0.98. Figure 4.6 shows the R^2 values greater than 0.5 for different numbers of hidden neurons.

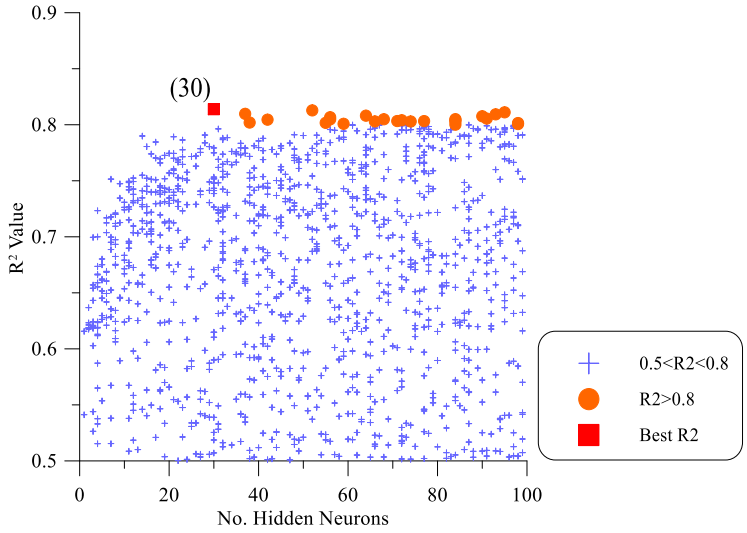

Figure 4.6 – Relationship between number of neurons and R² value, 1-layer model with 14 inputs.

Finally, a network consisting of two hidden layers and 14-input was defined. The optimal architecture was composed of 14-71-342-1 neurons (the sequence represents the number of neurons established for input layer (14), number of neurons in each hidden layers (71 and 342) and neurons in the output layer (1), respectively). A momentum coefficient of 0.3 and optimal learning rate of 2.33 was determined as the best value for network performance. Figure 4.7 displays R² values (greater than 0.6) for various combinations of neurons in the hidden layers. Figure 4.7 also displays a 2D representation corresponding to the sum of neurons in each hidden layer, enabling a clearer visualization.

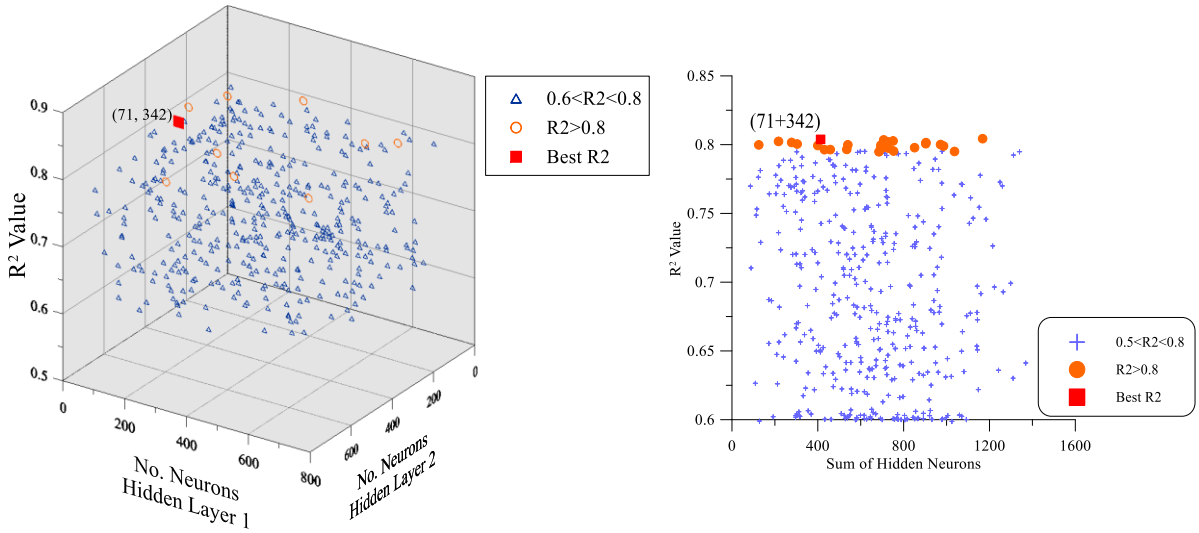

Figure 4.7 – Relationship between number of neurons and R² value, 2-layer model with 14 inputs.

Table 4.3 summarizes the optimal architecture obtained for each artificial neural network model according with the previous results.

Table 4.3 – Optimal architecture for each ANN model.

Model	No. Inputs	No. Hidden layers	No. Hidden neurons	No. Output
1	9	1	60	1
2	9	2	44/42	1
3	14	1	30	1
4	14	2	71/342	1

4.2.2 TRAINING/TESTING PHASE AND EVALUATION OF THE ANN MODEL

The training and testing phases were performed for each previously defined architecture, using a random distribution of 80-20% of the data respectively, with 342 data samples for training and 86 data samples for testing. The models predict the values of the sand-geomembrane interface strength using the synaptic weight and bias values obtained during the training phase. After calculating the predicted values, they can be compared with the actual values obtained from the collected laboratory data.

Figure 4.8 to Figure 4.11 display comparison charts of the actual and predicted values for the single-layer and two-layer models, with nine (9) and fourteen (14) input parameters. The central line on the graphs represents a regression line, which illustrates the relationship between the two data sets. The closer the data points to the trend line, the more accurate the model's predictions are.

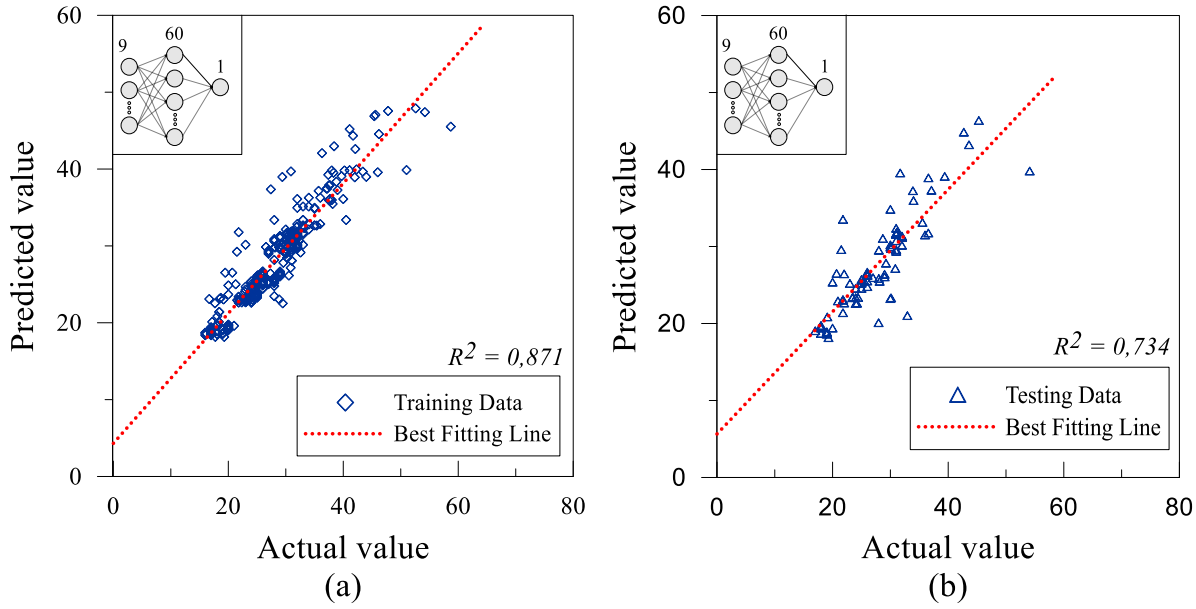

Figure 4.8 – Correlation graph of actual and predicted interface friction angle values in ANN with 1 hidden layer model and 9 input neurons: (a) Training phase and (b) Testing phase.

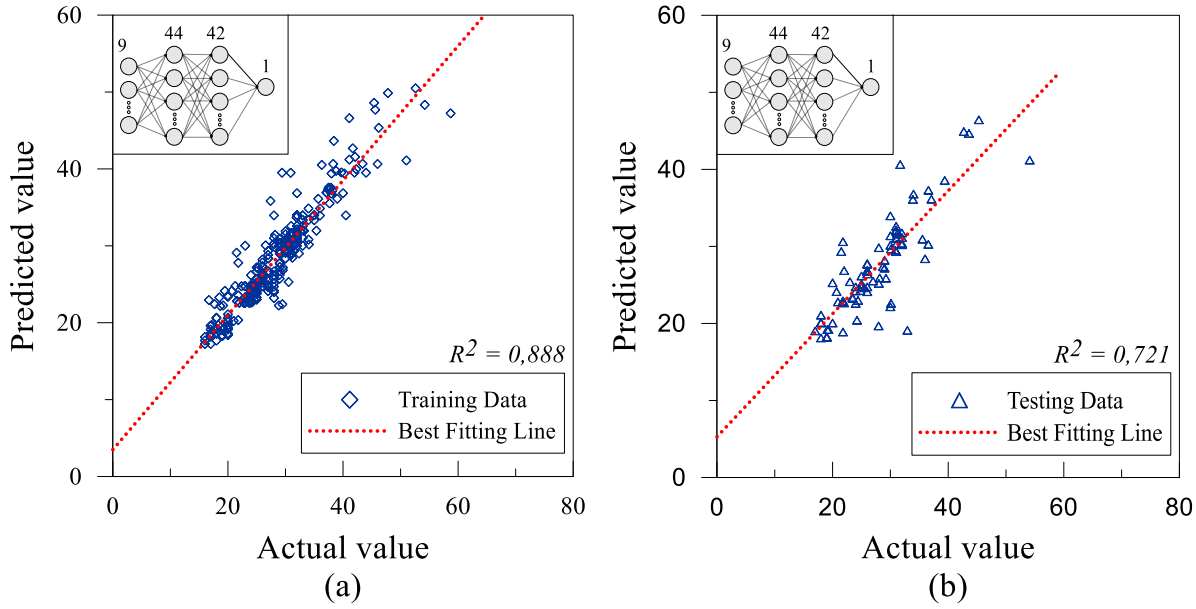

Figure 4.9 – Correlation graph of actual and predicted interface friction angle values in ANN with 2 hidden layer model and 9 input neurons: (a) Training phase and (b) Testing phase.

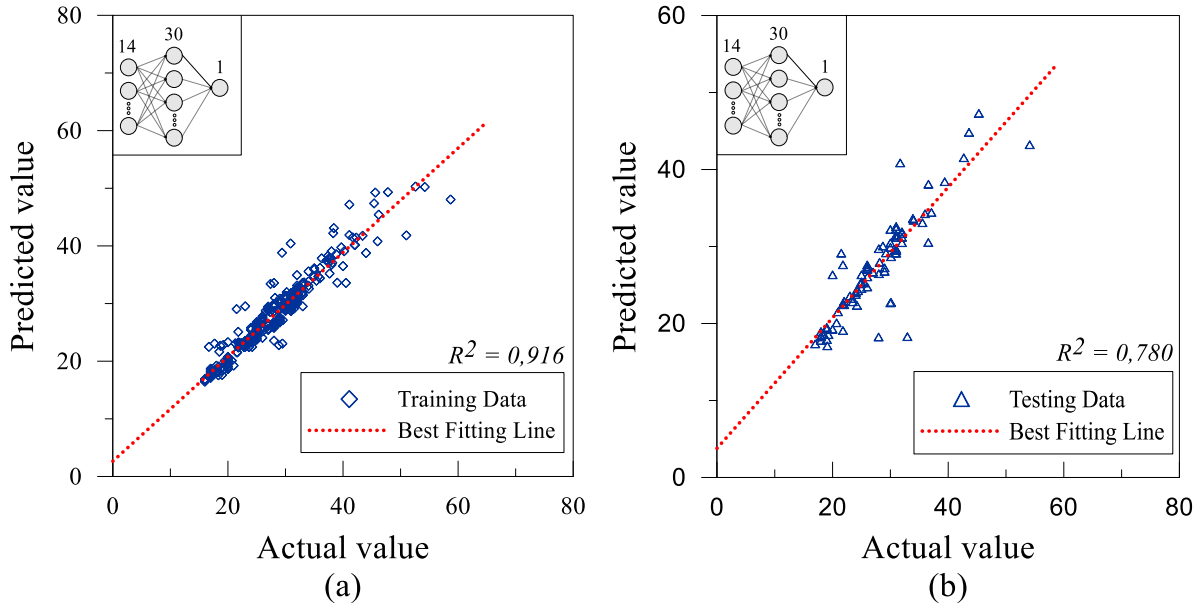

Figure 4.10 – Correlation graph of actual and predicted interface friction angle values in ANN with 1 hidden layer model and 14 input neurons: (a) Training phase and (b) Testing phase.

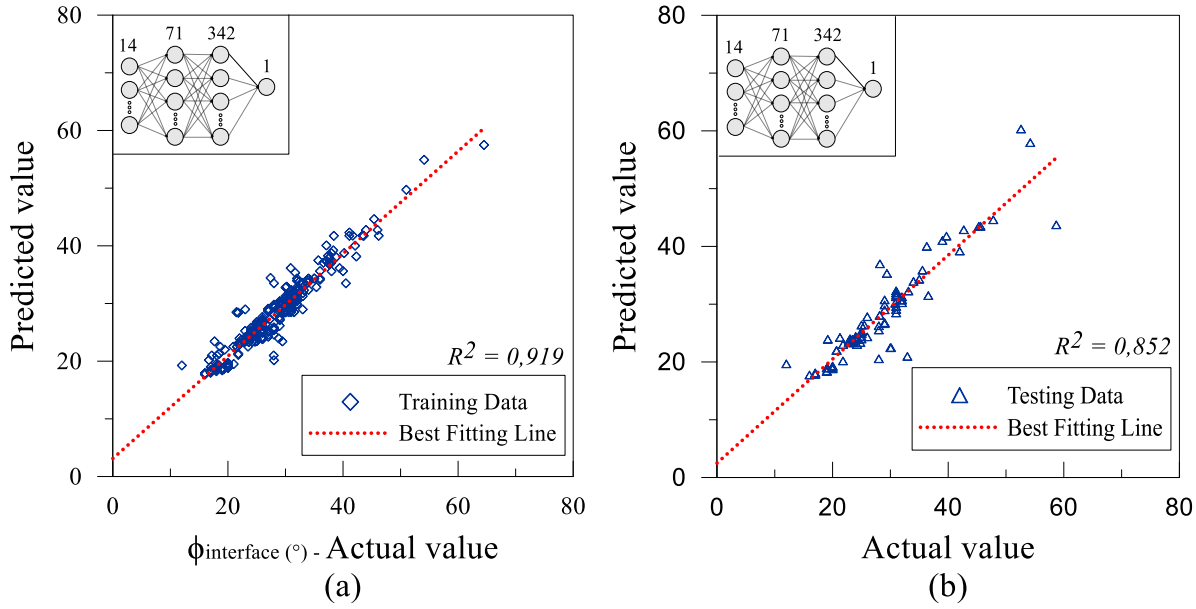

Figure 4.11 – Correlation graph of actual and predicted interface friction angle values in ANN with 2 hidden layer model and 14 input neurons: (a) Training phase and (b) Testing phase.

The graphs also show the coefficient of determination (R^2) values obtained from the trend line for both the actual and predicted values. Overall, the R^2 values obtained during the testing phase do not exhibit a significant difference compared to those obtained in the training phase, suggesting that the models do not generalize (over-fit) the data during the learning process, thereby enabling new data analysis (Haykin, 1999; Nunes da Silva et al., 2016).

The analysis reveals a noticeable dispersion of data points in the 9-input models when compared to the 14-input models. This dispersion is characterized by a larger number of samples deviating from the trend line. That observation suggests that for the present study removing the nominal parameter (type of test) as well as those with lower linear correlation (GM thickness and contact area), leads to a decrease in the accuracy and performance of the model. In other words, even though these parameters exhibit low linear correlation or do not correspond to a specific value, including them in the analysis helps the model capture the complexity of the data used.

To validate the accuracy of model results, the residual values were calculated by finding the difference between the predicted and the actual values. Figure 4.12 to Figure 4.15 show the distribution of the laboratory-measured values, as well as the predicted and residual ones (difference between measured and predicted) obtained for each model. The horizontal lines represent the variation of ±5 in the interface shear strength. The differences in the predicted values may be attributed to the significant variation in the data for certain input parameters, where the standard deviations exceed 50, and the coefficients of variation are above 100%. Although the data heterogeneity contributes to enhancing the network's learning, the model employs approximation factors that impact each parameter's influence on establishing a correlation with the desired outcome (which varies across each sample).

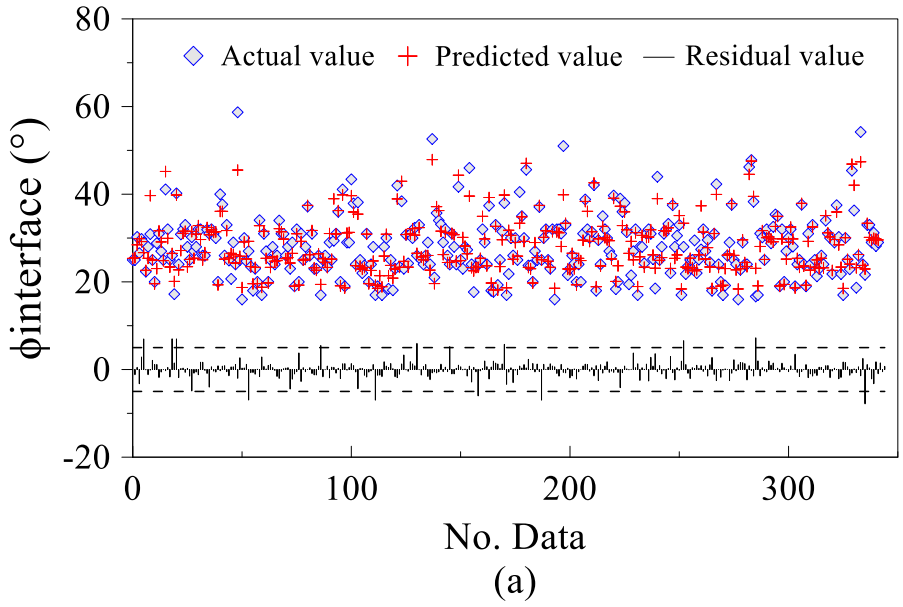

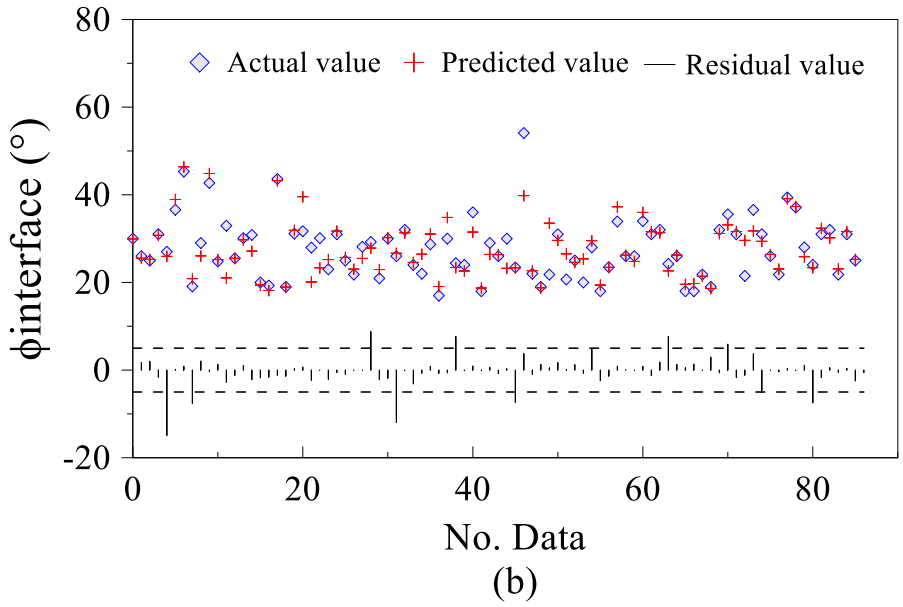

Figure 4.12 – Actual, predicted and residual values for 1 hidden layer model and 9 inputs: (a) Training phase and (b) Testing phase.

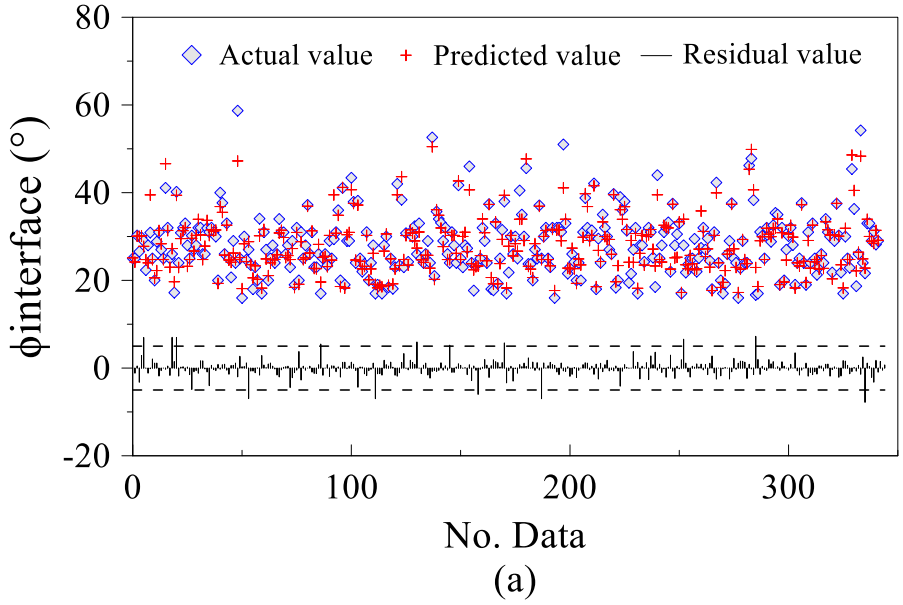

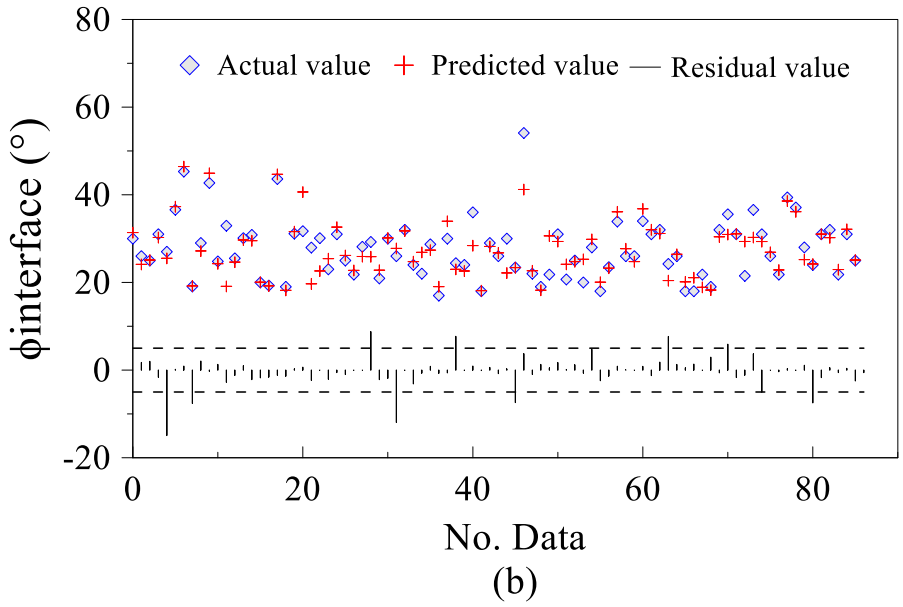

Figure 4.13 – Actual, predicted and residual values for 2 hidden layers model and 9 inputs: (a) Training phase and (b) Testing phase.

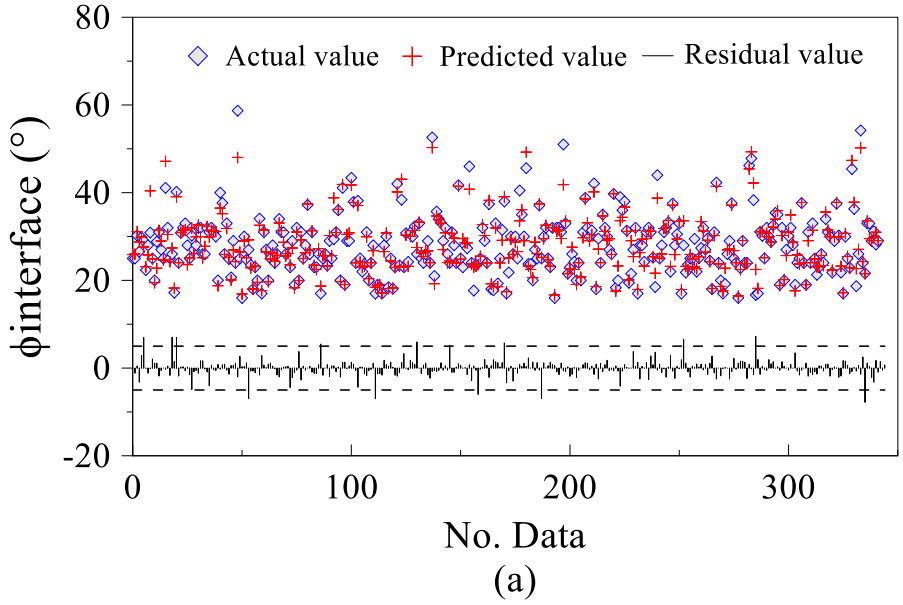

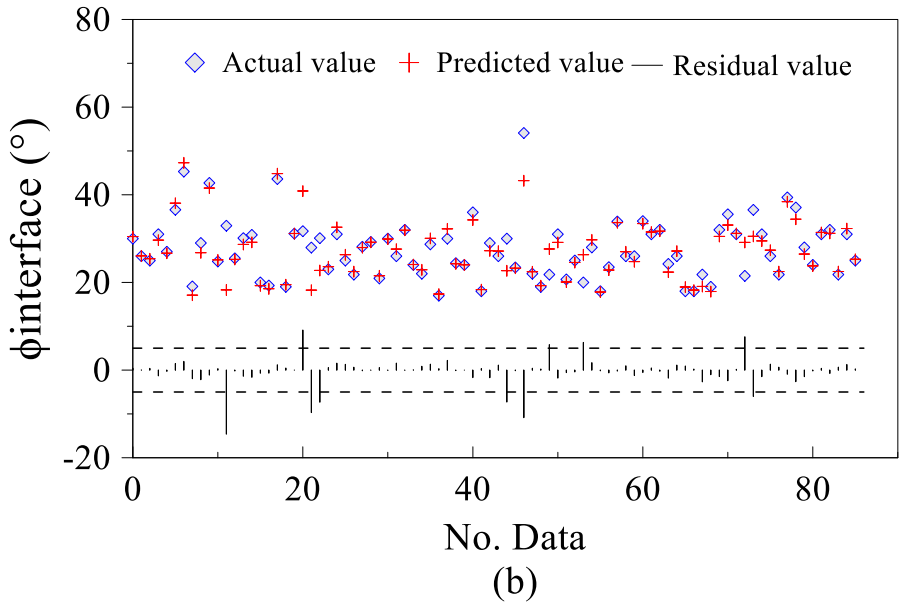

Figure 4.14 – Actual, predicted and residual values for 1 hidden layer model and 14 inputs: (a) Training phase and (b) Testing phase.

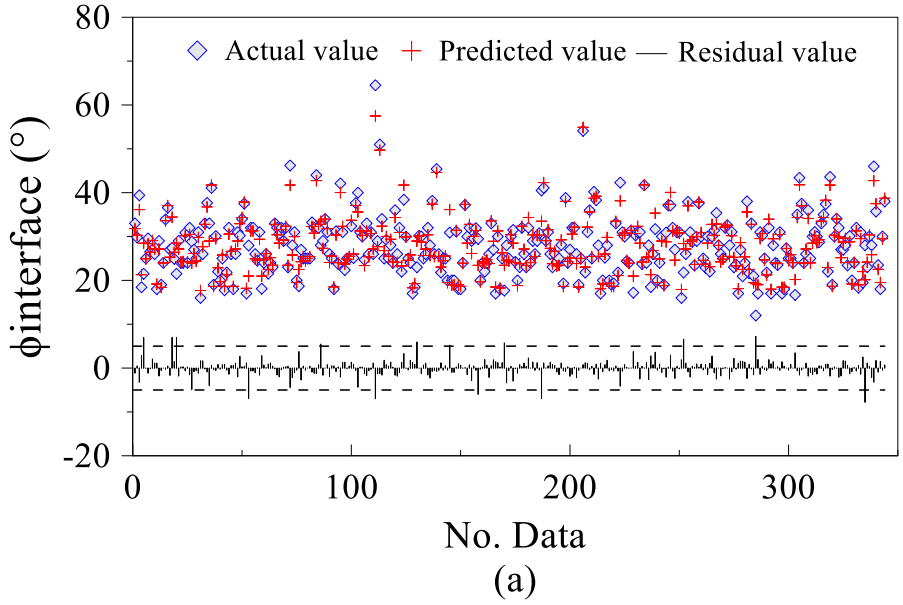

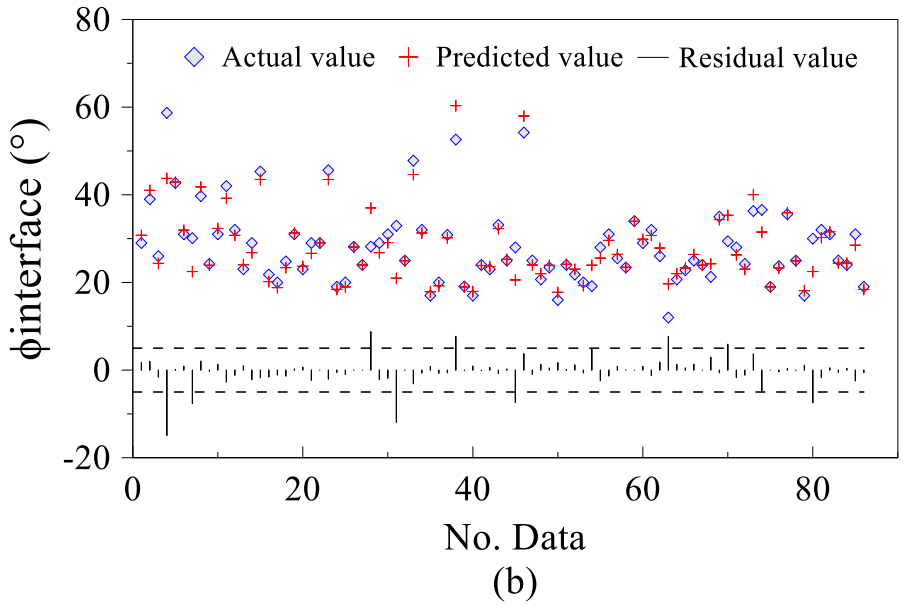

Figure 4.15 – Actual, predicted and residual values for 2 hidden layers model and 14 inputs: (a) Training phase and (b) Testing phase.

The percentages of predicted data that were observed outside the considered acceptable range of ±5 degrees were determined by calculating the residual quantity. For training phase, the residual percentage yielded to 5.6%, 5.3%, 5% and 4% for each model respectively. Conversely, the testing phase produces 11.6%, 12.8%, 11.6% and 11.6% for each model respectively. The frequency values of residual percentage can be visualized in Figure 4.16 to Figure 4.19, which correspond to the frequency histograms of residual values. The histograms are divided in three groups, values between 0 and ±5%, values higher than ±5% and values higher than ±10%, represented by the yellow, blue and red colour, respectively. Generally, it can be observed that the occurrence of residual values outside the acceptable range is minimal, and a considerable proportion of the deviations from the predicted data are centred around the range of 0° to ±2.5°. This concentration suggests that the model provides a satisfactory approximation of the results.

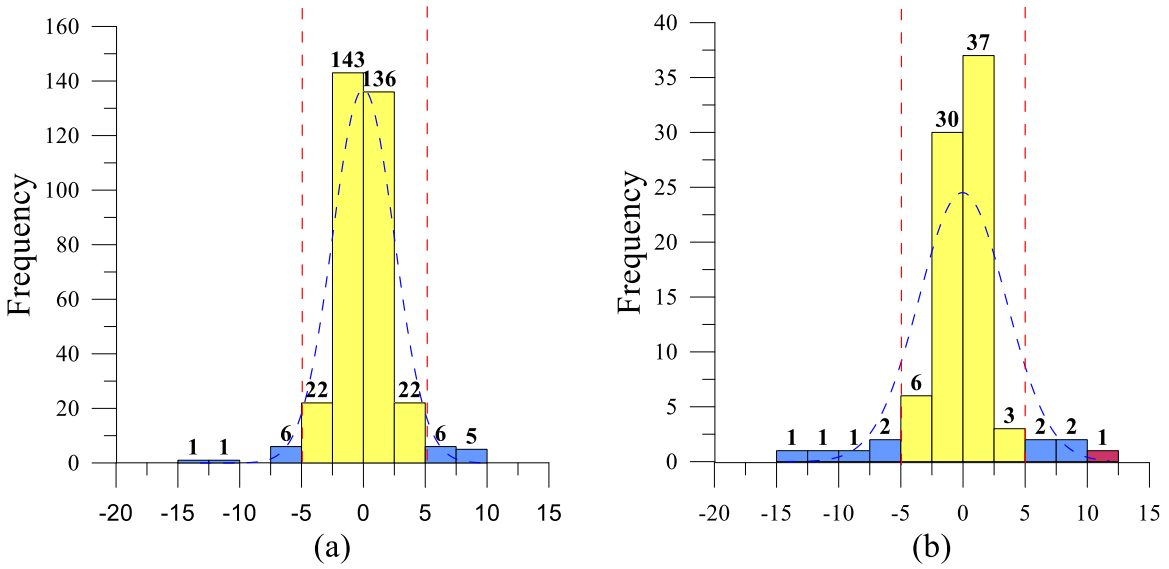

Figure 4.16 – Histogram of residual values for 1 hidden layers model and 9 inputs: (a) Training phase, 19 out of 342 data and (b) Testing phase, 10 out of 86 data.

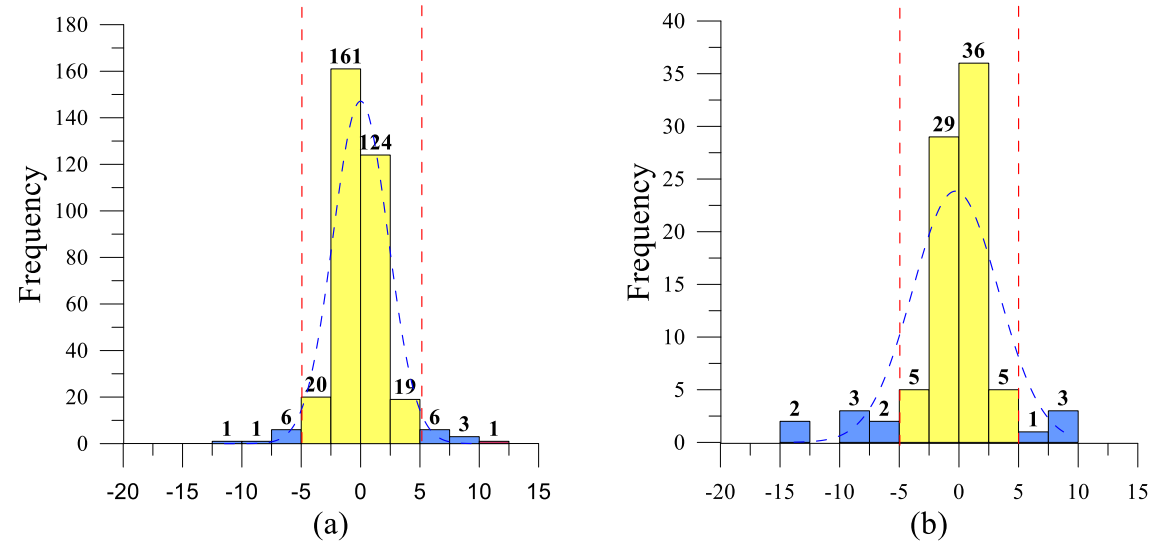

Figure 4.17 – Histogram of residual values for 2 hidden layers model and 9 inputs: (a) Training phase, 18 out of 342 data and (b) Testing phase, 11 out of 86 data.

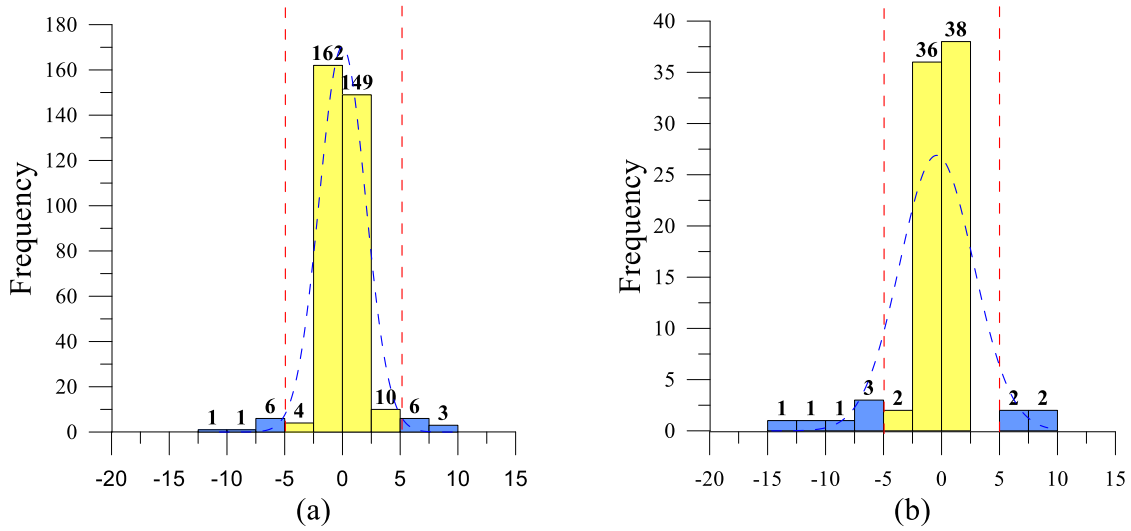

Figure 4.18 – Histogram of residual values for 1 hidden layers model and 14 inputs: (a) Training phase, 17 out of 342 data and (b) Testing phase, 10 out of 86 data.

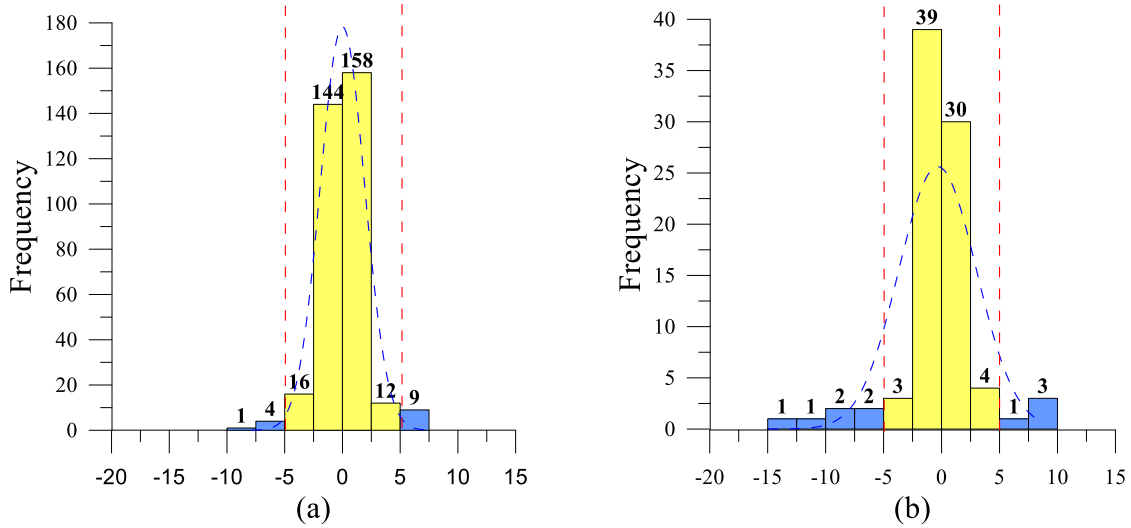

Figure 4.19 – Histogram of residual values for 2 hidden layers model and 14 inputs: (a) Training phase, 14 out of 342 data and (b) Testing phase, 10 out of 86 data.

From the relative residual values, it can be observed that only the testing phase of the models has between 10% and 15% of the data, with a relative difference greater than 15% concerning the predicted and actual results. On the other hand, the training phase of all the models show less than 10% of relative differences greater than 15%. That suggests a good overall performance of the models, considering that relative differences below 15% are acceptable for engineering analysis.

In addition, in order to evaluate the performance of each implemented model in predicting interface shear strength values, statistical errors such as RMSE, MAE, and MAPE were calculated as described in Chapter 3. Table 4.4 and Table 4.5 summarize the results of the four statistical evaluation criteria mentioned above.

Table 4.4 – Evaluation statistical metrics for training dataset.

Model	No. Inputs	No. Hidden layers	No. Hidden neurons	R^2	RMSE	MAE	MAPE%
1	9	1	60	0.871	2.49	1.64	6.06
2	9	2	44/42	0.888	2.32	1.56	5.71
3	14	1	30	0.916	2.00	1.23	4.38
4	14	2	71/342	0.919	1.92	1.32	5.03

Table 4.5 – Evaluation statistical metrics for testing dataset.

Model	No. Inputs	No. Hidden layers	No. Hidden neurons	R^2	RMSE	MAE	MAPE%
1	9	1	60	0.734	3.50	2.14	7.76
2	9	2	44/42	0.721	3.61	2.31	8.31
3	14	1	30	0.780	3.22	1.80	6.33
4	14	2	71/342	0.852	3.36	2.03	7.13

The analysis comparing predicted and actual values and the statistical criteria mentioned indicates that using more input parameters results in greater accuracy in the neural network model. Models with 14 input parameters exhibit better performance but do not achieve a perfect relationship, indicated by an R^2 value of 1 and zero errors. That can be attributed to the influence of missing data in certain parameters, which were completed using the average of the available data, affecting the network's learning process. For instance, according to the correlation presented in the heat map showed in Figure 4.2, the GM asperity height corresponds to the parameter with the highest correlation, a factor also highlighted by various authors as significantly influencing the interface strength with geomembrane (see Chapter 2). However, it is one of the least presented values in the collected data (see Figure 4.1).

There is no clear performance trend for the models regarding the number of hidden layers, as they have similar coefficients of determination. Also, the statistical error indices vary, with

better accuracy for both one and two layers and lower residual percentages for the training phase but constant or higher for the testing phase.

According to the above and to establish the more accurate model between one and two hidden layers, the external validation methodology developed by Golbraikh & Tropsha (2002) was applied to the testing phase of the 14 input models. Table 4.6 shows the determination coefficients for the testing data to a fitting line passing through the origin ($R_o{}^2, R_o{}'^2$), their respective slopes (k, k'), and the verification of compliance with the validation criteria defined in Chapter 3. It is possible to observe that both 14-input models met at least two defined conditions, showing that both are reliable. However, the two-layer model satisfies one more condition, making it more accurate.

Table 4.6 – External validation for testing phase models.

Model	R^2	$R_o{}^2$	$R_o{}'^2$	k	k'	R_s	**Cond. 1**	**Cond. 2**	**Cond. 3**	**Cond. 4**
2-layers	0.852	0.999	0.996	1.01	0.98	0.52	Yes	Yes	Not	Yes
1-layer	0.780	0.998	0.991	1.01	0.98	0.42	Yes	Yes	Not	Not

Based on the previous results, it becomes evident that utilizing two hidden layers in the neural network enhances the learning process for result prediction, surpassing the performance of a single layer (Ali et al., 2022). This improvement is reflected in higher R^2 values, indicating a stronger correlation between the predicted and actual values. It is possible to infer that in complex problems, the first layer captures the influence of the input parameters, while the second layer establishes meaningful relationships among them.

5 CONCLUSIONS

5.1 GENERAL CONCLUSIONS

The focus of this study is to assess the effectiveness of using ANN methodology to predict the shear strength at the interface of sand-geomembrane. An MLP architecture was chosen to configure the ANN models, and the training process is a supervised one that involves a BP training algorithm coupled with the DE optimization algorithm. The input data for the implemented models were defined from laboratory tests reported in previous research. Four hundred twenty-eight data, including 14 input parameters and sand-geomembrane interface strength results, were finally used. Once the results obtained from the various conducted analyses have been evaluated, it is possible to establish the following findings:

- The statistical information of the collected data reveals a wide distribution for each parameter, enabling a better characterization and analysis for different soil and geomembrane conditions.
- The correlation analysis of the collected data showed that the geomembrane asperity height has the highest correlation with the interface shear strength. In contrast, soil properties and displacement rate have a medium correlation. The thickness of the geomembrane and contact area has the lowest correlation coefficients. Although the results provide a reference measure for the established database, they are inconclusive compared to laboratory tests.
- Four ANN models were analysed, differentiated in terms of their number of inputs (9 or 14) and the number of hidden layers (1 or 2). Models with more input parameters showed greater accuracy based on distribution analysis, residual values, and statistical criteria obtained by comparing predicted and actual values.
- External validation methodology was applied between the 14-input models, finding that the architecture with two hidden layers met more selection criteria and was, therefore, the most accurate model.
- A perfect correlation between the predicted and actual data was not achieved, possibly due to the influence of missing values in the input parameters during the network's learning process.
- The ANN model with the architecture 14-71-342-1 displayed satisfactory results in terms of the predicted values' distribution compared to the trend line, a lower number of residual

values outside the acceptable range (4% for training and 11.6% for testing), and excellent prediction performance according to statistical metrics for both phases.

- It can be concluded that the ANN algorithm is a suitable method for predicting sand-geomembrane interface strength values (friction angle) for the collected data.

5.2 LIMITATIONS OF THE MODEL

The model's main limitation concerns the properties of the materials under evaluation. Specifically, the model focuses solely on the interaction between sandy soil and geomembrane. Additionally, it is necessary to have the most information possible about the input parameters, which must be within the ranges of the data used in the learning algorithms.

Due to the limited detailed information in the available data, the model does not consider other factors influencing the interface shear strength, such as saturation degree or thermal conditions.

5.3 SUGGESTIONS FOR FUTURE RESEARCH

The findings of this study provide some recommendations for further research on the subject of the soil-geosynthetic interface using machine learning technics:

- Develop or gather additional tests for sand-geomembrane interface behaviour, which can supplement the current database and provide more samples for training and validation.
- Implement different training and/or optimization algorithms and other ML techniques, to compare the results obtained and to establish the most accurate methodology.
- Initiate research with other materials for soil and geosynthetics, establishing a general behaviour for different types of interfaces.

REFERENCES

Abdalla, J. A., Attom, M. F., & Hawileh, R. (2015). Prediction of minimum factor of safety against slope failure in clayey soils using artificial neural network. *Environmental Earth Sciences*, *73*(9), 5463–5477. https://doi.org/10.1007/s12665-014-3800-x

Abdalla, K. M., & Stavroulakis, G. E. (1995). A Backpropagation Neural Network Model for Semi-rigid Steel Connections. *Computer-Aided Civil and Infrastructure Engineering*, *10*(2), 77–87. https://doi.org/10.1111/j.1467-8667.1995.tb00271.x

ABNT NBR ISO 12957-1. (2013). Geossintéticos – Determinação das Características de Atrito. Parte 1: Ensaio de Cisalhamento Direto, 8 p.

ABNT NBR ISO 12957-2. (2013). Geossintéticos – Determinação das Características de Atrito. Parte 2: Ensaio de Plano Inclinado, 12 p.

Abraham, A. (2005). Artificial Neural Networks. In P. H. Sydenham & R. Thorn (Eds.), *Handbook of Measuring System Design* (p. mm421). John Wiley & Sons, Ltd. https://doi.org/10.1002/0471497398.mm421

Abuel-Naga, H. M., & Bouazza, A. (2014). Numerical experiment-artificial intelligence approach to develop empirical equations for predicting leakage rates through GM/GCL composite liners. *Geotextiles and Geomembranes*, *42*(3), 236–245. https://doi.org/10.1016/j.geotexmem.2014.04.002

Adeli, H. (2001). Neural Networks in Civil Engineering: 1989–2000. *Computer-Aided Civil and Infrastructure Engineering*, *16*(2), 126–142. https://doi.org/10.1111/0885-9507.00219

Adeli, H., & Park, H. S. (1995). Optimization of space structures by neural dynamics. *Neural Networks*, *8*(5), 769–781. https://doi.org/10.1016/0893-6080(95)00026-V

Aditian, A., Kubota, T., & Shinohara, Y. (2018). Comparison of GIS-based landslide susceptibility models using frequency ratio, logistic regression, and artificial neural network in a tertiary region of Ambon, Indonesia. *Geomorphology*, *318*, 101–111. https://doi.org/10.1016/j.geomorph.2018.06.006

Afonso, M. R. F. L. (2009). Ensaios de corte directo na caracterização da interface solo-geossintético: Efeito da variação da tensão normal. Dissertação de Mestrado, Universidade de Porto, Porto, Portugal, 62 p.

Afzali-Nejad, A., Lashkari, A., & Martinez, A. (2021). Stress-Displacement Response of Sand–Geosynthetic Interfaces under Different Volume Change Boundary Conditions. *Journal of Geotechnical and Geoenvironmental Engineering*, *147*(8), 04021062. https://doi.org/10.1061/(ASCE)GT.1943-5606.0002544

Afzali-Nejad, A., Lashkari, A., & Shourijeh, P. T. (2017). Influence of particle shape on the shear strength and dilation of sand-woven geotextile interfaces. *Geotextiles and Geomembranes*, *45*(1), 54–66. https://doi.org/10.1016/j.geotexmem.2016.07.005

Aghajani, H. F., Salehzadeh, H., & Shahnazari, H. (2015). Application of artificial neural network for calculating anisotropic friction angle of sands and effect on slope stability. *Journal of Central South University*, *22*(5), 1878–1891. https://doi.org/10.1007/s11771-015-2707-3

Aguiar, V. R. (2003). Ensaios de rampa para estudo da resistência de interfaces solo-geossintético. Dissertação de Mestrado, Universidade Federal do Rio Grande do Sul, Brasil, 105 p.

Aguiar, V. R. (2008). Resistência de interfaces solo-geossintético-desenvolvimento de equipamento e ensaios. Tese de Doutorado, Pontifícia Universidade Católica do Rio de Janeiro, RJ, Brasil, 372 p.

Ahmad, I., Hesham El Naggar, M., & Khan, A. N. (2007). Artificial neural network application to estimate kinematic soil pile interaction response parameters. *Soil Dynamics and Earthquake Engineering*, *27*(9), 892–905. https://doi.org/10.1016/j.soildyn.2006.12.009

Aleshin, Y., & Torgoev, I. (2013). Landslide Prediction Based on Neural Network Modelling. In C. Margottini, P. Canuti, & K. Sassa (Eds.), *Landslide Science and Practice* (pp. 311–317). Springer Berlin Heidelberg. https://doi.org/10.1007/978-3-642-31319-6_41

Ali, T., Haider, W., Ali, N., & Aslam, M. (2022). A Machine Learning Architecture Replacing Heavy Instrumented Laboratory Tests: In Application to the Pullout Capacity of Geosynthetic Reinforced Soils. *Sensors*, *22*(22), 8699. https://doi.org/10.3390/s22228699

Alzahrani, S. (2017). Effect of Time on Soil-Geomembrane Interface Shear Strength. Master's thesis, University of Dayton, USA, 95 p. https://doi.org/10.13140/RG.2.2.25743.28320

Alzo'ubi, A. K., & Ibrahim, F. (2019). Predicting Loading–Unloading Pile Static Load Test Curves by Using Artificial Neural Networks. *Geotechnical and Geological Engineering*, *37*(3), 1311–1330. https://doi.org/10.1007/s10706-018-0687-4

Alzo'Ubi, A. K., & Ibrahim, F. (2021). Predicting the pile static load test using backpropagation neural network and generalized regression neural network – a comparative study. *International Journal of Geotechnical Engineering*, *15*(7), 810–821. https://doi.org/10.1080/19386362.2018.1519975

Amjad Raja, M. N., Abbas Jaffar, S. T., Bardhan, A., & Shukla, S. K. (2023). Predicting and validating the load-settlement behavior of large-scale geosynthetic-reinforced soil abutments using hybrid intelligent modeling. *Journal of Rock Mechanics and Geotechnical Engineering*, *15*(3), 773–788. https://doi.org/10.1016/j.jrmge.2022.04.012

Anderson, D., Hines, E. L., Arthur, S. J., & Eiap, E. L. (1997). Application of artificial neural networks to the prediction of minor axis steel connections. *Computers & Structures*, *63*(4), 685–692. https://doi.org/10.1016/S0045-7949(96)00080-6

Anderson, D., & McNeill, G. (1992). *Artificial neural networks technology: A DACS State-of-the-Art Report* (No. F30602-89-C–0082; p. 87). Kaman Sciences Corporation.

https://csiac.org/state-of-the-art-reports/artificial-neural-networks-technology/

Araújo, G. L. S., Sánchez, N. P., Palmeira, E. M., & Almeida, M. das G. G. de. (2022). Influence of micro and macroroughness of geomembrane surfaces on soil-geomembrane and geotextile-geomembrane interface strength. *Geotextiles and Geomembranes*, *50*(4), 751–763. https://doi.org/10.1016/j.geotexmem.2022.03.015

Ari, A., & Akbulut, S. (2022). Effect of fractal dimension on sand-geosynthetic interface shear strength. *Powder Technology*, *401*, 117349. https://doi.org/10.1016/j.powtec.2022.117349

ASTM D5321-12. (2012). Standard Test Method for Determining the Shear Strength of Soil-Geosynthetic and Geosynthetic-Geosynthetic Interfaces by Direct Shear. 8 p.

Atangana Njock, P. G., Shen, S.-L., Zhou, A., & Modoni, G. (2021). Artificial neural network optimized by differential evolution for predicting diameters of jet grouted columns. *Journal of Rock Mechanics and Geotechnical Engineering*, *13*(6), 1500–1512. https://doi.org/10.1016/j.jrmge.2021.05.009

Attoh-Okine, N. O. (2001). Grouping Pavement Condition Variables for Performance Modeling Using Self-Organizing Maps. *Computer-Aided Civil and Infrastructure Engineering*, *16*(2), 112–125. https://doi.org/10.1111/0885-9507.00218

Bacas, B. M., Cañizal, J., & Konietzky, H. (2015). Shear strength behavior of geotextile/geomembrane interfaces. *Journal of Rock Mechanics and Geotechnical Engineering*, *7*(6), 638–645. https://doi.org/10.1016/j.jrmge.2015.08.001

Baghbani, A., Choudhury, T., Costa, S., & Reiner, J. (2022). Application of artificial intelligence in geotechnical engineering: A state-of-the-art review. *Earth-Science Reviews*, *228*, 103991. https://doi.org/10.1016/j.earscirev.2022.103991

Bagińska, M., & Srokosz, P. E. (2019). The Optimal ANN Model for Predicting Bearing Capacity of Shallow Foundations trained on Scarce Data. *KSCE Journal of Civil Engineering*, *23*(1), 130–137. https://doi.org/10.1007/s12205-018-2636-4

Bahrami, A., Monjezi, M., Goshtasbi, K., & Ghazvinian, A. (2011). Prediction of rock fragmentation due to blasting using artificial neural network. *Engineering with Computers*, *27*(2), 177–181. https://doi.org/10.1007/s00366-010-0187-5

Barbosa, R. L., & Evangelista Jr, F. (2020). Machine Learning models to predict nonlinear simulations of net section resistance in steel structures. XLI Iberian Latin American Congress on Computational Methods in Engineering, Foz do Iguaçú.

Basheer, I. A., & Hajmeer, M. (2000). Artificial neural networks: Fundamentals, computing, design, and application. *Journal of Microbiological Methods*, *43*(1), 3–31. https://doi.org/10.1016/S0167-7012(00)00201-3

Basheer, I. A., Reddi, L. N., & Najjar, Y. M. (1996). Site Characterization by Neuronets: An Application to the Landfill Siting Problem. *Ground Water*, *34*(4), 610–617. https://doi.org/10.1111/j.1745-6584.1996.tb02048.x

Bekdaş, G., & Temür, R. (2018). Grey wolf optimizer for optimum design of reinforced concrete cantilever retaining walls. 260008. https://doi.org/10.1063/1.5043893

Bekhor, S., & Livneh, M. (2014). Using the Artificial Neural Networks Methodology to Predict the Vertical Swelling Percentage of Expansive Clays. *Journal of Materials in Civil Engineering*, *26*(6), 06014007. https://doi.org/10.1061/(ASCE)MT.1943-5533.0000931

Bhardwaj, A., & Venkatachalam, G. (2014). Landslide Hazard Evaluation Using Artificial Neural Networks and GIS. In K. Sassa, P. Canuti, & Y. Yin (Eds.), *Landslide Science for a Safer Geoenvironment* (pp. 397–403). Springer International Publishing. https://doi.org/10.1007/978-3-319-05050-8_62

Bilal, Pant, M., Zaheer, H., Garcia-Hernandez, L., & Abraham, A. (2020). Differential Evolution: A review of more than two decades of research. *Engineering Applications of Artificial Intelligence*, *90*, 103479. https://doi.org/10.1016/j.engappai.2020.103479

Bilgin, Ö., & Shah, B. (2021). Temperature Influence on High-Density Polyethylene Geomembrane and Soil Interface Shear Strength. *International Journal of Geosynthetics and Ground Engineering*, *7*(3), 66. https://doi.org/10.1007/s40891-021-00311-9

Boadu, F. K., Owusu-Nimo, F., Achampong, F., & Ampadu, S. I. K. (2013). Artificial neural network and statistical models for predicting the basic geotechnical properties of soils from electrical measurements. *Near Surface Geophysics*, *11*(6), 599–612. https://doi.org/10.3997/1873-0604.2013011

Briançon, L., Girard, H., & Gourc, J. P. (2011). A new procedure for measuring geosynthetic friction with an inclined plane. *Geotextiles and Geomembranes*, *29*(5), 472–482. https://doi.org/10.1016/j.geotexmem.2011.04.002

Caglar, N., & Arman, H. (2007). The applicability of neural networks in the determination of soil profiles. *Bulletin of Engineering Geology and the Environment*, *66*(3), 295–301. https://doi.org/10.1007/s10064-006-0075-9

Cal, Y. (1995). Soil classification by neural network. *Advances in Engineering Software*, *22*(2), 95–97. https://doi.org/10.1016/0965-9978(94)00035-H

Camarena-Martinez, R., Lizarraga-Morales, R. A., & Baeza-Serrato, R. (2021). Classification of Geomembranes as Raw Material for Defects Reduction in the Manufacture of Biodigesters Using an Artificial Neuronal Network. *Energies*, *14*(21), 7345. https://doi.org/10.3390/en14217345

Cascardi, A., Micelli, F., & Aiello, M. A. (2017). An Artificial Neural Networks model for the prediction of the compressive strength of FRP-confined concrete circular columns. *Engineering Structures*, *140*, 199–208. https://doi.org/10.1016/j.engstruct.2017.02.047

Cen, W.-J., Wang, H., & Sun, Y.-J. (2018). Laboratory Investigation of Shear Behavior of High-Density Polyethylene Geomembrane Interfaces. *Polymers*, *10*(7), 734. https://doi.org/10.3390/polym10070734

Chang, D. (2000). Estimation of Soil Physical Properties Using Remote Sensing and Artificial Neural Network. *Remote Sensing of Environment*, *74*(3), 534–544. https://doi.org/10.1016/S0034-4257(00)00144-9

Chao, Z., Fowmes, G., & Dassanayake, S. M. (2021). Comparative Study of Hybrid Artificial Intelligence Approaches for Predicting Peak Shear Strength Along Soil-Geocomposite Drainage Layer Interfaces. *International Journal of Geosynthetics and Ground Engineering*, *7*(3), 60. https://doi.org/10.1007/s40891-021-00299-2

Chao, Z., Shi, D., Fowmes, G., Xu, X., Yue, W., Cui, P., Hu, T., & Yang, C. (2023). Artificial intelligence algorithms for predicting peak shear strength of clayey soil-geomembrane interfaces and experimental validation. *Geotextiles and Geomembranes*, *51*(1), 179–198. https://doi.org/10.1016/j.geotexmem.2022.10.007

Chatterjee, S., Sarkar, S., Hore, S., Dey, N., Ashour, A. S., & Balas, V. E. (2017). Particle swarm optimization trained neural network for structural failure prediction of multistoried RC buildings. *Neural Computing and Applications*, *28*(8), 2005–2016. https://doi.org/10.1007/s00521-016-2190-2

Chauhan, S., Sharma, M., Arora, M. K., & Gupta, N. K. (2010). Landslide Susceptibility Zonation through ratings derived from Artificial Neural Network. *International Journal of Applied Earth Observation and Geoinformation*, *12*(5), 340–350. https://doi.org/10.1016/j.jag.2010.04.006

Chaves, J. F. N. (2021). Previsão da resistência à compressão do cimento Portland comum com utilização de técnica de Machine Learning. Dissertação de Mestrado, Universidade de Brasília, Brasil, 133 p.

Chaves, J. F. N., Evangelista Junior, F., Rego, J. H. S., & Vasques, L. P. (2023). Dataset construction and data science analysis of physicochemical characterization of ordinary Portland cement. *Revista Ibracon de Estruturas e Materiais*, *16(6)*, e16609. https://doi.org/10.1590/S1983-41952023000600009

Chen, R.-P., Zhang, P., Kang, X., Zhong, Z.-Q., Liu, Y., & Wu, H.-N. (2019). Prediction of maximum surface settlement caused by earth pressure balance (EPB) shield tunneling with ANN methods. *Soils and Foundations*, *59*(2), 284–295. https://doi.org/10.1016/j.sandf.2018.11.005

Chen, W.-B., Xu, T., & Zhou, W.-H. (2021). Microanalysis of smooth Geomembrane–Sand interface using FDM–DEM coupling simulation. *Geotextiles and Geomembranes*, *49*(1), 276–288. https://doi.org/10.1016/j.geotexmem.2020.10.022

Cheu, R. L., & Ritchie, S. G. (1995). Automated detection of lane-blocking freeway incidents using artificial neural networks. *Transportation Research Part C: Emerging Technologies*, *3*(6), 371–388. https://doi.org/10.1016/0968-090X(95)00016-C

Choudhary, A., Krishna, A. M. (2016). Experimental Investigation of Interface Behaviour of Different Types of Granular Soil/Geosynthetics. *International Journal of Geosynthetics and Ground Engineering*, 1(2), 4. DOI 10.1007/s40891-016-0044-8

Costa e Lopes, C. P. F. (2001). Estudo da interacção solo-geossintético através de ensaios de

corte em plano inclinado. Dissertação de Mestrado, Universidade de Porto, Porto, Portugal, 194 p.

Costa Junior, S. L. (2020). Avaliação da resistência de interface entre geomembranas e diferentes geossintéticos. Dissertação de Mestrado, Universidade Estadual Paulista, Brasil, 128 p.

Costa Junior, S. L., Aparicio-Ardila, M. A., Palomino, C. F., & Lins da Silva, J. (2023). Analysis of Textured Geomembrane–Soil Interface Strength to Mining Applications. *International Journal of Geosynthetics and Ground Engineering*, *9*(1), 3. https://doi.org/10.1007/s40891-022-00423-w

Crespo, J. L., & Mora, E. (1995). Neural Networks as Inference and Learning Engines. *Computer-Aided Civil and Infrastructure Engineering*, *10*(2), 89–96. https://doi.org/10.1111/j.1467-8667.1995.tb00272.x

Das, S. K., Samui, P., Sabat, A. K., & Sitharam, T. G. (2010). Prediction of swelling pressure of soil using artificial intelligence techniques. *Environmental Earth Sciences*, *61*(2), 393–403. https://doi.org/10.1007/s12665-009-0352-6

Das, S., & Suganthan, P. N. (2011). Differential Evolution: A Survey of the State-of-the-Art. *IEEE Transactions on Evolutionary Computation*, *15*(1), 4–31. https://doi.org/10.1109/TEVC.2010.2059031

David Frost, J., Kim, D., & Lee, S.-W. (2012). Microscale geomembrane-granular material interactions. *KSCE Journal of Civil Engineering*, *16*(1), 79–92. https://doi.org/10.1007/s12205-012-1476-x

Debnath, P., & Dey, A. K. (2017). Prediction of Laboratory Peak Shear Stress Along the Cohesive Soil–Geosynthetic Interface Using Artificial Neural Network. *Geotechnical and Geological Engineering*, *35*(1), 445–461. https://doi.org/10.1007/s10706-016-0119-2

Dede, T., Kankal, M., Vosoughi, A. R., Grzywiński, M., & Kripka, M. (2019). Artificial Intelligence Applications in Civil Engineering. *Advances in Civil Engineering*, *2019*, 1–3. https://doi.org/10.1155/2019/8384523

Deo, M. C., & Rao, V. V. (1997). Neural Networks for Wave Height Interpolation. *Computer-Aided Civil and Infrastructure Engineering*, *12*(3), 217–225. https://doi.org/10.1111/0885-9507.00058

Ebid, A. M. (2021). 35 Years of (AI) in Geotechnical Engineering: State of the Art. *Geotechnical and Geological Engineering*, *39*(2), 637–690. https://doi.org/10.1007/s10706-020-01536-7

Enayatollahi, I., Aghajani Bazzazi, A., & Asadi, A. (2014). Comparison Between Neural Networks and Multiple Regression Analysis to Predict Rock Fragmentation in Open-Pit Mines. *Rock Mechanics and Rock Engineering*, *47*(2), 799–807. https://doi.org/10.1007/s00603-013-0415-6

Ermini, L., Catani, F., & Casagli, N. (2005). Artificial Neural Networks applied to landslide

susceptibility assessment. *Geomorphology*, *66*(1–4), 327–343. https://doi.org/10.1016/j.geomorph.2004.09.025

Erzin, Y. (2007). Artificial neural networks approach for swell pressure versus soil suction behaviour. *Canadian Geotechnical Journal*, *44*(10), 1215–1223. https://doi.org/10.1139/T07-052

Erzin, Y., & Ecemis, N. (2015). The use of neural networks for CPT-based liquefaction screening. *Bulletin of Engineering Geology and the Environment*, *74*(1), 103–116. https://doi.org/10.1007/s10064-014-0606-8

Fausett, L. V. (1994). Fundamentals of neural networks: Architectures, algorithms, and applications (1st ed.). Prentice-Hall, Englewood Cliffs, NJ, 461 p.

Ferentinou, M. D., & Sakellariou, M. G. (2007). Computational intelligence tools for the prediction of slope performance. *Computers and Geotechnics*, *34*(5), 362–384. https://doi.org/10.1016/j.compgeo.2007.06.004

Fleming, I. R., Sharma, J. S., & Jogi, M. B. (2006). Shear strength of geomembrane–soil interface under unsaturated conditions. *Geotextiles and Geomembranes*, *24*(5), 274–284. https://doi.org/10.1016/j.geotexmem.2006.03.009

Gangopadhyay, S., Gautam, T. R., & Gupta, A. D. (1999). Subsurface Characterization Using Artificial Neural Network and GIS. *Journal of Computing in Civil Engineering*, *13*(3), 153–161. https://doi.org/10.1061/(ASCE)0887-3801(1999)13:3(153)

García-Segura, T., Yepes, V., & Frangopol, D. M. (2017). Multi-objective design of post-tensioned concrete road bridges using artificial neural networks. *Structural and Multidisciplinary Optimization*, *56*(1), 139–150. https://doi.org/10.1007/s00158-017-1653-0

Geomatrix Colombia. (2023). Blog. https://geomatrix.co/es/blog/

Géron, A. (2019). Hands-on machine learning with Scikit-Learn, Keras, and TensorFlow: Concepts, tools, and techniques to build intelligent systems (Second edition). O'Reilly Media, Inc, Beijing, China, Sebastopol, CA, 819 p.

Ghaleini, E. N., Koopialipoor, M., Momenzadeh, M., Sarafraz, M. E., Mohamad, E. T., & Gordan, B. (2019). A combination of artificial bee colony and neural network for approximating the safety factor of retaining walls. *Engineering with Computers*, *35*(2), 647–658. https://doi.org/10.1007/s00366-018-0625-3

Girard, H., Fischer, S., & Alonso, E. (1990). Problems of friction posed by the use of geomembranes on dam slopes—Examples and measurements. *Geotextiles and Geomembranes*, *9*(2), 129–143. https://doi.org/10.1016/0266-1144(90)90010-A

Giroud, J. P., & Bonaparte, R. (1989). Leakage through liners constructed with geomembranes—Part I. Geomembrane liners. *Geotextiles and Geomembranes*, *8*(1), 27–67. https://doi.org/10.1016/0266-1144(89)90009-5

Glorot, X., Bordes, A., & Bengio, Y. (2011). Deep Sparse Rectifier Neural Networks. *15*, 315–

323. 14th International Conference on Articial Intelligence and Statistics (AISTATS), Fort Lauderdale, FL, USA.

Goh, A. T. C., Wong, K. S., & Broms, B. B. (1995). Estimation of lateral wall movements in braced excavations using neural networks. *Canadian Geotechnical Journal*, *32*(6), 1059–1064. https://doi.org/10.1139/t95-103

Golbraikh, A., & Tropsha, A. (2002). Beware of q2! *Journal of Molecular Graphics and Modelling*, *20*(4), 269–276. https://doi.org/10.1016/S1093-3263(01)00123-1

Gomes, R. C. (1993). Interação Solo-Reforço e Mecanismo de Ruptura em Solos Reforçados com Geotêxteis. Universidade de São Paulo, São Carlos, Brasil.

Gourc, J. P., Lalarakotoson, S., Müller-Rochholz, H., & Bronstein, Z. (1996). Friction measurement by direct shearing or tilting process—Development of a European standard. 1039–1046.

Gourc, J. P., & Reyes Ramírez, R. (2004). Dynamics-based interpretation of the interface friction test at the inclined plane. *Geosynthetics International*, *11*(6), 439–454. https://doi.org/10.1680/gein.2004.11.6.439

Govindaraju, R. S., & Rao, A. R. (2000). Artificial Neural Networks in Hydrology (Vol. 36). Springer Netherlands, Dordrecht. https://doi.org/10.1007/978-94-015-9341-0

Grubert, J. P. (1995). Prediction of Estuarine Instabilities with Artificial Neural Networks. *Journal of Computing in Civil Engineering*, *9*(4), 266–274. https://doi.org/10.1061/(ASCE)0887-3801(1995)9:4(266)

Guo, J. C. Y. (2001). A Semivirtual Watershed Model by Neural Networks. *Computer-Aided Civil and Infrastructure Engineering*, *16*(2), 106–111. https://doi.org/10.1111/0885-9507.00217

Hanandeh, S., Ardah, A., & Abu-Farsakh, M. (2020). Using artificial neural network and genetics algorithm to estimate the resilient modulus for stabilized subgrade and propose new empirical formula. *Transportation Geotechnics*, *24*, 100358. https://doi.org/10.1016/j.trgeo.2020.100358

Hanna, A. M., Morcous, G., & Helmy, M. (2004). Efficiency of pile groups installed in cohesionless soil using artificial neural networks. *Canadian Geotechnical Journal*, *41*(6), 1241–1249. https://doi.org/10.1139/t04-050

Hanna, A. M., Ural, D., & Saygili, G. (2007). Evaluation of liquefaction potential of soil deposits using artificial neural networks. *Engineering Computations*, *24*(1), 5–16. https://doi.org/10.1108/02644400710718547

Hasanipanah, M., Noorian-Bidgoli, M., Jahed Armaghani, D., & Khamesi, H. (2016). Feasibility of PSO-ANN model for predicting surface settlement caused by tunneling. *Engineering with Computers*, *32*(4), 705–715. https://doi.org/10.1007/s00366-016-0447-0

Hauke, J., & Kossowski, T. (2011). Comparison of Values of Pearson's and Spearman's

Correlation Coefficients on the Same Sets of Data. *QUAGEO*, *30*(2), 87–93. https://doi.org/10.2478/v10117-011-0021-1

Haykin, S. S. (1999). Neural networks: A comprehensive foundation (2. ed.). Prentice-Hall, Upper Saddle River, NJ, 842 p.

Hecht-Nielsen. (1989). Theory of the backpropagation neural network. *International Joint Conference on Neural Networks*, 593–605 vol.1. https://doi.org/10.1109/IJCNN.1989.118638

Hegazy, T., Tully, S., & Marzouk, H. (1998). A neural network approach for predicting the structural behavior of concrete slabs. *Canadian Journal of Civil Engineering*, *25*(4), 668–677. https://doi.org/10.1139/l98-009

Hsieh, C., & Hsieh, M.-W. (2003). Load plate rigidity and scale effects on the frictional behavior of sand/geomembrane interfaces. *Geotextiles and Geomembranes*, *21*(1), 25–47. https://doi.org/10.1016/S0266-1144(02)00034-1

Hsieh, C., Hsieh, M.-W., Chein, J. (2002). Direct shear behaviour of sand geomembrane systems of various shear boxes. Geosynthetics – 7th ICG, 671 – 676.

Huang, C.-C., & Loh, C.-H. (2001). Nonlinear Identification of Dynamic Systems Using Neural Networks. *Computer-Aided Civil and Infrastructure Engineering*, *16*(1), 28–41. https://doi.org/10.1111/0885-9507.00211

Huang, Y., Li, J., & Fu, J. (2019). Review on Application of Artificial Intelligence in Civil Engineering. *Computer Modeling in Engineering & Sciences*, *121*(3), 845–875. https://doi.org/10.32604/cmes.2019.07653

Hutter, F., Kotthoff, L., & Vanschoren, J. (2019). Automated Machine Learning: Methods, Systems, Challenges. Springer International Publishing, USA, 219 p. https://doi.org/10.1007/978-3-030-05318-5

IGS. (2015a). Funções dos geossintéticos. 2 p.

IGS. (2015b). Geossintéticos em projetos hidráulicos. 2 p.

Ikizler, S. B., Aytekin, M., Vekli, M., & Kocabaş, F. (2010). Prediction of swelling pressures of expansive soils using artificial neural networks. *Advances in Engineering Software*, *41*(4), 647–655. https://doi.org/10.1016/j.advengsoft.2009.12.005

Ingold, T. S. (1991). Friction Testing. Geomembranes –Identification and Performance Testing. *RILEM – Reportof Technical Committee 103-MGH Mechanical AndHydraulic Testing of Geomembranes*, 176–218.

ISO 10318-1. (2015). Geosynthetics—Terms and definitions.

Izgin, M. (1997). Geomembrane-sand interface friction. Master's thesis, Middle East Technical University, Turkey, 171 p.

Izgin, M., & Wasti, Y. (1998). Geomembrane–sand interface frictional properties as determined by inclined board and shear box tests. *Geotextiles and Geomembranes*, *16*(4), 207–219.

https://doi.org/10.1016/S0266-1144(98)00010-7

Jain, A. K., Jianchang Mao, & Mohiuddin, K. M. (1996). Artificial neural networks: A tutorial. *Computer*, *29*(3), 31–44. https://doi.org/10.1109/2.485891

Jeremiah, J. J., Abbey, S. J., Booth, C. A., & Kashyap, A. (2021). Results of Application of Artificial Neural Networks in Predicting Geo-Mechanical Properties of Stabilised Clays—A Review. *Geotechnics*, *1*(1), 147–171. https://doi.org/10.3390/geotechnics1010008

Jewell, R. A. (1990). Reinforcement bond capacity. *Géotechnique*, *40*(3), 513–518. https://doi.org/10.1680/geot.1990.40.3.513

Jewell, R. A. (1996). Soil reinforcement with geotextiles. Construction Industry Research and Information Association, London, 332 p.

Jewell, R. A., Milligan, G. W. E., Sarsby, R. W., & Dubois, D. (1984). Interaction Between Soil and Geogrids. In *Polymer Grid Reinforcement* (pp. 18–30). Thomas Telford Ltd.

Jogi, M. (2005). A method for measuring smooth geomembrane/soil interface shear behaviour under unsaturated conditions. Master's thesis, University of Saskatchewan, Canada, 91 p.

Kalinli, A., Acar, M. C., & Gündüz, Z. (2011). New approaches to determine the ultimate bearing capacity of shallow foundations based on artificial neural networks and ant colony optimization. *Engineering Geology*, *117*(1–2), 29–38. https://doi.org/10.1016/j.enggeo.2010.10.002

Kao, J.-J., & Liao, Y.-Y. (1996). IAC Network for Composition of Waste-Incineration Facility. *Journal of Computing in Civil Engineering*, *10*(2), 168–171. https://doi.org/10.1061/(ASCE)0887-3801(1996)10:2(168)

Karademir, T. (2011). Elevated temperature effects on interface shear behaviour. Phd Thesis, Georgia Institute of Technology, USA, 592 p.

Karademir, T., & Frost, J. D. (2021). Elevated Temperature Effects on Geotextile–Geomembrane Interface Shear Behavior. *Journal of Geotechnical and Geoenvironmental Engineering*, *147*(12), 04021148. https://doi.org/10.1061/(ASCE)GT.1943-5606.0002698

Karunanithi, N., Grenney, W. J., Whitley, D., & Bovee, K. (1994). Neural Networks for River Flow Prediction. *Journal of Computing in Civil Engineering*, *8*(2), 201–220. https://doi.org/10.1061/(ASCE)0887-3801(1994)8:2(201)

Khan, R., & Latha, G. M. (2023). Multi-scale understanding of sand-geosynthetic interface shear response through Micro-CT and shear band analysis. *Geotextiles and Geomembranes*, *51*(3), 437–453. https://doi.org/10.1016/j.geotexmem.2023.01.006

Kiefa, M. A. A. (1998). General Regression Neural Networks for Driven Piles in Cohesionless Soils. *Journal of Geotechnical and Geoenvironmental Engineering*, *124*(12), 1177–1185. https://doi.org/10.1061/(ASCE)1090-0241(1998)124:12(1177)

Kim, J.-T., Jung, H.-J., & Lee, I.-W. (2000). Optimal Structural Control Using Neural Networks. *Journal of Engineering Mechanics*, *126*(2), 201–205. https://doi.org/10.1061/(ASCE)0733-9399(2000)126:2(201)

Koerner, R. M. (2012). Designing with geosynthetics (6th ed.). Vol. 1. Prentice Hall, Inc. New Jersey, USA. p.761.

Koerner, R. M., & Soong, T.-Y. (1997). The evolution of geosynthethics. *Civil Engineering*, *67*(7), 62–64.

Koutsourais, M. M., Sprague, C. J., & Pucetas, R. C. (1991). Interfacial friction study of cap and liner components for landfill design. *Geotextiles and Geomembranes*, *10*(5–6), 531–548. https://doi.org/10.1016/0266-1144(91)90045-X

Kumar, D., Singh, A., Kumar, P., Jha, R. K., Sahoo, S. K., & Jha, V. (2020). Sobol sensitivity analysis for risk assessment of uranium in groundwater. *Environmental Geochemistry and Health*, *42*(6), 1789–1801. https://doi.org/10.1007/s10653-020-00522-5

Kumar, V., kumar, V., & Yeetendra, K. (2012). Liquefaction potential evaluation of alluvial soil by neuro-Fuzzy technique. *International Journal of Emerging Technology and Advanced Engineering*, *2*(3), 174–184.

Kumari, S., & Dutta, R. K. (2019). Leakage rate prediction through composite liner due to geomembrane defect using neural network. *Journal of Geotechnical Engineering*, *6*(3), 8–17.

Kung, G. T. C., Hsiao, E. C. L., Schuster, M., & Juang, C. H. (2007). A neural network approach to estimating deflection of diaphragm walls caused by excavation in clays. *Computers and Geotechnics*, *34*(5), 385–396. https://doi.org/10.1016/j.compgeo.2007.05.007

Lachtermacher, G., & Fuller, J. D. (1994). Backpropagation in Hydrological Time Series Forecasting. In K. W. Hipel, A. I. McLeod, U. S. Panu, & V. P. Singh (Eds.), *Stochastic and Statistical Methods in Hydrology and Environmental Engineering* (Vol. 10/3, pp. 229–242). Springer Netherlands. https://doi.org/10.1007/978-94-017-3083-9_18

Lagaros, N. D., & Plevris, V. (2022). Artificial Intelligence (AI) Applied in Civil Engineering. *Applied Sciences*, *12*(15), 7595. https://doi.org/10.3390/app12157595

Lapedes, A., & Farber, R. (1989). How Neural Nets Work. In Y. C. Lee, *Evolution, Learning and Cognition*, 331–346. WORLD SCIENTIFIC. https://doi.org/10.1142/9789814434102_0012

Lashkari, A., & Jamali, V. (2021). Global and local sand–geosynthetic interface behaviour. *Géotechnique*, *71*(4), 346–367. https://doi.org/10.1680/jgeot.19.P.109

Lee, C., & Sterling, R. (1992). Identifying probable failure modes for underground openings using a neural network. *International Journal of Rock Mechanics and Mining Sciences & Geomechanics Abstracts*, *29*(1), 49–67. https://doi.org/10.1016/0148-9062(92)91044-6

Lee, S., Ryu, J.-H., Lee, M.-J., & Won, J.-S. (2006). The Application of Artificial Neural

Networks to Landslide Susceptibility Mapping at Janghung, Korea. *Mathematical Geology*, *38*(2), 199–220. https://doi.org/10.1007/s11004-005-9012-x

Lee, S., Ryu, J.-H., Min, K., & Won, J.-S. (2003). Landslide susceptibility analysis using GIS and artificial neural network. *Earth Surface Processes and Landforms*, *28*(12), 1361–1376. https://doi.org/10.1002/esp.593

Leite, A. R. S. (2019). Aplicações de redes neurais artificiais para previsão do comportamento cisalhante em descontinuidades de maciços rochosos. Dissertação de Mestrado, Universidade Federal do Ceará, Brasil, 156 p.

Lima Junior, N. R. (2000). Estudo da interação solo-geossintético em obras de proteção ambiental com o uso do equipamento de plano inclinado. Dissertação de Mestrado, Universidade de Brasília, Brasil, 148 p.

Lima, J. P. S., Evangelista, F., & Soares, C. G. (2023). Bi-fidelity Kriging model for reliability analysis of the ultimate strength of stiffened panels. *Marine Structures*, *91*, 103464. https://doi.org/10.1016/j.marstruc.2023.103464

Ling, H. I., Burke, C., Mohri, Y., & Matsushima, K. (2002). Shear Strength Parameters of Soil-Geosynthetic Interfaces Under Low Confining Pressure Using a Tilting Table. *Geosynthetics International*, *9*(4), 373–380. https://doi.org/10.1680/gein.9.0223

Lingras, P., & Adamo, M. (1996). Average and Peak Traffic Volumes: Neural Nets, Regression, Factor Approaches. *Journal of Computing in Civil Engineering*, *10*(4), 300–306. https://doi.org/10.1061/(ASCE)0887-3801(1996)10:4(300)

Liong, S.-Y., Lim, W.-H., & Paudyal, G. N. (2000). River Stage Forecasting in Bangladesh: Neural Network Approach. *Journal of Computing in Civil Engineering*, *14*(1), 1–8. https://doi.org/10.1061/(ASCE)0887-3801(2000)14:1(1)

Lopes, M. J., & Lopes, M. L. (1999). Soil-Geosynthetic Interaction—Influence of Soil Particle Size and Geosynthetic Structure. *Geosynthetics International*, *6*(4), 261–282. https://doi.org/10.1680/gein.6.0153

Lopes, P. C., Lopes, M. L., & Lopes, M. P. (2001). Shear Behaviour of Geosynthetics in the Inclined Plane Test – Influence of Soil Particle Size and Geosynthetic Structure. *Geosynthetics International*, *8*(4), 327–342. https://doi.org/10.1680/gein.8.0198

Lu, P., Chen, S., & Zheng, Y. (2012). Artificial Intelligence in Civil Engineering. *Mathematical Problems in Engineering*, *2012*, 1–22. https://doi.org/10.1155/2012/145974

Maglogiannis, I. G. (Ed.). (2007). Emerging artificial intelligence applications in computer engineering: Real word AI systems with applications in eHealth, HCI, information retrieval and pervasive technologies. IOS Press, Ansterdam, Whashington D.C., 407 p.

Mahesh, B. (2020). Machine Learning Algorithms—A Review. *International Journal of Science and Research (IJSR)*, *9*(1), 381–386. https://doi.org/DOI: 10.21275/ART20203995

Manevitz, L., Yousef, M., & Givoli, D. (1997). Finite-Element Mesh Generation Using Self-

Organizing Neural Networks. *Computer-Aided Civil and Infrastructure Engineering*, *12*(4), 233–250. https://doi.org/10.1111/0885-9507.00060

Markou, I. N., & Evangelou, E. D. (2018). Shear Resistance Characteristics of Soil–Geomembrane Interfaces. *International Journal of Geosynthetics and Ground Engineering*, *4*(4), 29. https://doi.org/10.1007/s40891-018-0146-6

Masri, S. F., Chassiakos, A. G., & Caughey, T. K. (1993). Identification of Nonlinear Dynamic Systems Using Neural Networks. *Journal of Applied Mechanics*, *60*(1), 123–133. https://doi.org/10.1115/1.2900734

Mayoraz, F., & Vulliet, L. (2002). Neural Networks for Slope Movement Prediction. *International Journal of Geomechanics*, *2*(2), 153–173. https://doi.org/10.1061/(ASCE)1532-3641(2002)2:2(153)

Mello, L. G. R. (2001). Estudo da interação solo-geossintético em taludes de obras de disposição de resíduos. Dissertação de Mestrado, Universidade de Brasília, Brasil, 137 p.

Messner, J. I., Sanvido, V. E., & Kumara, S. R. T. (1994). StructNet: A Neural Network for Structural System Selection. *Computer-Aided Civil and Infrastructure Engineering*, *9*(2), 109–118. https://doi.org/10.1111/j.1467-8667.1994.tb00366.x

Monteiro, C. B. (2012). Estudo de interface solo-geomembrana como variações de níveis de saturação do solo. Dissertação de Mestrado, Universidade de Brasília, Brasil, 131 p.

Moraci, N., Cardile, G., Gioffrè, D., Mandaglio, M. C., Calvarano, L. S., & Carbone, L. (2014). Soil Geosynthetic Interaction: Design Parameters from Experimental and Theoretical Analysis. *Transportation Infrastructure Geotechnology*, *1*(2), 165–227. https://doi.org/10.1007/s40515-014-0007-2

Mukherjee, A., Deshpande, J. M., & Anmala, J. (1996). Prediction of Buckling Load of Columns Using Artificial Neural Networks. *Journal of Structural Engineering*, *122*(11), 1385–1387. https://doi.org/10.1061/(ASCE)0733-9445(1996)122:11(1385)

Naderpour, H., Rafiean, A. H., & Fakharian, P. (2018). Compressive strength prediction of environmentally friendly concrete using artificial neural networks. *Journal of Building Engineering*, *16*, 213–219. https://doi.org/10.1016/j.jobe.2018.01.007

O'Rourke, T. D., Druschel, S. J., & Netravali, A. N. (1990). Shear Strength Characteristics of Sand-Polymer Interfaces. *Journal of Geotechnical Engineering*, *116*(3), 451–469. https://doi.org/10.1061/(ASCE)0733-9410(1990)116:3(451)

Owusu-Ababio, S. (1998). Effect of Neural Network Topology on Flexible Pavement Cracking Prediction. *Computer-Aided Civil and Infrastructure Engineering*, *13*(5), 349–355. https://doi.org/10.1111/0885-9507.00113

Pain, C. C., De Oliveira, C. R. E., & Goddard, A. J. H. (1999). A neural network graph partitioning procedure for grid-based domain decomposition. *International Journal for Numerical Methods in Engineering*, *44*(5), 593–613. https://doi.org/10.1002/(SICI)1097-0207(19990220)44:5<593::AID-

NME516>3.0.CO;2-0

Palmeira, E. M. (1987). The study of soil-reinforcement interaction by means of large scale laboratory tests. Phd Thesis, University of Oxford, England, 237 p.

Palmeira, E. M. (2009). Soil–geosynthetic interaction: Modelling and analysis. *Geotextiles and Geomembranes*, *27*(5), 368–390. https://doi.org/10.1016/j.geotexmem.2009.03.003

Palmeira, E. M., Lima, N. R., & Mello, L. G. R. (2002). Interaction Between Soils and Geosynthetic Layers in Large-Scale Ramp Tests. *Geosynthetics International*, *9*(2), 149–187. https://doi.org/10.1680/gein.9.0214

Palmeira, E. M., & Milligan, G. W. E. (1989). Scale and other factors affecting the results of pull-out tests of grids buried in sand. *Géotechnique*, *39*(3), 511–542. https://doi.org/10.1680/geot.1989.39.3.511

Pant, A., & Ramana, G. V. (2022). Novel application of machine learning for estimation of pullout coefficient of geogrid. *Geosynthetics International*, *29*(4), 342–355. https://doi.org/10.1680/jgein.21.00021a

Paruchuri, B. (2011). Effects of Freezing Temperature on Interface Shear Strength of Landfill Geosynthetic Liners. Phd Thesis, The University of Toledo, USA, 120 p.

Pavanello, P., Carrubba, P., & Moraci, N. (2021). The characterisation of geosynthetic interface friction by means of the inclined plane test. *Geotextiles and Geomembranes*, *49*(1), 257–275. https://doi.org/10.1016/j.geotexmem.2020.10.027

Pavanello, P., Carrubba, P., & Moraci, N. (2022). Geosynthetic Interface Friction at Low Normal Stress: Two Approaches with Increasing Shear Loading. *Applied Sciences*, *12*(3), 1065. https://doi.org/10.3390/app12031065

Pham, T. A., Ly, H.-B., Tran, V. Q., Giap, L. V., Vu, H.-L. T., & Duong, H.-A. T. (2020). Prediction of Pile Axial Bearing Capacity Using Artificial Neural Network and Random Forest. *Applied Sciences*, *10*(5), 1871. https://doi.org/10.3390/app10051871

Phoon, K.-K., & Zhang, W. (2022). Future of machine learning in geotechnics. *Georisk: Assessment and Management of Risk for Engineered Systems and Geohazards*, 1–16. https://doi.org/10.1080/17499518.2022.2087884

Pitanga, H. N., Gourc, J.-P., & Vilar, O. M. (2009). Interface shear strength of geosynthetics: Evaluation and analysis of inclined plane tests. *Geotextiles and Geomembranes*, *27*(6), 435–446. https://doi.org/10.1016/j.geotexmem.2009.05.003

Pooya Nejad, F., & Jaksa, M. B. (2017). Load-settlement behavior modeling of single piles using artificial neural networks and CPT data. *Computers and Geotechnics*, *89*, 9–21. https://doi.org/10.1016/j.compgeo.2017.04.003

Priyadarshee, A., Chandra, S., Gupta, D., & Kumar, V. (2020). Neural Models for Unconfined Compressive Strength of Kaolin Clay Mixed with Pond Ash, Rice Husk Ash and Cement. *Journal of Soft Computing in Civil Engineering*, *4*(2). https://doi.org/10.22115/scce.2020.223774.1189

Qadir, A., Gazder, U., & Choudhary, K. U. N. (2020). Artificial Neural Network Models for Performance Design of Asphalt Pavements Reinforced with Geosynthetics. *Transportation Research Record: Journal of the Transportation Research Board*, *2674*(8), 319–326. https://doi.org/10.1177/0361198120924387

Rahman, M. S., Wang, J., Deng, W., & Carter, J. P. (2001). A neural network model for the uplift capacity of suction caissons. *Computers and Geotechnics*, *28*(4), 269–287. https://doi.org/10.1016/S0266-352X(00)00033-1

Raja, M. N. A., & Shukla, S. K. (2021). Predicting the settlement of geosynthetic-reinforced soil foundations using evolutionary artificial intelligence technique. *Geotextiles and Geomembranes*, *49*(5), 1280–1293. https://doi.org/10.1016/j.geotexmem.2021.04.007

Raja, M. N. A., Shukla, S. K., & Khan, M. U. A. (2022). An intelligent approach for predicting the strength of geosynthetic-reinforced subgrade soil. *International Journal of Pavement Engineering*, *23*(10), 3505–3521. https://doi.org/10.1080/10298436.2021.1904237

Ray, S. (2019). A Quick Review of Machine Learning Algorithms. *2019 International Conference on Machine Learning, Big Data, Cloud and Parallel Computing (COMITCon)*, 35–39. https://doi.org/10.1109/COMITCon.2019.8862451

Rebelo, K. M. W. (2003). Resistência de Interface entre geomembranas e solos através do ensaio de Ring Shear. Mestrado em Geotecnia, Universidade de São Paulo, Brasil, 194 p. https://doi.org/10.11606/D.18.2003.tde-10052004-164052

Reich, Y. (1997). Machine Learning Techniques for Civil Engineering Problems. *Computer-Aided Civil and Infrastructure Engineering*, *12*(4), 295–310. https://doi.org/10.1111/0885-9507.00065

Reyes Ramirez, R., & Gourc, J. P. (2003). Use of the inclined plane test in measuring geosynthetic interface friction relationship. *Geosynthetics International*, *10*(5), 165–175. https://doi.org/10.1680/gein.2003.10.5.165

Rowe, R. K., Rimal, S., & Sangam, H. (2009). Ageing of HDPE geomembrane exposed to air, water and leachate at different temperatures☆. *Geotextiles and Geomembranes*, *27*(2), 137–151. https://doi.org/10.1016/j.geotexmem.2008.09.007

Roy, P. P., & Roy, K. (2008). On Some Aspects of Variable Selection for Partial Least Squares Regression Models. *QSAR & Combinatorial Science*, *27*(3), 302–313. https://doi.org/10.1002/qsar.200710043

Russell, S. J., Norvig, P., & Davis, E. (2010). Artificial intelligence: A modern approach (3rd ed). Prentice Hall, Upper Saddle River, USA, 1132 p.

Sadrossadat, E., Heidaripanah, A., & Osouli, S. (2016). Prediction of the resilient modulus of flexible pavement subgrade soils using adaptive neuro-fuzzy inference systems. *Construction and Building Materials*, *123*, 235–247. https://doi.org/10.1016/j.conbuildmat.2016.07.008

Salahudeen, A. B., Sadeeq, J. A., Badamasi, A., & Onyelowe, K. C. (2020). *Prediction of*

unconfined compressive strength of treated expansive clay using back-propagation artificial neural networks. *27*(1).

Saleh, A. Y., Nuzly, H., Hameed, B. A., & Salleh, M. (2014). A Novel hybrid algorithm of Differential evolution with Evolving Spiking Neural Network for pre-synaptic neurons Optimization. *International Journal of Advances in Soft Computing and Its Applications*, *6*(1), 16.

Salehi, H., & Burgueño, R. (2018). Emerging artificial intelligence methods in structural engineering. *Engineering Structures*, *171*, 170–189. https://doi.org/10.1016/j.engstruct.2018.05.084

Sánchez, N. P. (2018). Estudo de alguns aspectos que influenciam a aderência entre geossintéticos e diferentes materiais. Tese de Doutorado, Universidade de Brasília, Brasil, 168 p.

Schober, P., Boer, C., & Schwarte, L. A. (2018). Correlation Coefficients: Appropriate Use and Interpretation. *Anesthesia & Analgesia*, *126*(5), 1763–1768. https://doi.org/10.1213/ANE.0000000000002864

Shahin, M. A. (2013). Artificial Intelligence in Geotechnical Engineering. In *Metaheuristics in Water, Geotechnical and Transport Engineering* (pp. 169–204). Elsevier. https://doi.org/10.1016/B978-0-12-398296-4.00008-8

Shahin, M. A. (2016). State-of-the-art review of some artificial intelligence applications in pile foundations. *Geoscience Frontiers*, *7*(1), 33–44. https://doi.org/10.1016/j.gsf.2014.10.002

Shahin, M. A., & Jaksa, M. B. (2005). Neural network prediction of pullout capacity of marquee ground anchors. *Computers and Geotechnics*, *32*(3), 153–163. https://doi.org/10.1016/j.compgeo.2005.02.003

Shahin, M. A., Jaksa, M. B., & Maier, H. R. (2005). Neural network based stochastic design charts for settlement prediction. *Canadian Geotechnical Journal*, *42*(1), 110–120. https://doi.org/10.1139/t04-096

Shahin, M. A., Jaksa, M. B., & Maier, H. R. (2008). State of the Art of Artificial Neural Networks in Geotechnical Engineering. *Electronic Journal of Geotechnical Engineering*, 26.

Shahin, M. A., Jaksa, M. B., & Maier, H. R. (2009). Recent Advances and Future Challenges for Artificial Neural Systems in Geotechnical Engineering Applications. *Advances in Artificial Neural Systems*, *2009*, 1–9. https://doi.org/10.1155/2009/308239

Shahin, M. A., Maier, H. R., & Jaksa, M. B. (2002). Predicting Settlement of Shallow Foundations using Neural Networks. *Journal of Geotechnical and Geoenvironmental Engineering*, *128*(9), 785–793. https://doi.org/10.1061/(ASCE)1090-0241(2002)128:9(785)

Shang, J. Q., Ding, W., Rowe, R. K., & Josic, L. (2004). Detecting heavy metal contamination in soil using complex permittivity and artificial neural networks. *Canadian*

Geotechnical Journal, *41*(6), 1054–1067. https://doi.org/10.1139/t04-051

Shukla, S. K., & Yin, J.-H. (2006). Fundamentals of Geosynthetic Engineering (1st ed.). CRC Press, London, 432 p. https://doi.org/10.1201/9781482288445

Silva, I. N., Spatti, D. H., & Flauzino, R. A. (2016). Redes Neurais Artificiais para engenharia e ciências aplicadas (2nd ed.). Artliber Editora Ltda, São Paulo, Brasil, 431 p.

Soleimanbeigi, A., & Hataf, N. (2006). Prediction of settlement of shallow foundations on reinforced soils using neural networks. *Geosynthetics International*, *13*(4), 161–170. https://doi.org/10.1680/gein.2006.13.4.161

Stark, T. D., Williamson, T. A., & Eid, H. T. (1996). HDPE Geomembrane/Geotextile Interface Shear Strength. *Journal of Geotechnical Engineering*, *122*(3), 197–203. https://doi.org/10.1061/(ASCE)0733-9410(1996)122:3(197)

Tanga, A. T. (2022). Machine learning for geomembrane-sand interface analysis. Dissertação de Mestrado, Universidade de Brasília, Brasil, 71 p.

Theocaris, P. S., & Panagiotopoulos, P. D. (1993). Neural networks for computing in fracture mechanics. Methods and prospects of applications. *Computer Methods in Applied Mechanics and Engineering*, *106*(1–2), 213–228. https://doi.org/10.1016/0045-7825(93)90191-Y

Tyche. (2020). Data Science and Artificial Intelligence Software. Machine Learning Module, versão 1.0. Nexum Research Group. Universidade de Brasilia, Brasilia, Brasil.

Vangla, P., & Gali, M. L. (2016). Shear behavior of sand-smooth geomembrane interfaces through micro-topographical analysis. *Geotextiles and Geomembranes*, *44*(4), 592–603. https://doi.org/10.1016/j.geotexmem.2016.04.001

Vangla, P., & Latha, G. M. (2015). Influence of Particle Size on the Friction and Interfacial Shear Strength of Sands of Similar Morphology. *International Journal of Geosynthetics and Ground Engineering*, *1*(1), 6. https://doi.org/10.1007/s40891-014-0008-9

Vanluchene, R. D., & Sun, R. (1990). Neural Networks in Structural Engineering. *Computer-Aided Civil and Infrastructure Engineering*, *5*(3), 207–215. https://doi.org/10.1111/j.1467-8667.1990.tb00377.x

Vesterstrom, J., & Thomsen, R. (2004). A comparative study of differential evolution, particle swarm optimization, and evolutionary algorithms on numerical benchmark problems. *Proceedings of the 2004 Congress on Evolutionary Computation (IEEE Cat. No.04TH8753)*, 1980–1987. https://doi.org/10.1109/CEC.2004.1331139

Viana, H. N. de L. (2007). Estudo da interação solo-geossintético em taludes de obras de disposição de resíduos. Tese de Doutorado, Universidade de Brasília, Brasil, 207 p.

Wasti, Y., & Özdüzgün, Z. B. (2001). Geomembrane–geotextile interface shear properties as determined by inclined board and direct shear box tests. *Geotextiles and Geomembranes*, *19*(1), 45–57. https://doi.org/10.1016/S0266-1144(00)00002-9

Wu, H., & Shu, Y. (2012). Stability of geomembrane surface barrier of earth dam considering

strain-softening characteristic of geosynthetic interface. *KSCE Journal of Civil Engineering*, *16*(7), 1123–1131. https://doi.org/10.1007/s12205-012-1466-z

Yan, F., Lin, Z., Wang, X., Azarmi, F., & Sobolev, K. (2017). Evaluation and prediction of bond strength of GFRP-bar reinforced concrete using artificial neural network optimized with genetic algorithm. *Composite Structures*, *161*, 441–452. https://doi.org/10.1016/j.compstruct.2016.11.068

Yeh, Y., Kuo, Y., & Hsu, D. (1993). Building KBES for Diagnosing PC Pile with Artificial Neural Network. *Journal of Computing in Civil Engineering*, *7*(1), 71–93. https://doi.org/10.1061/(ASCE)0887-3801(1993)7:1(71)

Yi, Y., Zhang, W., Xu, X., Zhang, Z., & Wu, X. (2022). Evaluation of neural network models for landslide susceptibility assessment. *International Journal of Digital Earth*, *15*(1), 934–953. https://doi.org/10.1080/17538947.2022.2062467

Young-Su, K., & Byung-Tak, K. (2006). Use of Artificial Neural Networks in the Prediction of Liquefaction Resistance of Sands. *Journal of Geotechnical and Geoenvironmental Engineering*, *132*(11), 1502–1504. https://doi.org/10.1061/(ASCE)1090-0241(2006)132:11(1502)

Yun, C.-B., & Bahng, E. Y. (2000). Substructural identification using neural networks. *Computers & Structures*, *77*(1), 41–52. https://doi.org/10.1016/S0045-7949(99)00199-6

Zaman, M., Solanki, P., Ebrahimi, A., & White, L. (2010). Neural Network Modeling of Resilient Modulus Using Routine Subgrade Soil Properties. *International Journal of*

Zupan, J., & Gasteiger, J. (1993). Neural networks for chemists: An introduction. *Journal of Chemometrics*, *8*, 297–298. https://doi.org/10.1002/cem.1180080410

Zurada, J. M. (1992). Introduction to artificial neural systems. West. Saint Paul, USA, 683 p.